From drones to *Daphnia*:
Exploring eutrophication and climate change impacts on algal blooms at various scales

by

Edna G. Fernandez-Figueroa

A dissertation submitted to the Graduate Faculty of
Auburn University
in partial fulfillment of the
requirements for the Degree of
Doctor of Philosophy

Auburn, Alabama
May 1, 2021

Keywords: cyanobacteria, *Daphnia*, drinking water, harmful algal blooms (HAB), unoccupied aerial systems (AUS), eutrophication

Copyright 2021 by Edna G. Fernandez-Figueroa

Approved by

Alan E. Wilson, Chair, Full Professor, of Fisheries, Aquaculture, and Aquatic Sciences
Mark Liles, Marguerite Scharnagel Endowed Professor of Biological Sciences
Stephanie Rogers, Assistant Professor of Geosciences
Matthew Waters, Associate Professor of Crop, Soil, and Environmental Sciences

Abstract

Climactic variations and cultural eutrophication alter aquatic ecosystems by promoting harmful algal blooms (HABs) that destabilize aquatic food webs and degrade the quality and safety of aquacultured fish, recreational waterbodies, and drinking water sources. The goal of my dissertation work was to gain a holistic understanding of these complex events by studying HABs at multiple scales. At the food web level, many aquatic organisms will have to cope with toxic cyanobacteria and thermal stress. I tested the potential energetic trade-offs associated with local adaptations to toxic cyanobacteria in the keystone zooplankton grazer, *Daphnia pulicaria*, under multiple stressor conditions. Results from this lab study suggest local adaptations to toxic cyanobacteria and elevated temperatures are synergistic, leading to higher survivorship during summer HAB events. At the aquaculture production level, I tested whether unoccupied aerial systems (i.e., drones) were a viable tool for monitoring the abundance of potentially toxic cyanobacteria in small eutrophic systems. Four sensors were used to monitor 54 eutrophic ponds that varied in size and trophic state. Results indicate that while drones are well-equipped for estimating total phytoplankton abundance, commercial sensors are not equipped to reliably monitor cyanobacteria abundance. At the state level, a comprehensive two-year sampling of all drinking water utilities in Alabama was used to determine the prevalence of cyanobacteria, cyanotoxins, and off-flavor compounds in the state's surface drinking water sources. Raw water samples show that drinking water sources were high in nutrients (i.e., nitrogen and phosphorus), but deficient. In cyanobacteria, cyanotoxins, and off-flavor compounds. These results suggest that cultural eutrophication does not necessarily lead to HABs, and therefore monitoring phytoplankton abundance is a better indicator of the trophic state of these systems than nutrients. Finally, to understand algal bloom intensification trends at the national level, a 30 year survey of

650 lakes located across 11 freshwater ecoregions was completed to determine if spatial patterns were associated with algal bloom intensification. Results indicate that 65% of lakes are not significantly increasing or decreasing in algal bloom intensity and algal bloom trends were closely related to eutrophication. These findings suggest researchers may be overestimating the widespread intensification of algal blooms.

Acknowledgments

To my parents: Dr. David Fernandez and Dra. Edna Figueroa. Thank you for all the sacrifices you made to further my education. Your intelligence, kindness, and work ethic inspire me daily.

This work could not have been possible without the support of the Wilson Lab members, the aquaculture farmers that kindly allowed me to collect areal imagery and water samples from their systems, the drinking water utility managers that provided intake samples, and the support staff at Swingle Hall and E. W. Shell Fisheries Center. A special thank you to Evann R. Martin for his assistance with data collection and general unwavering support. Much of this work was financial supported by an NSF GRFP Fellowship. Thank you to my research committee and university reader for dedicating time from your busy schedule to support and review my progress as a graduate student. My path has been unconventional, but I appreciate you allowing me to forge it in a safe space. Finally, thank you to Dr. Alan Wilson for encouraging me to explore research and professional development opportunities within and outside our lab.

Table of Contents

List of Tables

List of Figures

Chapter 1

Local adaptation mediates direct and indirect effects of multiple stressors on consumer fitness

Abstract

Anthropogenic impacts are expected to increase the co-occurrence of stressors that can fundamentally alter ecosystem structure and function. To cope with stress, many organisms locally adapt, but how such adaptations affect the ability of an organism to manage co-occurring stressors is not well understood. In aquatic ecosystems, elevated temperatures and harmful algal blooms are common co-stressors. To better understand the role and potential trade-offs of local adaptations for mitigating the effects of stressors, *Daphnia pulicaria* genotypes that varied in their ability to consume toxic cyanobacteria prey (i.e., three tolerant and three sensitive) were exposed to five diets that included combinations of toxic cyanobacteria, *Microcystis aeruginosa*, and green algae, *Ankistrodesmus falcatus*, under two temperatures (20°C vs. 28°C). A path analysis was conducted to understand how local adaptations affect energy allocation to intermediate life history traits (i.e., somatic growth, fecundity, survival) that maximize *Daphnia* fitness (i.e., population growth rate). Results from the 10-day study show that tolerant *Daphnia* genotypes had higher fitness than sensitive genotypes regardless of diet or temperature treatment, suggesting toxic cyanobacteria tolerance did not cause a decrease in fitness in the absence of cyanobacteria or under elevated temperatures. Results from the path analysis demonstrated that toxic cyanobacteria had a stronger effect on life history traits than temperature and that population growth rate was mainly constrained by reduced fecundity. These findings suggest that local adaptations to toxic cyanobacteria and elevated temperatures are synergistic, leading to higher survivorship of cyanobacteria-tolerant genotypes during summer cyanobacterial bloom events.

Introduction

The ability of a population to manage stressors dictates its fitness, ultimately shaping population dynamics, community structure, and ecosystem function. The mechanisms through which adaptive traits improve fitness are complex given that the value of adaptive traits may vary based on the magnitude and duration of exposure as well as the presence of additional stressors that often lead to unpredictable responses. Anthropogenic activities have been shown to increase the severity, frequency, and co-occurrence of stressors. Therefore untangling the interactive effects of multiple stressors and the strategies employed by organisms to tolerate them is critical for increasing our basic understanding of ecological interactions as well as managing ecosystems (Nõges et al. 2016).

Aquatic ecosystems are particularly sensitive to anthropogenic stressors (Dudgeon et al. 2007), such as temperature increases, agricultural fertilizer run-off, and water flow disruptions, that affect the life history patterns and distribution of aquatic organisms by changing the physical (i.e., thermal stratification) and chemical (i.e., nutrient cycling) conditions of aquatic ecosystems (Hering et al. 2015). These changes are known to alter food web dynamics by expanding the thermal range and promoting the growth of undesirable or detrimental taxa (e.g., toxic or invasive species, Strayer 2010). In lentic systems, these anthropogenic impacts often disrupt freshwater aquatic food webs by promoting cyanobacteria that thrive in eutrophic systems with elevated surface water temperatures, enabling them to outcompete phytoplankton with lower temperature optima for growth, such as chlorophytes and diatoms (Jöhnk et al. 2008; Dupuis and Hann 2009). Cyanobacterial dominance can disrupt the trophic transfer of energy through aquatic food webs, as cyanobacteria lack essential polyunsaturated fatty acids necessary for zooplankton grazer growth (Müller-Navarra et al. 2000). Furthermore, many cyanobacteria

species mechanically inhibit grazing by aggregating into colonies or by producing toxic secondary metabolites that may weaken or kill grazers as well as other phytoplankton (Lampert 1987; Wilson et al. 2006). The large-bodied cladoceran genus, *Daphnia,* is a dominant grazer of phytoplankton as well as an important prey for planktivorous fishes in lakes (Dodson and Hanazato 1995; Ebert 2005). As climate change increases global surface water temperatures, *Daphnia* will have to cope with thermal stress and cyanobacterial blooms more frequently and for longer periods (Griffith and Gobler 2020).

Ectothermic aquatic organisms, such as *Daphnia,* are particularly sensitive to environmental changes. For example, as temperatures rise, metabolic rate increases resulting in accelerated maturation, somatic growth, population growth, and higher energy demands (Orcutt and Porter 1984; Lampert and Trubetskova 1996; Hietala et al. 1997; Paul et al. 2004; Masclaux et al. 2009). Elevated temperatures can have a detrimental effect on *Daphnia* exposed to sterol-deficient cyanobacteria, such as *Microcystis,* with sterol demands positively correlated with temperature (Sperfeld and Wacker 2009; Przytulska et al. 2015). The common freshwater cyanobacterium, *Microcystis,* can outcompete nutritious algal species and kill some grazers by producing toxic secondary metabolites (i.e., microcystin), mechanically inhibiting grazing by aggregating into colonies or producing large filaments, and depriving grazers of unsaturated fatty acids necessary for growth (Dupuis and Hann 2009). The effect of temperature on *Daphnia* sensitivity to toxic cyanobacteria appears to be dependent on the intensity and duration of thermal stress, *Daphnia* species and local adaptations, and cyanobacterial species, abundance and toxicity (Chislock et al. 2013; Hochmuth and Schamphelaere 2014). For example, Hietala et al. (1997) showed that *Daphnia pulex* fed the nutritious green algae, *Scenedesmus obtusiusculus,* had a higher rate of instantaneous increase (*r*) when cultured at 24°C than 19°C. Yet, when fed

toxic *Microcystis aeruginosa,* the same *Daphnia* had lower *r* when cultured at 24°C than 19°C. Clearly, there are important interactions between temperature and food quality that influence zooplankton-phytoplankton interactions.

However, studies have found the effect of temperature on *Daphnia* life history patterns varies depending on the cyanobacteria in the diet. Claska and Gilbert (1998) showed that higher temperature treatments (12°, 14°, 19° and 25°C) reduced the population growth rate, survivorship and fecundity of *Daphnia pulex* when fed two toxic cyanobacterial species, *Anabaena flos-aquae* and *A. affinis*. This idea was expanded by Hochmuth and Schamphelaere (2014) who tested the effect of temperature (15°, 19°, 23°C) on the reproduction of *Daphnia magna* when fed 6 cyanobacterial species. The authors found that higher culture temperatures further reduced the reproduction of *Daphnia* fed *Anabaena* and *Oscillatoria,* but decreased the harmful effects on reproduction of *Daphnia* fed *Microcystis, Nodularia,* and *Aphanizomenon*. Another study focused on *Daphnia magna* fed high vs. low quality food at different temperatures (12°, 15°, 20°, 25°C) and showed that the negative effect of food quality on somatic growth and reproduction decreased at higher temperatures (Masclaux et al. 2009).

Few studies have explored how combined temperature and cyanobacterial stressors affect multiple genotypes of the same *Daphnia* species. Hietala et al. (1997) found intraspecific variations in the effect of stressors on life-history traits but did not consider the role of adaptations due to previous exposure to cyanobacteria. Recent research has shown that some *Daphnia* clones from eutrophic systems with frequent cyanobacterial blooms can locally adapt to toxic cyanobacteria (i.e., cyanobacteria-tolerant genotypes) and ultimately control toxic cyanobacteria (Hairston et al. 1999; Sarnelle and Wilson 2005; Chislock et al. 2013, 2019b). In contrast, *Daphnia* clones from oligotrophic systems with limited prior exposure to cyanobacteria

(i.e., cyanobacteria-sensitive genotypes) cannot control cyanobacteria *in situ* (Chislock et al. 2013). In this study, we asked whether cyanobacterial tolerance in *Daphnia* comes at a cost through higher sensitivity to thermal stress or relatively slower population growth when cyanobacteria are rare (Chislock et al. 2013).

Daphnia adaptations to tolerate toxic cyanobacteria can have significant effects on ecosystem-evolutionary dynamics (Chislock et al. 2013, 2019a), yet the mechanisms driving these patterns are not well understood. Moreover, it is unclear how temperature stress will affect the ability of *Daphnia* to tolerate cyanobacteria. In this study, we explore how contrasting temperatures (20°C and 28°C) affect the fitness of cyanobacteria-sensitive and -tolerant *Daphnia pulicaria* genotypes directly through thermal stress as well as indirectly by promoting cyanobacterial dominance. Cyanobacteria-tolerant *Daphnia* genotypes are expected to optimize life history traits, such as survival, fecundity, and somatic growth, to maximize fitness differently than cyanobacteria-sensitive *Daphnia* genotypes when fed diets containing greater concentrations of cyanobacteria. To test these hypotheses, empirically generated data were used to create a path diagram to track the mechanisms by which temperature and cyanobacteria affected life history traits (i.e., survivorship, fecundity, and somatic growth) and, ultimately, fitness (i.e., population growth) of cyanobacteria-sensitive and -tolerant *Daphnia pulicaria* genotypes.

Materials and methods

Daphnia pulicaria genotypes were collected as diapausing (ephippial) eggs from the surface sediment of six small glacial lakes in southern Michigan and hatched via light-induced hatching in 2017 (Weider et al., 1997). Three of the lakes are oligotrophic with low

cyanobacterial abundance, while the additional three lakes are eutrophic and are known to experience cyanobacterial blooms (Table A1; Sarnelle and Wilson 2005). Parthenogenetic lines were maintained for each *Daphnia* genotype at room temperature conditions (~24°C) in filtered and autoclaved lake water and fed *Ankistrodesmus falcatus ad libitum* for at least 30 generations to minimize maternal effects. Juvenile survivorship assays were then conducted to confirm the sensitivity of each genotype to toxic cyanobacteria, as described by Sarnelle and Wilson (2005) (Table A1).

Daphnia culture medium was prepared by filtering water from an oligotrophic lake (Lake Martin, Alabama) through a 1.2 µm glass microfiber filter followed by a 0.45 µm cellulose nitrate membrane filter and then sterilized in an autoclave. The nutritious chlorophyte, *Ankistrodesmus falcatus* (unicellular, mean cell dimensions 2.5 µm x 45 µm), and toxic cyanobacterium, *Microcystis aeruginosa* (UTEX 2667, uni- or bicellular, mean cell diameter 4 µm), were maintained in a nutrient-rich medium (modified BG-11, Vanderploeg et al., 2001) as semi-continuous cultures at 25°C with a 8 hr light : 16 hr dark conditions in an incubator. Microcystin content of the diets containing *Microcystis aeruginosa* was determined via enzyme-linked immunosorbent assay (ELISA, An and Carmichael, 1994) after extraction in 75% aqueous, acidified methanol followed by removing the solvent and resuspending the extract in 5 ml of phosphate buffer (Wilson et al. 2008).

Prior to the experiment, neonates from each genotype were placed in individual vials filled with *Daphnia* culture medium and fed *Ankistrodesmus ad libitum* until maturity. Neonates (<24 hrs) from mature females were then pooled by genotype and placed in *Daphnia* culture medium without food for 5 hours to purge their guts. To determine *Daphnia* neonate lengths at the beginning of the experiment (L_{t0}), a random subset from each genotype was placed onto a

water droplet on a slide and measured with a compound light microscope. Two neonates from each tolerant or sensitive genotype (6 neonates total/jar) were added to 500 ml jars of the corresponding diet mixture equivalent to 1 mg carbon per liter (Kilham et al. 1997). Diets were prepared by centrifuging cultures of exponentially growing cells, discarding the supernatant, and then re-suspending the cells in *Daphnia* culture medium. Food concentrations were determined by counting 10 fields of two replicate 0.18 ml subsamples of each culture using a Palmer-Maloney chamber. Diet treatments included a 100% *Ankistrodesmus* (highest quality diet), 75% *Ankistrodesmus* + 25% *Microcystis*, 50% *Ankistrodesmus* + 50% *Microcystis*, and 25% *Ankistrodesmus* + 75% *Microcystis* (lowest quality diet) treatments. A starvation treatment of only *Daphnia* culture medium was included to determine if the effect of toxic cyanobacteria was greater than the effect of starvation. The jars were then sealed and placed in incubators set to either 20°C or 28°C in an 8 hr light: 16 hr dark cycle. Jars were inverted to resuspend algae and randomly reorganized daily to minimize variation in light exposure across jars.

Daphnia survivorship and number of neonates were recorded daily. *Daphnia* were transferred to new jars with fresh diet mixtures every 72 hours for 10 days. After each 72 hr span, the number of females carrying eggs and number of eggs per female was determined and neonates were counted, measured, and discarded. Three *Daphnia* from each jar were placed onto a water droplet on a slide and measured with a compound light microscope to determine length (L_{tx}). *Daphnia* length measurements were used to estimate juvenile somatic growth rate (length, µm/day) based on the formula: $(\ln L_{tx} - \ln L_{t0})/\text{time}$, where L_{t0} and L_{tx} are animal lengths at day 0 and day x, respectively.

Daphnia percent survival was calculated using the formula: $(A_{t10} / A_{t0})*100$, where A_{t0} and A_{t10} are the number of live *Daphnia* females at day 0 and day 10, respectively. The time

needed to kill 50% of the *Daphnia* (LT50) under multiple stressor combinations was calculated using the open-source *ecotox* R package based on probit analysis (Hlina 2019). *Daphnia* fecundity was estimated by calculating the total number of neonates produced per female by dividing the number of neonates produced in each jar by the number of live females and then summing these values for each day across the entire experiment.

The intrinsic rate of population increase (*r*) was calculated for each jar using the Euler equation: $1 = \sum_{x=0}^{10} e^{-rx} l(x)m(x)$, where *r* is the rate of population growth per day, x is the age class (day; 0 to 10), l(x) is the probability of surviving to age x, and m(x) is the number of neonates produced per *Daphnia* per jar on day x. For jars with no reproduction, *r* was determined from changes in *Daphnia* abundance over time based on the formula: $r = [\ln \text{density}_{t+1} - \ln \text{density}_t]/$ time (Allan 1976; Wilson and Hay 2007).

Statistical differences among treatment effects were analyzed using analysis of variance (ANOVA). One-way, two-way, and three-way ANOVAs were calculated to assess the importance of interactions of temperature, diet, and *Daphnia* genotypes. Extra sum of squares *F*-tests were calculated to determine whether models that included interactions were a significant improvement in fit to the data. Differences among treatments were determined via Tukey's HSD post-hoc test. All statistical analyses were performed with the open-source software RStudio version 4.0.2 (RStudio Team 2015). A path model was used to determine how sensitive and tolerant *Daphnia* genotypes differed in how they allocated resources across three life history traits (i.e., percent survival, fecundity, and somatic growth) to maximize fitness (i.e., population growth). The path model includes causal arrows from the two experimental treatments to the three life history traits that mediate population growth. The indirect effect of the treatments on fitness through each intermediate life history trait was determined by calculating the product of

path coefficients from a treatment through an intermediate life history trait to fitness. The total effect of each experimental variable was determined by adding the direct and indirect effects of the variable on fitness. A structural equation model (SEM) was generated using the *sem* R package (Fox et al. 2017) to test the causal structure of the path model. Diets were ranked for the model from most nutritious to least nutritious (100% *Ankistrodesmus* and 0% *Microcystis* = 0, 75% *Ankistrodesmus* and 25% *Microcystis* = 25, 50% *Ankistrodesmus* and 50% *Microcystis* =50, 25% *Ankistrodesmus* and 75% *Microcystis* = 75). To evaluate the fit of the data for the models, Goodness of Fit Tests were conducted and showed that the models are a good fit to the data (sensitive $p = 0.27$ and tolerant $p = 0.44$). The two treatments and three intermediate life history traits included in the path models explained 91.4% and 93.5% of the observed patterns in population growth of sensitive and tolerant *Daphnia* genotypes, respectively. The AIC of the sensitive (41.2) and tolerant (40.6) models were relatively high, but all parameters had to be included in the model to understand the effect of all measured parameters on population growth.

Results

The combined effects of toxic cyanobacteria and elevated temperature on cyanobacteria-tolerant and cyanobacteria-sensitive *Daphnia* genotypes were measured as *Daphnia* survival (percent survival and LT50), juvenile somatic growth rate, fecundity (total number of neonates produced per *Daphnia* female), and population growth (intrinsic rate of population increase (r)). Both cyanobacteria-sensitive and -tolerant *Daphnia* had significantly lower ($p < 0.05$) population growth when fed diets containing no food (starvation) or ≥50% *Microcystis* compared to the high quality 100% *Ankistrodesmus* diet at 28°C (Figure 1.1). Sensitive genotypes had significantly lower ($p < 0.05$) population growth when starved or fed any diet containing *Microcystis* relative

to 100% *Ankistrodesmus* at 28°C, which suggests cyanobacteria, even at low concentrations, had a detrimental impact on the population growth of sensitive genotypes at elevated temperatures. Tolerant *Daphnia* genotypes had similar growth rates ($p > 0.05$) when exposed to 25% *Microcystis* and 100% *Ankistrodesmus* diets under both temperature treatments, which suggests tolerant genotypes can tolerate low cyanobacterial densities even under elevated temperature conditions. Cyanobacteria-sensitive genotypes exhibited significantly higher population growth at 28°C than 20°C ($p < 0.0001$) when fed 100% *Ankistrodesmus* diets. Elevated temperatures also accelerated the population growth of tolerant *Daphnia* genotypes fed 100% *Ankistrodesmus* and 25% *Microcystis*, though these effects were not significant ($p > 0.05$). There was a significant interaction between temperature and diet as well as *Daphnia* genotype and diet, which suggests the effect of diet on population growth was dependent on both temperature and *Daphnia* genotype ($p \leq 0.0003$, Table 1.1).

The effect of temperature on the survival of both genotypes was dependent on diet (Table B1). Both genotypes had higher LT50 when fed 100% *Ankistrodesmus* under elevated temperatures (28°C), but LT50 decreased as cyanobacterial density increased (Figure B1). The effect of diet on survival was weaker at 20°C, and tolerant genotypes had lower LT50 when fed 100% *Ankistrodesmus* than diets containing cyanobacteria or starved diets. There was a significant effect of cyanobacteria on survival, and it appears the effect of temperature on *Daphnia* survival is dependent on the presence of cyanobacteria, based on the significant interaction between these two variables ($p = 0.01$, Table B1).

The juvenile somatic growth rate of both sensitive and tolerant genotypes decreased as cyanobacterial abundance in diets increased under both temperature conditions (Figure C1). Tolerant *Daphnia* neonates grew significantly faster than sensitive genotypes when fed 25%

Microcystis at 28°C (p <0.001). There was a significant interaction between temperature and diet as well as *Daphnia* genotype and diet, which suggests the effect of diet on somatic growth was dependent on temperature and local adaptations to cyanobacteria ($p \leq 0.05$, Table C1). There are no data for the somatic growth of sensitive *Daphnia* genotype females fed 50% and 75% *Microcystis* at 28°C because all adult females died prior to day 7.

Fecundity was the main driver of population growth of both genotypes. Both *Daphnia* genotypes had higher fecundity at 28°C than 20°C when fed 100% *Ankistrodesmus* and 25% *Microcystis* diets, though these patterns were not statistically significant (p >0.05, Figure D1). Neither sensitive nor tolerant *Daphnia* genotypes reproduced under starvation treatments. Tolerant *Daphnia* genotypes cultured at 20°C were unique in their ability to produce offspring when fed high cyanobacteria diets (50-75% *Microcystis*). Tolerant *Daphnia* genotypes also produced more offspring than sensitive genotypes (p <0.0001) when fed 25% *Microcystis* diets at 28°C. There was a significant interaction between temperature and diet as well as *Daphnia* genotype and diet, which suggests that the effect of diet on fecundity was dependent on temperature and *Daphnia* genotype ($p \leq 0.002$, Table D1).

Local adaptations allow organisms to allocate resources among life history traits to maximize fitness. A path diagram was generated to better understand how local adaptations of *Daphnia pulicaria* to toxic cyanobacteria affected their allocation of resources to somatic growth, reproduction, and survival to maximize population growth when exposed to various temperatures and cyanobacterial diets. The path diagram suggests that a reduction in fecundity due to exposure to cyanobacteria was the main determinant of population growth of both cyanobacteria-sensitive and -tolerant genotypes (Figure 1.2). Interestingly, temperature had a significant effect on the survivorship (0.55, p = 0.003) of cyanobacteria-sensitive *Daphnia*

genotypes but did not significantly affect the intermediate life history traits of tolerant genotypes (Table 1.2). The significant direct effects of temperature (0.19, $p = 0.003$) on tolerant *Daphnia* population growth suggests these treatments affected population growth through a life history trait or behavioral modification not measured in this study. Although cyanobacterial diets significantly affected the somatic growth rate of cyanobacteria-sensitive (-0.43, $p = 0.03$) and -tolerant genotypes (-0.68, $p < 0.0001$), there was no direct effect of somatic growth on the population growth rate of either genotype. This suggests that although cyanobacterial diets decrease the somatic growth rate of *Daphnia*, it did not cause a significant decrease in overall fitness.

Discussion

Daphnia pulicaria genotypes collected from eutrophic lakes are known to locally adapt to tolerate, and potentially control, toxic cyanobacteria that are common in these systems (Chislock et al. 2013, 2019b). Cyanobacteria-tolerant *Daphnia* genotypes maintained positive population growth and fecundity when exposed to low concentrations of toxic cyanobacteria (25% *Microcystis*) under both temperature conditions (20° and 28°C), whereas cyanobacteria-sensitive *Daphnia* genotypes were negatively affected regardless of cyanobacterial concentration in the diet (25-75% *Microcystis*) or temperature treatment. In fact, tolerant genotypes performed as well or better than sensitive *Daphnia* genotypes under the various temperature and diet combinations for all life history traits recorded. These results suggest tolerance to cyanobacteria did not come at a cost of lower fitness when *Daphnia* were exposed to elevated temperatures. Cyanobacterial blooms are well documented climate change co-stressors, therefore cyanobacterial and thermal tolerance are likely coupled due to simultaneous exposure in nature

(Griffith and Gobler 2020). However, trade-offs have been recorded by others. For example, Schaffner et al. (2019) documented the change in *Daphnia mendotae* clonal diversity throughout a growing season, culminating in a summer cyanobacterial bloom, and found a drastic decrease in clonal diversity as cyanobacteria increased in dominance. The authors then isolated cyanobacteria-sensitive and -tolerant *D. mendotae* clones and found tolerant clones had lower juvenile growth rate than sensitive clones when fed spring diets (i.e., mixture of diatoms, cryptophytes and chlorophytes) when compared to summer diets (i.e., mixture of cyanobacteria and chlorophytes), which suggests there was an unidentified cost of cyanobacterial tolerance. Although results from the present study suggest that local adaptations to toxic cyanobacteria do not lead to a decrease in fitness when exposed to elevated temperatures (i.e., energetic trade-off), findings by Schaffner et al. (2019) suggest cyanobacterial tolerance may decrease *Daphnia* fitness when exposed to other environmental parameters not considered in this study.

Although *Daphnia* tolerance to toxic cyanobacteria has been well-documented through space and time (Hairston et al. 1999; Sarnelle and Wilson 2005), how adaptations allow *Daphnia* to prioritize life history traits to maximize fitness is not well understood. A path analysis was generated to quantify how cyanobacteria-sensitive and -tolerant *Daphnia* genotypes allocate finite resources between life history traits to maximize fitness. Path analysis results show toxic cyanobacteria had a stronger effect than temperature on the fitness of both *Daphnia* genotype groups, mainly by decreasing fecundity (Table 1.2). Toxic cyanobacterial abundance was also the main driver of survivorship, fecundity, and somatic growth of both sensitive and tolerant *Daphnia*, except for survivorship of sensitive *Daphnia* which was controlled by temperature (Figure 1.2). Fecundity was the life history trait most sensitive to exposure to toxic

cyanobacteria, likely because the sterol content of cyanobacteria does not meet the high energetic demands of reproduction.

While cyanobacteria had a clear negative impact on *Daphnia* fitness, the effect of temperature was dependent on diet. In fact, elevated temperatures (28°C) either significantly increased or had no significant effect on the life history traits, and ultimately fitness, of cyanobacteria-sensitive and -tolerant *Daphnia* fed the nutritious green algae, *Ankistrodesmus falcatus.* Temperature increases the metabolic rate of ectothermic organisms, such as *Daphnia*, which accelerates somatic growth, maturation times and increases fecundity as long as sufficient nutritious food is available and temperatures do not exceed the thermal optimum of an organism (Orcutt and Porter 1984; Korpelainen 1986; Hietala et al. 1997). However, elevated temperatures further decreased the population growth of *Daphnia* genotypes fed diets that included the sterol-deficient and toxic cyanobacteria, *Microcystis aeruginosa*, though these differences were not statistically significant (Figure 1.1). Minimal effects of temperature on *Daphnia* physiology may indicate that the 28°C treatment was not sufficient to induce thermal stress. Interactive effects between temperature and diet have been recorded in other *Daphnia* studies (Hietala et al. 1997; Hochmuth and Schamphelaere 2014), as well as other ectothermic organisms, such as copepods (Malzahn et al. 2016), fish (Vagner et al. 2015), mollusks (Wacker and von Elert 2003) and insects (Clissold and Simpson 2015).

Juvenile somatic growth rate is frequently used as a predictor of population growth (*r*) of *Daphnia* fed high quality diets (Lampert and Trubetskova 1996). While somatic growth was significantly affected by cyanobacteria for both *Daphnia* genotypes, it did not significantly affect population growth rate (Figure 1.2). Somatic growth rate was significantly correlated with the fecundity and survival of tolerant genotypes, but not overall fitness. Fecundity is directly

correlated to body size of *Daphnia* (Lampert 1993), which suggests the fecundity of tolerant *Daphnia* was controlled by somatic growth rate. Fecundity and somatic growth were not closely related in sensitive genotypes, likely due to low reproduction (Figure D1). The negligible direct effect of somatic growth on *r* suggest somatic growth rate may not be a reliable predictor of population growth rate when *Daphnia* are exposed to multiple stressors, including cyanobacteria in their diet. Lampert and Trubetskova (1996) found that juvenile growth rates were a reliable index of fitness, as long as *Daphnia* had sufficient quantities of high-quality food. When *Daphnia* were exposed to temperature stress, or when comparing *Daphnia* of different strains and adaptations, somatic growth was less of a reliable estimate of fitness.

Conclusions

Climate change is expected to negatively affect aquatic environments directly through changes in temperature and precipitation patterns, as well as indirectly by promoting the growth of sterol-deficient and toxic cyanobacteria (O'Neil et al. 2012). This study shows that under the culture conditions tested, *Daphnia pulicaria* adaptations to toxic cyanobacteria lead to higher population growth rate in the presence of toxic cyanobacteria as well as elevated temperatures. Future studies should consider climate change stressors across multiple trophic levels by taking into account effects on predator feeding rates (Beisner et al. 1996), chemical signaling (Larsson and Dodson 1993), and susceptibility to parasites (Manzi et al. 2020). Additionally, exploring additional indirect effect of elevated temperature on *Daphnia* fitness, such as hypolimnetic oxygen depletion, as well as additional stressors associated with climate change, such as acidification, will be important for understanding the value of adaptive traits.

Table 1.1. Analysis of variance results for population growth (r, day^{-1}) over 10 days of cyanobacteria-sensitive and cyanobacteria-tolerant *Daphnia pulicaria* genotypes exposed to two temperatures (20°C and 28°C) and five diet treatments (*Ankistrodesmus* only (0% *Microcystis*), 75% *Ankistrodesmus* and 25% *Microcystis* (25% *Microcystis*), 50% *Ankistrodesmus* and 50% *Microcystis* (50% *Microcystis*), and 25% *Ankistrodesmus* and 75% *Microcystis* (75% *Microcystis*), and a starvation treatment (starved)). Extra sum of squares *F*-test results determine whether two- and three-way ANOVAs are a significant improvement in fit to the data compared to one-way ANOVA. df = degrees of freedom; MS= means square error.

Test	**Source**	**df**	**MS**	**F-ratio**	***p*-value**
One-way ANOVA	Temperature	1	0.0014	0.18	0.67
	Genotype	1	0.1511	20.36	<0.0001
	Cyanobacteria	4	0.2081	28.04	<0.0001
	Error	73	0.0074		
Two-way ANOVA	Temperature	1	0.0014	0.35	0.55
	Genotype	1	0.1511	39.31	<0.0001
	Cyanobacteria	4	0.2081	54.14	<0.0001
	Temperature x Genotype	1	0.0005	0.13	0.72
	Temperature x Cyanobacteria	4	0.0502	13.07	<0.0001
	Cyanobacteria x Genotype	4	0.0236	6.14	0.0003
	Error	64	0.0038		
				F-Test *p*-value:	<0.0001
Three-way ANOVA	Temperature	1	0.0014	0.36	0.55
	Genotype	1	0.1511	40.93	<0.0001
	Cyanobacteria	4	0.2081	56.37	<0.0001
	Temperature x Genotype	1	0.0005	0.13	0.72
	Temperature x Cyanobacteria	4	0.0502	13.61	<0.0001
	Cyanobacteria x Genotype	4	0.0236	6.39	0.0002
	Genotype x Temperature x Cyanobacteria	4	0.0061	1.66	0.17
	Error	60	0.0037		
				F-Test test *p*-value:	0.17

Table 1.2. Effect of temperature and cyanobacterial diets on the population growth (*r*) of cyanobacteria-sensitive and cyanobacteria-dominant *Daphnia pulicaria* genotypes. Path coefficients are listed for the direct effects of each causal variable. Indirect effects are the products of the direct effect of the two treatments and the path coefficients for the intermediate life history trait variables, including percent survival, fecundity and somatic growth. Total effects are the sum of direct and indirect effects.

Causal variable	Direct effect	Indirect effect via survivorship	Indirect effect via fecundity	Indirect effect via somatic growth	Total effect
Sensitive genotypes					
Temperature	0.12	0.03	0.23	0.01	0.39
Cyanobacteria	0.02	-0.02	-0.61	-0.01	-0.62
Survivorship	0.05				0.05
Fecundity	**0.89**				**0.89**
Somatic Growth	0.02				0.02
Tolerant genotypes					
Temperature	**0.19**	0.11	-0.01	0.01	0.30
Cyanobacteria	0.09	-0.05	-0.57	-0.10	-0.63
Survivorship	**0.39**				0.41
Fecundity	**0.70**				0.83
Somatic Growth	0.14				0.09

Bolded values: *p*-value <0.05

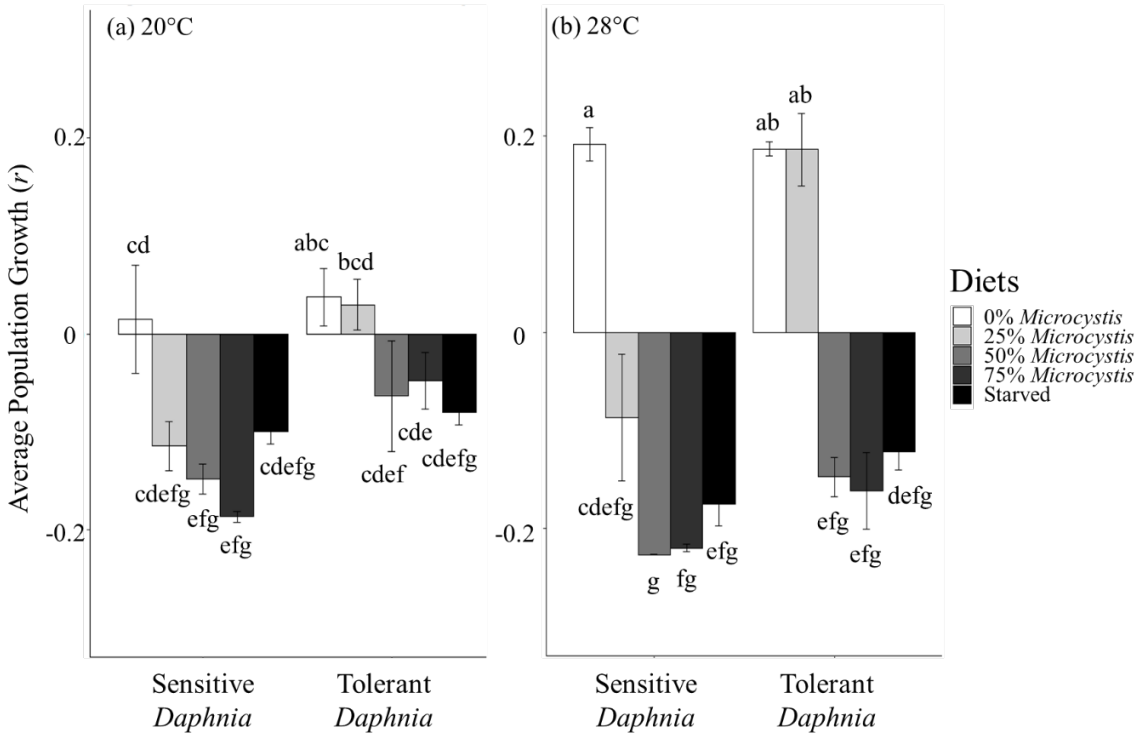

Figure 1.1. Average population growth rates (r, day^{-1}) of cyanobacteria-sensitive and cyanobacteria-tolerant *Daphnia pulicaria* genotypes cultured over 10 days at (a) 20°C and (b) 28°C. Diet treatments include *Ankistrodesmus* only (0% *Microcystis*), 75% *Ankistrodesmus* and 25% *Microcystis* (25% *Microcystis*), 50% *Ankistrodesmus* and 50% *Microcystis* (50% *Microcystis*), 25% *Ankistrodesmus* and 75% *Microcystis* (75% *Microcystis*), and a starvation treatment (starved). Unique letters represent statistically different observations (p <0.05) across both genotypes and temperature treatments. Error bars= ± SE. Sample size per treatment = 4.

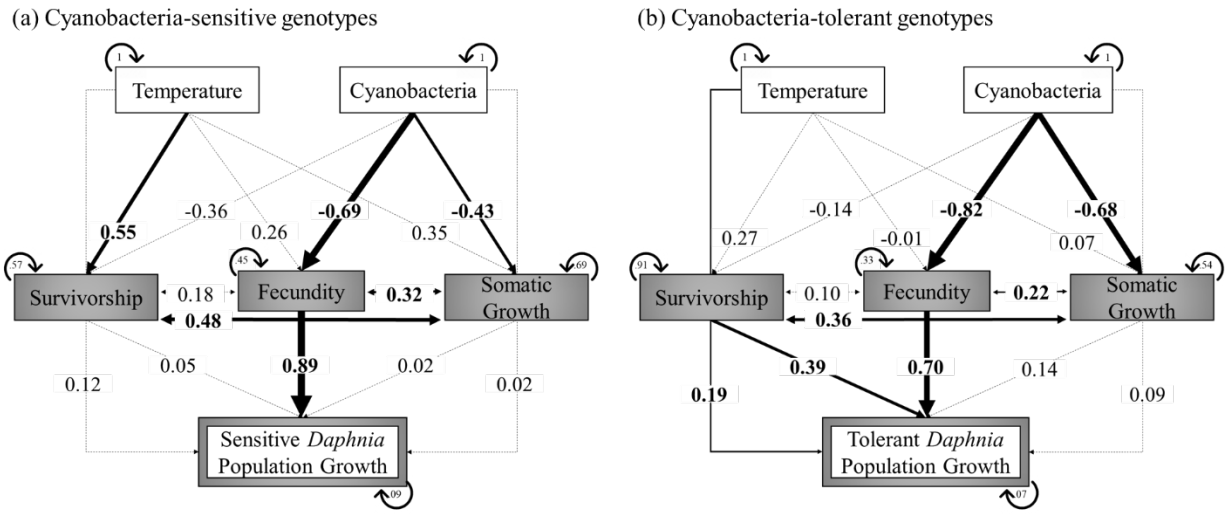

Figure 1.2. Path model of direct and indirect effects of temperature and cyanobacteria on the population growth (*r*) of (a) cyanobacteria-sensitive and (b) cyanobacteria-tolerant *Daphnia pulicaria* genotypes. Solid arrows represent significant paths (p <0.05), and the arrow thickness represents effect strength. Double-sided arrows represent correlations between the three intermediate life history traits: survivorship, fecundity, and somatic growth. Looped arrows represent the variance terms of each variable.

Chapter 2

Commercially available unoccupied aerial systems for monitoring harmful algal blooms: a comparative study

Abstract

Reliable remote sensing platforms and methods for monitoring phytoplankton are needed for mitigating the detrimental impacts of cyanobacterial harmful algal blooms (CyanoHABs) on small inland waterbodies. Commercial unoccupied aerial systems (UAS) present an affordable high-resolution solution for rapid assessment of cyanobacterial abundance in small (<30 m) aquatic systems by recording the reflectance of photosynthetic pigments found in all phytoplankton (i.e., chlorophyll-*a*) and those unique to cyanobacteria (i.e., phycocyanin). This study evaluates the performance of four sensors, including visible light spectra (RGB) sensors on the Phantom 4 and Phantom 4 Professional platforms, the MAPIR Survey3W modified multispectral (near-infrared, green, blue) sensor, and the Parrott Sequoia multispectral (green, red, near-infrared, red-edge) sensor for estimating cyanobacterial abundance. Each sensor's performance was determined by comparing 26 vegetation indices to chlorophyll-*a* and phycocyanin measurements of 54 ponds that varied in productivity. Vegetation indices that included the red and near-infrared wavelengths generated from Parrot Sequoia aerial images provided the best chlorophyll-*a* (i.e., NDVI, $r^2 = 0.78$, $p < 0.0001$) and phycocyanin (i.e., EVI2, $r^2 = 0.57$, $p < 0.0001$) estimates. The RGB sensors were moderately effective for estimating chlorophyll-*a*, whereas the MAPIR Survey3W generated poor estimates of both pigments due to differences in recorded wavelengths.

Introduction

Harmful algal blooms dominated by cyanobacteria (CyanoHABs) threaten freshwater ecosystems worldwide (Huisman et al. 2018). Cyanobacteria are photosynthetic prokaryotes able to outcompete other phytoplankton species, such as green algae and diatoms, when surface water temperatures exceed 25°C and anthropogenic eutrophication increases nutrient availability (i.e., nitrogen and phosphorus, Downing et al. 2001; O'Neil et al. 2012). Cyanobacteria impair freshwater systems through the production of toxins (i.e., cyanotoxins) linked to illness and fatality in livestock, pets, and humans (Merel et al. 2013). Some cyanobacteria can also produce off-flavor compounds (i.e., geosmin and 2-methylisoborneol) that impart a musty scent and flavor on drinking water and farm-raised fish, leading to significant economic losses to aquaculture and drinking water industries (Tucker and Schrader 2020). CyanoHABs are traditionally monitored via cell counts or by measuring the concentration of photosynthetic pigments found in all phytoplankton (i.e., chlorophyll-*a*) relative to accessory pigments unique to cyanobacteria (i.e., phycocyanin). Reliable tools that can rapidly and accurately quantify the abundance of ecologically important phytoplankton (i.e., green algae and diatoms) relative to toxin-producing cyanobacteria in drinking water sources, aquaculture farms, and recreational water bodies are necessary for implementing monitoring, response, and forecasting tools for mitigating the ecologic, economic and health impacts of CyanoHABs.

Bloom-forming cyanobacterial taxa often accumulate near the surface, forming patchy surface scums that can amass downwind or mix throughout the water column due to wind and wave action (Walsby et al. 1997). Traditional water sampling is often not sufficient for the quantitative monitoring of spatially and temporally heterogeneous CyanoHABs (Kutser 2004). *In situ* water sampling programs typically collect samples from a limited number of fixed locations and depths

and rarely consider the effect of wind on the horizontal and vertical distribution of cyanobacteria. Moreover, collecting representative surface samples from research vessels can be challenging as vessels often disrupt algal assemblages leading to inaccurate estimates (Kutser 2004). The turn-around time and cost of traditional laboratory methods, such as microscopic cell counts and pigment measurement techniques (i.e., fluorescence or high-performance liquid chromatography), can also restrict the application of *in situ* sampling for monitoring and predicting CyanoHABs (Merel et al. 2013). Satellite remote sensing platforms can surpass many of these challenges, as satellites can regularly monitor large spatial ranges for prolonged periods.

Satellite data have been useful for recording long-term and seasonal bloom dynamics and understanding how external factors, such as surface water temperature, meteorological events, and anthropogenic nutrient loading drive CyanoHAB occurrence (Wynne et al. 2010; Shi et al. 2017). Several satellites generate reliable data for monitoring the spatial and temporal distribution of algal blooms, including satellites from the Landsat series, Moderate Resolution Imaging Spectroradiometer (MODIS) Aqua and Terra, MEdium Resolution Imaging Spectrometer (MERIS), Sentinel 2-A/B, and Hyperion (Brivio et al. 2001; Kutser 2004; Kutser et al. 2006; Yacobi et al. 2011; Shi et al. 2017; Drozd et al. 2020). Yet, low spatial and temporal resolution, atmospheric correction challenges, cloud cover, slow image turn-around times, and cost of some satellite products can limit the application of satellite remote sensors for monitoring CyanoHABs in small inland systems (Lomax et al. 2005). For example, MERIS is a multispectral sensor used to detect and measure cyanobacteria when present at high densities (Kutser et al. 2006; Wynne et al. 2010). However, the spatial resolution of 300 m and revisit times of two days limit its application for smaller waterbodies. The hyperspectral imager in space, Hyperion, collects data from 196 spectral bands in the 400-2500 nm region. Although Hyperion data have been useful for

monitoring water quality parameters, such as chlorophyll-*a* and chromophoric dissolved organic matter (Brando and Dekker 2003), its 30 m spatial resolution is not sufficient for studying inland CyanoHABs, particularly in the presence of patchy surface scum (Kutser 2004). Therefore, satellite data are not reliable for monitoring small inland systems (<30 m) such as ponds, lakes, and rivers, especially if cyanobacteria are present.

Unoccupied aerial systems (UASs), remotely-piloted remote sensing platforms (i.e., drones), show great potential for bridging the gap between *in situ* water sampling and satellite remote sensing. UASs collect high-resolution aerial data with minimal atmospheric disturbance from cloud coverage, allow flexible flight planning with rapid turn-around times, and are available in a variety of wavelength combinations (Kislik et al. 2018). Commercially available UAS sensors are classified as visible wavelength (RGB), modified or multiband multispectral, thermal, or hyperspectral. Multispectral sensors record wavelengths that fall within and outside the visible light spectrum (i.e., RGB and near-infrared, respectively) and are classified as multiband or modified. Multiband multispectral sensors collect data for 4-6 bands, and each band typically has a dedicated sensor. While more expensive, multiband sensors generate high-resolution results, and many are designed to measure the photosynthetic activity of terrestrial crops. For example, the Parrot Sequoia multiband multispectral sensor records green, red, red-edge, and near-infrared bands, which can be used to calculate the Normalized Difference Vegetation Index (NDVI) and is marketed for measuring crop health. Sensors that measure the red-edge (735 nm) region of high reflectance between the red and near-infrared wavelengths can be as effective at estimating the chlorophyll concentration of crops as hyperspectral sensors (Lu et al. 2019). However, the value of the red-edge wavelength for monitoring CyanoHABs can be dependent on the trophic status of the waterbody (Cillero Castro et al. 2020). Modified multispectral sensors are a low-cost

alternative to multiband multispectral sensors. One such example is the MAPIR Survey3W near-infrared, green, blue (NGB), which is an RGB sensor with a filter that sacrifices the red wavelength to record the near-infrared wavelength. Although modified multispectral sensors typically have lower resolutions than multiband multispectral sensors, they have been used to estimate cyanobacterial buoyant packed cell volume (Van der Merwe and Price 2015). Lastly, many UASs, such as the DJI Phantom series, are equipped with an integrated RGB sensor that provides a cost-effective alternative to multispectral sensors. RGB sensors can detect algal cover and biomass in coastal systems (Xu et al. 2018; Cheng et al. 2020), but further research is needed before these sensors can reliably estimate cyanobacterial abundance.

Monitoring CyanoHABs with UAS has been hindered by the lack of standardized methods for aerial image collection, validation techniques, and universal algorithms for processing UAS data (Kislik et al. 2018). Additionally, there is no consensus on which sensor type or vegetation index works best for estimating chlorophyll-*a*, and few have been used to estimate phycocyanin concentration. Chlorophyll-*a*, present in all phytoplankton, including green algae and cyanobacteria, absorbs red and blue wavelengths at approximately 430 and 662 nm, respectively, and reflects green and near-infrared wavelengths at approximately 500 and 700-1300 nm, respectively (Figure 2.1). Cyanobacterial accessory pigments such as phycocyanin (absorbance at 620 nm) allow cyanobacteria to absorb light at a broader spectrum and protects them from solar radiation (Oliver et al. 2012). The absorbance and reflection characteristics of chlorophyll-*a* and phycocyanin can be magnified by calculating band ratio algorithms (i.e., vegetation indices) that emphasize the spectral characteristics of photosynthetic pigments, water, and soil leading to better estimates than single band measurements (Xue and Su 2017). The goal of this study is to determine whether commercially available UAS sensors are adequate for estimating algal and cyanobacterial

abundance in small (<30 m) eutrophic waterbodies. To determine which sensor and vegetation index combination is best for monitoring chlorophyll-*a* and phycocyanin, aerial images collected by four sensors that vary in measured wavelengths, bandwidths, resolution, and price were used to calculate 26 vegetation indices. The four sensors chosen are commonly used for agricultural research and include two visible RGB sensors (DJI Phantom 4 and Phantom 4 Pro), one modified multispectral sensor (MAPIR Survey3W), and a multiband multispectral sensor (Parrot Sequoia). Vegetation index values were compared to *in situ* chlorophyll-*a* and phycocyanin measurements, to determine which sensor and vegetation index combination should be considered for monitoring CyanoHABs in small aquatic systems.

Materials and methods

Study area and field survey methods

Aerial images were collected over several research, aquaculture, and recreational ponds from September 2019 to July 2020 (Table 2.1). UAS flights 1, 2 and 3 were collected at a commercial aquaculture facility in Alabama, USA (32.396, -87.367; Figure 2.2). Flight 1 surveyed 7 ponds, flight 2 surveyed 8 ponds, and flight 3 surveyed 5 ponds. UAS flights 4, 5, 6, and 7 were conducted at the E.W. Shell Fisheries Center of Auburn University in Auburn, Alabama, USA (32.662, -85.496), which is a 1,600-acre research facility equipped with over 300 man-made experimental aquaculture ponds ranging in size, depth, and productivity (Figure 2.3). Flight 4 surveyed 5 ponds, flight 5 surveyed 16 ponds, flight 6 surveyed 1 pond, and flight 7 surveyed 19 ponds. Research and commercial aquaculture ponds frequently experience high cyanobacterial abundance due to long residence times and high nutrient inputs in the form of fish feed. Flights 8, 9 and 10 were conducted over the man-made aesthetic pond at the Jule Collins Smith Museum of Fine Art at

Auburn University (32.588, -85.484), which frequently experiences dense cyanobacterial blooms (Figure 2.4).

Aerial images were collected on clear days when the solar altitude was less than 43˚ to avoid sun glint effects (Ortega-Terol et al. 2017). Flights were fully automated based on specified flight plans on the free mobile device application Pix4Dcapture (Pix4D SA, Lausanne, Switzerland). Details for each flight are found in Table 2.1. Ground control targets were positioned around the survey area prior to flights as horizontal ground control points (GCP). Geographic coordinates were collected for each GCP target and water sample collection site using a Trimble Geo7x Handheld GNSS System (Trimble Inc., California, USA). Geographical point data was then post-processed with the Global Navigation Satellite System (GNSS) post-processing program Trimble GPS Pathfinder Office (Trimble Inc., California, USA) to improve geospatial accuracy during aerial image processing.

UAS description

Due to the weight of the modified and multiband multispectral sensors, two separate UAVs were used (Table 2.2). Flights were conducted immediately one after the other to minimize sun angle variation between flights.

The Survey3W NGB modified 3-band multispectral sensor (MAPIR, Inc., California, USA) was mounted on a DJI Phantom 4 quadcopter (SZ DJI Technology Co., Shenzhen, China). The Survey3W NGB is a Sony Exmor R IMX117 12MP (Bayer RGB) camera that sacrifices the red band to measure the near-infrared wavelength (Figure 2.5). The Survey3W was programmed to capture aerial images at a 0.5 second interval at a 90˚ angle and collect both RAW data (GPS location, 12bit per channel) and JPEG images (8bit per channel). The Survey3W was equipped with a Survey3 Advanced GPS Receiver (20.6 g) that generates a geolocation stamp for each JPEG

image captured. The Survey3W was mounted on the Phantom 4 quadcopter using a plastic tilting camera mount in a way that did not obstruct the Phantom 4's RGB camera. Visual light spectrum reflectance data were collected with the Phantom 4's integrated visual spectrum 12.4M RGB camera (Figure 2.5). The Phantom 4 was equipped with a GPS/GLONASS integrated system that GPS tags the images with latitude, longitude, and altitude information (Table 2.2).

The Parrot Sequoia 4.0 multiband multispectral sensor was mounted on a DJI Phantom 4 Pro quadcopter (SZ DJI Technology Co., Shenzhen, China). The Parrot Sequoia multispectral sensor is equipped with green, red, red-edge and near-infrared sensors, an RGB sensor and an integrated GPS and light sensor (Figure 2.5). Images were captured at a 1.5 second interval at a 90˚ angle. The Parrot Sequoia was mounted on the Phantom 4 Pro using a plastic mount that did not block the field of view of the UAV's integrated RGB camera. Visual light spectrum images were collected at a 90˚ angle with the Phantom 4 Pro's integrated 20M RGB camera, and latitude, longitude, and altitude information were collected with the UAV's GPS/GLONASS (Table 2.2).

Image processing

Prior to photogrammetric processing, Survey3W NGB JPEG images were combined with GPS-tagged RAW images using the MAPIR Camera Control software to create a TIFF file with all metadata included (MAPIR CAMERA 2020). Georeferenced Survey3W NGB images were then calibrated based on images of the MAPIR Calibration Target V2 collected immediately before UAS flights.

The Pix4Dmapper software (Pix4D SA, Lausanne, Switzerland) was utilized for photogrammetric processing of the images from each sensor. A camera profile had to be added to Pix4Dmapper based on manufacturer specifications for the Survey3W NGB sensor. The Survey3W NGB, Phantom 4 RGB, and Phantom 4 Pro RGB cameras capture images by scanning

the scene rapidly (i.e., rolling shutter), which often causes aerial image distortion or warping. To correct for rolling shutter effects, the rolling shutter correction setting was enabled for these sensors on the Pix4Dmapper software. The Parrot Sequoia multispectral sensor employs a global shutter, which captures the entire frame simultaneously, therefore the rolling shutter correction was not necessary. GCP GPS data collected prior to flights were used to georeference images to improve spatial accuracy. Reflectance values for the Parrot Sequoia multispectral sensor were radiometrically calibrated based on images of the Parrot Sequoia radiometric calibration target collected immediately before UAS flights. Point cloud densification, digital surface models (DSM), orthomosaics, and reflection map generation for all the sensors were processed on Pix4Dmapper and exported to ArcGIS Pro for spectral calculations. GPS data collected at the time of water sample collection was used to determine the sampling point on the aerial image (seen as black dots on Figures 2.2-2.5), and vegetation index values was collected for that area for correlation analysis (see *Data analysis* section for details).

Post-processing was successful for most UAS flights, with the exception of flights 2 and 3. During these flights, incoming storms generated wind gusts that destabilized the aircraft causing it to tilt and shift from the pre-specified flight plan leading to image tie point generation failure in some areas and causing gaps in the final orthomosaic (Figure 2.2).

Vegetation indices

The 26 vegetation indices (i.e., band ratio algorithms) calculated in this study are specified in Table 2.3. Vegetation index calculations were performed on ArcGIS Pro using the Raster Calculator Tool.

Water sample collection and analysis

Water samples were collected using a rigid tube sampler. Integrated sample collection depth was based on transparency measured as Secchi depth (cm) using a Secchi disk. Multiple water samples were collected and processed from several areas within larger ponds to account for spatial heterogeneity due to wind and aquaculture aerators pushing buoyant cyanobacteria to a localized section of the pond. Physical water parameters, such as temperature, conductivity and pH, were recorded using a handheld YSI ProDSS handheld multiparameter water quality meter (Xylem Inc., Ohio, USA). A known volume of well-mixed samples was filtered through Pall A/E filters and stored frozen in the dark for later algal pigment extraction. Chlorophyll-*a* samples were measured to estimate algal abundance using a Turner Designs Trilogy fluorometer with non-acidification chlorophyll module after a 24 hour extraction in 90% aqueous ethanol in the dark at 4˚C (Sartory and Grobbelaar 1984). Phycocyanin concentrations were measured to estimate cyanobacterial abundance using a Turner Designs Trilogy fluorometer with an orange module after grinding, extracting each filter in a 50 mM phosphate buffer in darkness for 4 hours, centrifuging, and filtering (<0.2 µm) each sample (Kasinak et al. 2015).

Data analysis

Chlorophyll-*a* and phycocyanin data were log-transformed prior to statistical analysis to normalize the data. Pearson correlations where then calculated between the two pigments (chlorophyll-*a* and phycocyanin) and the vegetation index values generated from each sensor using the *stats* package in the open source statistical software RStudio (RStudio Inc., MA, USA).

Results and Discussion

UASs provide a low-cost, high spatial and temporal resolution alternative for monitoring CyanoHABs in waterbodies too small to monitor via satellite remote sensing (<30 m). The ability

of four sensors that vary in measured wavelengths, resolution, and price for estimating phytoplankton abundance was determined by calculating 26 vegetation indices and comparing them to *in situ* chlorophyll-*a* and phycocyanin concentrations. The four sensors varied greatly in their ability to estimate algal and cyanobacterial abundance.

Seventy water samples were collected from 54 ponds that varied widely in their appearance, with some clear ponds and others containing suspended sediments, suspended algae, and thick cyanobacterial scum. The inclusion of clear and high sediment ponds was essential to ensure the sensors and vegetation indices were effective in a variety of systems, not just productive ponds. All ponds had sediment substrates with limited benthic macrophyte cover, therefore noise caused by macrophyte chlorophyll-*a* was not considered in this study. Primary productivity varied among the ponds sampled. Chlorophyll-*a* concentrations ranged from 3 to 3,090 µg/L (average 293.49 µg/L) and phycocyanin concentrations ranged from 0 to 17,210 µg/L (average 943.5 µg/L). High chlorophyll-*a* and phycocyanin concentrations are common in eutrophic and hypereutrophic systems, and some samples included a thick *Microcystis* sp. scum that was very dense, resulting in the extremely high pigment concentrations measured. Large ponds, such as the aesthetic pond sampled in flights 8-10 (Figure 2.4), that contained surface scum were sampled from areas with and without scum to account for spatial variation within the pond. Samples from the same pond were treated individually, therefore each sample represented a unique vegetation index value within the dataset. Water samples were collected based on water transparency (measured as Secchi depth) to ensure the chlorophyll-*a* and phycocyanin samples represented the water column layer visible from aerial images.

The four sensors and vegetation indices varied greatly in their ability to estimate chlorophyll-*a* and phycocyanin concentrations (Tables 2.4 and 2.5). RGB sensors on commercial UASs

provide a cost-effective tool for monitoring photosynthetic activity. Despite differences in resolution, the 12.4 M Phantom 4 and 20 M Phantom 4 Pro RGB sensors generated similar vegetation index values for both chlorophyll-*a* and phycocyanin. Of the 12 vegetation indices calculated from the two RGB sensors, the Color Index of Vegetation Extraction (CIVE) generated the best estimates of chlorophyll-*a* concentration for the aerial images collected from the Phantom 4 ($r^2 = 0.30$, $p < 0.0001$) and Phantom 4 Pro ($r^2 = 0.34$, $p < 0.0001$; Table 2.4). CIVE was originally developed to differentiate between vegetation and soil to estimate crop growth without the need to measure near-infrared wavelengths (Kataoka et al. 2003), and it is not typically included in UAS aquatic ecosystem monitoring studies. Both RGB sensors were more sensitive to chlorophyll-*a* than phycocyanin. The Green–Red Ratio Index (GRRI) and Visible Atmospherically Resistant Index (VARIgreen) vegetation indices were the best predictors of phycocyanin concentration (Table 2.5), though these correlations may be an artifact of chlorophyll-*a* content within cyanobacterial cells, as GRRI was also closely related to chlorophyll-*a*. Several studies have utilized RGB UAS sensors for mapping coastal floating green tides (Xu et al. 2017), attached green algae (Xu et al. 2018), benthic cyanobacterial mats (Bollard-Breen et al. 2015), and nuisance filamentous green algae (Flynn and Chapra 2014). For example, Xu et al. (2018) calculated the Normalized Green-Blue Difference Index (NGBDI), Normalized Green-Red Difference Index (NGRDI), Visible Band Difference Vegetation Index (VDVI), and Excess Green Index (EXG) indices from RGB UAS imagery to identify green algae growing on rafts, and found that NGRDI generated the most accurate results. These findings are consistent with our results, as of the four vegetation indices tested by Xu et al. (2018), NGRDI was closely related to both chlorophyll-*a* and phycocyanin. RGB UASs are primarily used for qualitative rather than quantitative assessment of CyanoHABs, but the low-cost and ease of use of RGB sensors warrants further research.

Vegetation index values generated from the modified multispectral MAPIR Survey3W NGB sensor indicate that it is not reliable for quantifying cyanobacterial abundance in the eutrophic aquatic systems monitored in this study. Of the five vegetation indices calculated, the Enhanced Normalized Difference Vegetation Index (ENDVI) was the best predictor of both chlorophyll-*a* (r^2 = 0.03, p = 0.14; Table 2.4) and phycocyanin (r^2 = 0.15, p = 0.002; Table 2.5). ENDVI was designed to inflate the chlorophyll-*a* reflection values by combining reflectance from near-infrared and green wavelengths (MaxMax 2015). Blue Normalized Vegetation Index (BNDVI) values generated from modified multispectral NGB sensors have been used for monitoring cyanobacterial buoyant packed cell volume (Van der Merwe and Price 2015). BNDVI was not significantly correlated with chlorophyll-*a* or phycocyanin in our study, potentially due to the high cyanobacterial densities in our systems, as BNDVI can become saturated and less reliable as buoyant packed cell volume increases.

Aerial images collected with the Parrot Sequoia multiband multispectral sensor generated the best estimates of chlorophyll-*a* and phycocyanin of the four sensors. Of the 15 vegetation indices calculated from multiband multispectral aerial images, Difference Vegetation Index (DVI), 2-Band Enhanced Vegetation Index (EVI2), Normalized Difference Vegetation Index (NDVI), and Normalized Difference Vegetation Structure Index (NDVSI) were highly correlated to chlorophyll-*a* concentration (Table 2.4). NDVI was originally developed for monitoring terrestrial vegetation using satellite remote sensors (Rouse et al. 1974). While satellite NDVI values are often distorted by atmospheric disturbances and cloud cover, UAS images are collected at a lower altitude which decreases atmospheric effects (Choo et al. 2018). Currently, NDVI is one of the most measured vegetation indices for precision agriculture, and it provided the best estimate of chlorophyll-*a* (r^2 =0.78, p <0.0001) of all the sensor and vegetation index combinations in this

study. Multiband multispectral aerial images also generated the best estimates of cyanobacterial abundance, with the Green Chlorophyll Index (CiGreen), Green Normalized Difference Vegetation Index (GNDVI), and NDVSI vegetation indices generating the best phycocyanin estimates of all four sensors and vegetation index combinations (Table 2.5). The red-edge wavelength is included in many multispectral sensors because it significantly improves crop health estimates (Lu et al. 2019). However, of the 15 vegetation indices generated from the multiband multispectral sensor, vegetation indices that included the red-edge wavelength, such as the Normalized Difference Red-Edge Index (NDRE) and Modified Simple Ratio Red-Edge (MSRre), generated the least reliable estimates of chlorophyll-*a* and phycocyanin.

Many multiband multispectral sensors are specifically designed to record peak reflectance and absorbance characteristics of terrestrial chlorophyll-*a*. Vegetation indices that included the red and near-infrared wavelengths provided the best chlorophyll-*a* and phycocyanin estimates, as near-infrared wavelengths are reflected at a higher degree than green wavelengths. Studies that utilized UASs and satellites for monitoring water quality in reservoirs also found that vegetation indices that include the red and near-infrared wavelengths, such as the Ratio Vegetation Index (RVI) and NDVI, performed the best for estimating chlorophyll-*a* (Beck et al. 2016; Cillero Castro et al. 2020). However, measuring the near-infrared wavelength did not necessarily generate more reliable results, as seen with the modified multispectral Survey3W NGB sensor. The Cigreen and GNDVI vegetation indices were both calculated from modified and multiband multispectral sensor aerial images, yet they vary greatly in their relationship to both chlorophyll-*a* and phycocyanin (Tables 2.4 and 2.5). Differences between the sensors could be attributed to the differences in wavelengths and bandwidths, as well as resolution (Figure 2.5 and Table 2.2). The Survey3W NGB records near-infrared data at the 850 nm range at a bandwidth of 30 nm, whereas the Parrot

Sequoia records near-infrared at the 790 nm range at a bandwidth of 40 nm (Figure 2.1). A study conducted by Lu, He and Dao (2019) compared the ability of wavelengths recorded by three-band modified multispectral, multiband multispectral, and hyperspectral sensors for estimating terrestrial crop cover and found wavelengths recorded by modified multispectral sensors generate low accuracy imagery that should be restricted to mapping rather than quantification (Lu et al. 2019). Such discrepancies were not found between vegetation index values generated from the two RGB sensors and the multiband multispectral sensors (i.e., GRRI, NGRDI, and RGRI; Tables 2.4 and 2.5). This suggests that the improved resolution of the multispectral sensor was not as important as the addition of the near-infrared band for estimating photosynthetic pigments.

Many of the vegetation indices designed for estimating algal abundance from satellite remote sensors, including the Floating Algae Index (FAI) generated from MODIS wavelengths (Hu 2009) and the Cyanobacterial Index (CI) generated from MERIS wavelengths (Wynne et al. 2010), require sensors that measure wavelengths most commercial drones are not equipped to record. Some vegetation indices such as KIVU, generated from Landsat 5 images, utilize visible wavelength data for determining chlorophyll-*a* in inland aquatic ecosystems (Brivio et al. 2001). However, KIVU was a poor measure of chlorophyll-*a* in our highly productive ponds (Table 2.4), likely because KIVU was generated from systems with relatively low chlorophyll-*a* concentrations (Brivio et al. 2001). There are currently no commercially available UAS sensors designed specifically for aquatic ecosystem monitoring, as most sensors and vegetation indices are designed for detecting terrestrial vegetation. The sensors included in this study were more sensitive to chlorophyll-*a* concentrations than phycocyanin, likely because phycocyanin absorbs light at 620 nm which is not measured by most commercially available sensors. Results from this study suggest multiband multispectral sensors can be utilized for estimating algal and cyanobacterial abundance,

but further research should be conducted to determine whether these tools can reliably differentiate between chlorophyll-*a* and phycocyanin. Although remote sensing imagery cannot estimate cyanotoxins (i.e., microcystin and cylindrospermopsin) or off-flavor compounds (i.e., geosmin and MIB), photosynthetic pigment estimates based on UAS images could be instrumental for early detection and management of CyanoHABs.

Conclusions

Traditional water sampling techniques provide a snapshot of cyanobacterial abundance, ecosystem conditions, and the presence of cyanotoxins but do not illustrate how the system changes spatially or temporally. Algorithms created for satellite remote sensing data are capable of monitoring cyanobacterial abundance in large water bodies, but the spatial resolution is not fine enough for measuring smaller systems (Kutser 2004). UASs are a cost-effective, rapid, and customizable tool for predicting and monitoring cyanobacterial abundance at smaller scales (<30 m). This study compared the performance of four UAS sensors that vary in recorded wavelengths, resolution, and price for estimating phytoplankton (measured as chlorophyll-*a)* and cyanobacterial (measured as phycocyanin) abundance in small eutrophic systems. Twenty-six vegetation indices were calculated based on the recorded wavelengths of each sensor, to determine the best band ratio algorithm for estimating cyanobacterial pigments. Results from this study show that RGB and multiband multispectral sensors are viable tools for estimating chlorophyll-*a* content in small eutrophic aquatic systems, with the multiband multispectral sensor generating the best estimates of both pigments. The RGB and multiband multispectral sensors were less sensitive to phycocyanin concentrations, likely due to the unique spectral absorbance of phycocyanin at 620 nm which is not commonly monitored by commercial sensors. The 3-band modified multispectral sensor was not effective for monitoring either photosynthetic pigment, regardless of calculated vegetation index. Future research should be conducted to determine whether vegetation index estimates are equally robust in other small waterbodies such as rivers, streams, and lakes.

Table 2.1. Unoccupied aerial system (UAS) flight details for this study. GSD – ground sampling distance, Lat – latitude, Long – longitude.

Flight ID	Figure	Date	Location	Lat	Long	Flight Altitude (m)	GSD (cm/px)	Image % Overlap	Flight Dimensions (m)	Water Samples
1	2.2a	11/20/19	Aquaculture Facility	32.390	-87.349	75	3.28	75	485 x 469	10
2	2.2b	04/14/20	Aquaculture Facility	32.413	-87.375	75	2.05	75	924 x 942	8
3	2.2c	04/14/20	Aquaculture Facility	32.396	-87.367	75	3.28	75	358 x 816	6
4	2.3a	09/03/19	Research Facility	32.662	-85.496	50	1.36	80	161 x 305	5
5	2.3b	02/21/20	Research Facility	32.662	-85.496	50	2.23	75	114 x 196	16
6	2.3d	06/18/20	Research Facility	32.654	-85.488	30	1.31	75	63 x 102	1
7	2.3c	07/17/20	Research Facility	32.662	-85.496	50	2.19	75	166 x 297	19
8	2.4a	03/18/20	Aesthetic Pond	32.588	-85.484	50	2.19	75	147 x 195	2
9	2.4b	05/31/20	Aesthetic Pond	32.588	-85.484	50	2.19	75	147 x 195	1
10	2.4c	07/10/20	Aesthetic Pond	32.588	-85.484	75	2.19	75	147 x 195	2

Table 2.2. Description of the two unoccupied aerial systems (UAS) utilized in this study. Each UAS was made up of the unoccupied aerial vehicle (UAV), its integrated visible wavelength red, green, blue (RGB) camera, and onboard multispectral sensors.

	Modified Multispectral UAS	**Multiband Multispectral UAS**
UAV Model	**DJI Phantom 4**	**DJI Phantom 4 Pro**
Type	Quadcopter	Quadcopter
Vertical Position Accuracy	±0.5 m	±0.5 m
Horizontal Position Accuracy	±1.5 m	±1.5 m
Max Flight Time	~28 minutes	~30 minutes
Max Speed	20 m/S	45 m/S
Estimated Payload Capacity	~462 g	~462 g
Diagonal Length	350 mm	350 mm
Weight With Batteries	1380 g	1388 g
Retail Value	$1,500	$1,500
RGB Camera	**DJI Phantom 4 RGB**	**DJI Phantom 4 Pro RGB**
FOV	94° 20 Mm	84° 8.8 Mm/24 Mm
Image Size	4000 x 3000	5472 x 3648
Spatial Resolution	3.4 cm/pixel 80 m altitude	2.6 cm/pixel 80 m altitude
Effective Pixels	12.4 M	20 M
Focal Length	20 mm	24 mm
Onboard Sensor	**MAPIR Survey3W**	**Parrot Sequoia**
HFOV	87° 19 mm	62° mm
Image Size	4032 x 3024	4608 x 3456
Spatial Resolution	5.519 cm/pixel 120 m altitude	11 cm/pixel 120 m altitude
Focal Length	3.37 mm	3.98 mm
Lens Type	Non-Fish Eye	Non-Fish Eye
Weight	75.4 g	90 g
Dimensions	41 x 59 x 25 mm	75 x 59 x 3 mm
Retail Value	$400	$3,500

Table 2.3. Vegetation indices calculated from DJI Phantom 4 and Phantom 4 Pro RGB sensors (RGB), MAPIR Survey3W NGB modified multispectral sensor (NGB), and Parrot Sequoia multiband multispectral (Multispec) imagery. B – Blue; G – Green; NIR – Near-infrared; R – Red; RE – Red-edge.

Vegetation Index	Formula	Sensor	Citation
2-Band Enhanced Vegetation Index (EVI2)	2.5((NIR – R)/(NIR + 2.4*R +1))	Multispec	(Jiang et al. 2007)
Blue Normalized Vegetation Index (BNDVI)	(NIR-B)/(NIR+B)	NGB	(Van der Merwe and Price 2015)
Color Index of Vegetation Extraction (CIVE)	0.441*R-0.881*G+0.385*B+18.787	RGB	(Kataoka et al. 2003)
Difference Vegetation Index (DVI)	NIR-R	Multispec	(Tucker 1979)
Enhanced Normalized Difference Vegetation Index (ENDVI)	((NIR+G)-(2*B))/((NIR+G)+(2*B))	NGB	(MaxMax 2015)
Excess Green Index (EXG)	2*G-R-B	RGB	(Xu et al. 2018)
Excess Green Minus Excess Red (ExGR)	ExG−1.4R−G	RGB	(Camargo Neto 2004)
Green Chlorophyll Index (CiGreen)	(NIR/G)-1	Multispec & NGB	(Gitelson et al. 2003)
Green Normalized Difference Vegetation Index (GNDVI)	(NIR-G)/(NIR+G)	Multispec & NGB	(Gitelson and Merzlyak 1998)
Green–Red Ratio Index (GRRI)	G/R	Multispec & RGB	(Tucker 1979)
KIVU	(B-R)/G	RGB	(Brivio et al. 2001)
Modified Simple Ratio Red-Edge (MSRre)	(NIR/RE-1)/ √ (NIR/RE+1)	Multispec	(Cao et al. 2013)
Modified Single Ratio (MSR)	(NIR/R)-1/(√NIR/R)+1	Multispec	(Chen 1996)
Normalized Difference Red-Edge Index (NDRE)	NIR−RE/NIR+RE	Multispec	(Barnes et al. 2000)
Normalized Difference Vegetation Index (NDVI)	(NIR-R)/(NIR+R)	Multispec	(Rouse et al. 1974)
Normalized Difference Vegetation Structure Index (NDVSI)	(NIR - (R+G) 0.5)/(NIR + (R+G) 0.5)	Multispec	(Yang et al. 2008)
Normalized Green-Blue Difference Index (NGBDI)	G-B/G+B	NGB & RGB	(Xu et al. 2017)
Normalized Green-Red Difference Index (NGRDI)	(G-R)/(G+R)	Multispec & RGB	(Xu et al. 2017)
Ratio Normalized Difference Vegetation Index (RNDVI)	((NIR-R)/(NIR+R)* NIR)R	Multispec	(Peng Gong et al. 2003)
Ratio Vegetation Index (RVI or SR)	NIR/R	Multispec	(Cillero Castro et al. 2020)
Red Green Blue Vegetation Index (RGBVI)	G^2−R×B/G^2+R×B	RGB	(Bendig et al. 2015)
Red-Edge Chlorophyll Index (CiRedEdge)	(NIR/RE)-1	Multispec	(Gitelson et al. 2003)
Red-Green Ratio Index (RGRI)	R/G	Multispec & RGB	(Gamon and Surfus 1999)
Visible Atmospherically Resistant Index (VARIgreen)	(G-R)/(G+R-B)	RGB	(Gitelson et al. 2002)
Visible Band Difference VI (VDVI)	(2*G-R-B)/(2*G+R+B)	RGB	(Xu et al. 2018)
Vegetativen (VEG)	G/(R^a*$B^{(1-a)}$) a = 0.667	RGB	(Hague et al. 2006)

Table 2.4. Pearson's correlations between log-transformed chlorophyll-*a* concentrations (µg/L) of 70 water samples and vegetation index values derived from UAS images captured with a DJI Phantom 4 integrated RGB camera, DJI Phantom 4 Pro integrated RGB camera, a MAPIR Surve3 NGB sensor, and a Parrot Sequoia multispectral sensor. Values are only shown for vegetation indices that could be calculated by that particular sensor.

	Phantom 4 RGB		**Phantom 4 Pro RGB**		**Survey3 NGB**		**Sequoia Multispectral**	
	r^2	*p*-value	r^2	*p*-value	r^2	*p*-value	r^2	*p*-value
BNDVI					0.01	0.40		
CiGreen					0.03	0.18	0.63	<0.0001
CIRedEdge							0.02	0.27
CIVE	0.30	<0.0001	0.34	<0.0001				
DVI							0.73	<0.0001
ENDVI					0.03	0.14		
EVI2							0.76	<0.0001
EXG	0.28	<0.0001	0.32	<0.0001				
ExGR	0.11	0.006	0.06	0.05				
GNDVI	-	-	-	-	0.01	0.54	0.66	<0.0001
GRRI	0.29	<0.0001	0.27	<0.0001			0.30	<0.0001
KIVU	0.01	0.39	0.07	0.03				
MSR							0.71	<0.0001
MSRre							0.02	0.27
NDRE							0.02	0.28
NDVI							0.78	<0.0001
NDVSI							0.75	<0.0001
NGBDI	0.04	0.08	0.03	0.19	0.00	0.80		
NGRDI	0.29	<0.0001	0.26	<0.0001			0.29	<0.0001
RGBVI	0.13	0.003	0.20	<0.0001				
RGRI	0.28	<0.0001	0.25	<0.0001			0.27	<0.0001
RNDVI							0.43	<0.0001
RVI							0.58	<0.0001
VARIgreen	0.30	<0.0001	0.25	<0.0001				
VDVI	0.25	<0.0001	0.23	<0.0001				
VEG	0.02	0.28	0.11	0.01				

Table 2.5. Pearson's correlations between log-transformed phycocyanin concentrations (µg/L) of 70 water samples and vegetation index values derived from UAS images captured with a DJI Phantom 4 integrated RGB camera, DJI Phantom 4 Pro integrated RGB camera, a MAPIR Surve3 NGB sensor, and a Parrot Sequoia multispectral sensor. Values are only shown for vegetation indices that could be calculated by that particular sensor.

	Phantom 4 RGB		**Phantom 4 Pro RGB**		**Survey3 NGB**		**Parrot Multispectral**	
	r^2	*p*-value	r^2	*p*-value	r^2	*p*-value	r^2	*p*-value
BNDVI					0.02	0.31		
CiGreen					0.01	0.57	0.55	<0.0001
CIRedEdge							0.07	0.05
CIVE	0.07	0.03	0.08	0.02				
DVI							0.44	<0.0001
ENDVI					0.15	0.002		
EVI2							0.51	<0.0001
EXG	0.06	0.04	0.08	0.02				
ExGR	0.05	0.06	0.04	0.13				
GNDVI					0.00	0.84	0.57	<0.0001
GRRI	0.19	<0.0001	0.14	0.002			0.08	0.03
KIVU	0.03	0.14	0.08	0.02				
MSR							0.50	<0.0001
MSRre							0.07	0.05
NDRE							0.07	0.05
NDVI							0.51	<0.0001
NDVSI							0.57	<0.0001
NGBDI	0.00	0.89	0.00	0.91	0.04	0.12		
NGRDI	0.16	0.001	0.13	0.003			0.08	0.04
RGBVI	0.02	0.32	0.05	0.07				
RGRI	0.14	0.002	0.12	0.004			0.07	0.04
RNDVI							0.39	0.01
RVI							0.43	<0.0001
VARIgreen	0.17	0.001	0.14	0.002				
VDVI	0.06	0.05	0.06	0.04				
VEG	0.01	0.33	0.05	0.06				

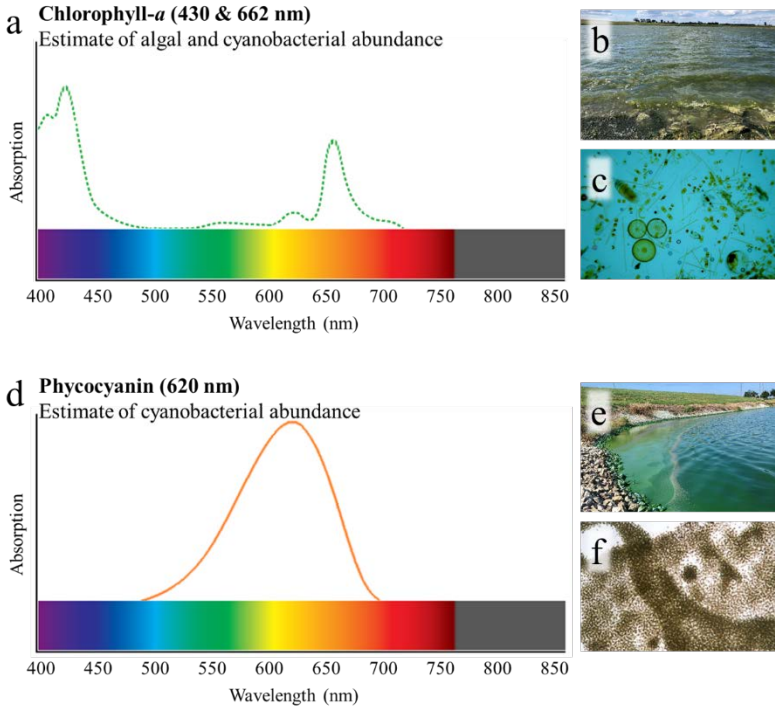

Figure 2.1. Spectral absorbance of chlorophyll-*a*, the photosynthetic pigment found in all phytoplankton (a). High chlorophyll-*a* concentrations cause waterbodies to appear green (b), due to high concentrations of phytoplankton including green algae, diatoms, and cyanobacteria (c). In contrast, the cyanobacterial accessory pigment phycocyanin has a spectral absorbance at 620nm (d). Elevated phycocyanin values are indicative of high cyanobacterial abundance, commonly associated with thick surface scums (e), as the release of cyanotoxins by cyanobacterial genera, such as *Microcystis aeruginosa* (f).

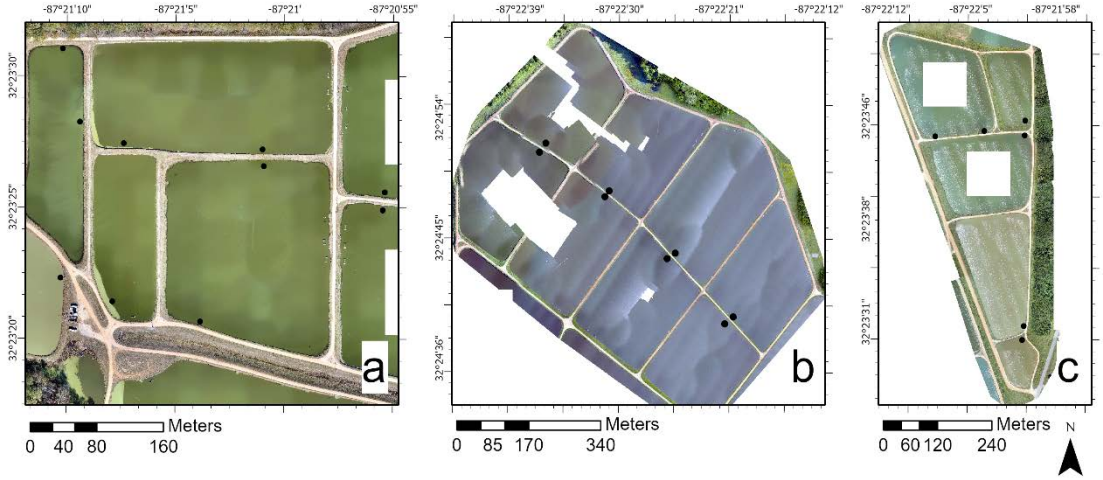

Figure 2.2. Orthomosaics generated from aerial images collected with the integrated RGB sensor of a Phantom 4 Pro at a commercial aquaculture facility in Alabama, USA. 10 water samples were collected to validate aerial data collected on 11/20/2019, which surveyed 7 ponds (Flight 1, panel a). 8 water samples were collected to validate aerial data collected on 04/14/20, which surveyed 8 ponds (Flight 2, panel b). 6 water samples were collected to validate aerial data collected on 04/14/20, which surveyed 5 ponds (Flight 3, panel c). Water sample collection locations are shown as black dots.

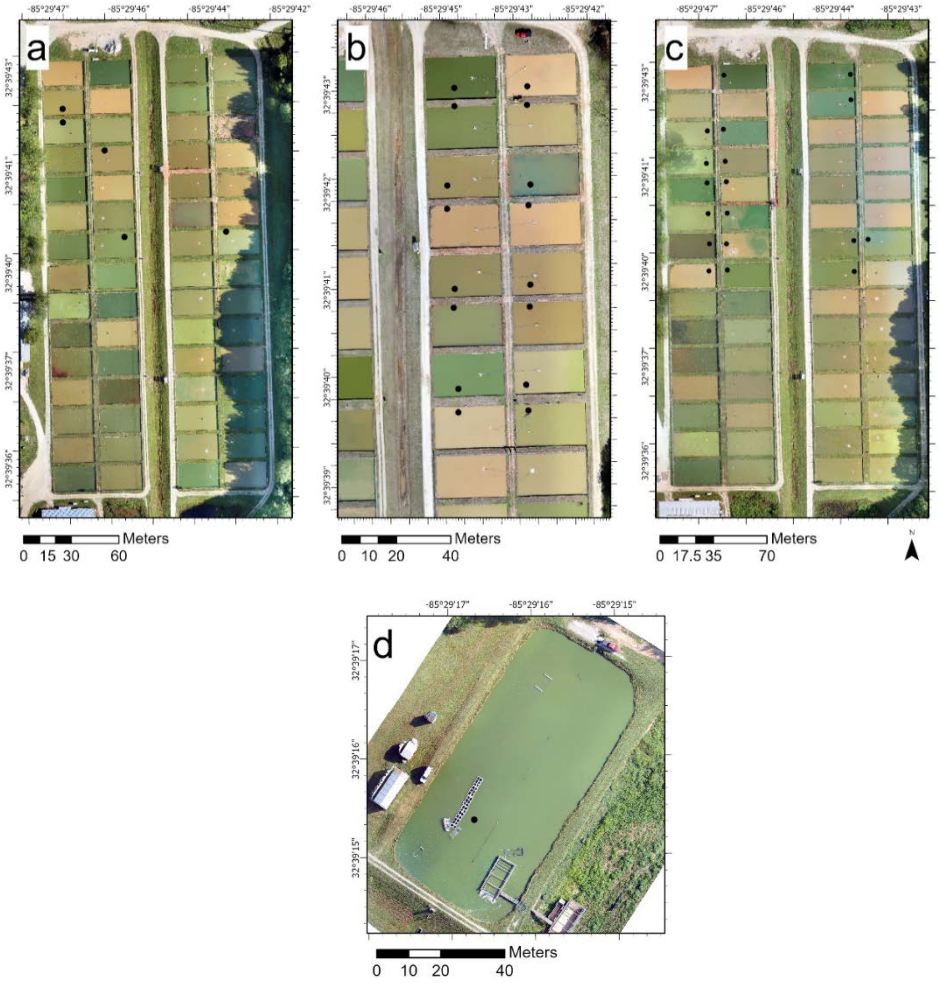

Figure 2.3. Orthomosaics generated from aerial images collected with the integrated RGB sensor of a Phantom 4 Pro at research ponds at Auburn University's E.W. Shell Fisheries Center. Water sample collection locations are shown as black dots. 5 water samples were collected to validate aerial data collected on 09/03/2019, which surveyed 5 ponds (Flight 4, panel a). 16 water samples were collected to validate aerial data collected on 02/21/2020, which surveyed 16 ponds (Flight 5, panel b). 19 water samples were collected to validate aerial data collected on 02/21/2020, which surveyed 19 ponds (Flight 7, panel c). 1 water sample was collected to validate aerial data collected on 06/18/2020, which surveyed 1 pond (Flight 6, panel d).

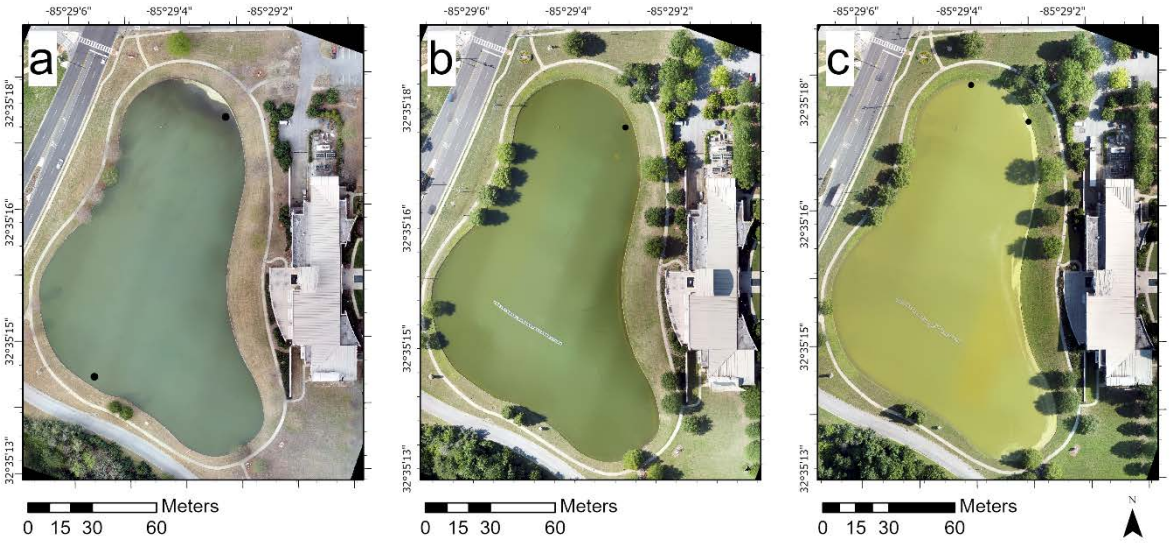

Figure 2.4. Orthomosaics generated from aerial images collected with the integrated RGB sensor of a Phantom 4 Pro at Auburn University's Jule Collins Smith Museum of Fine Art's pond. Water sample collection locations are shown as black dots. 2 water sample was collected to validate aerial data collected on 06/18/2020, which surveyed 1 pond (Flight 8, panel a). 1 water sample was collected to validate aerial data collected on 05/31/2020, which surveyed 1 pond (Flight 9, panel b). 2 water sample was collected to validate aerial data collected on 07/10/2020, which surveyed 1 pond (Flight 10, panel c).

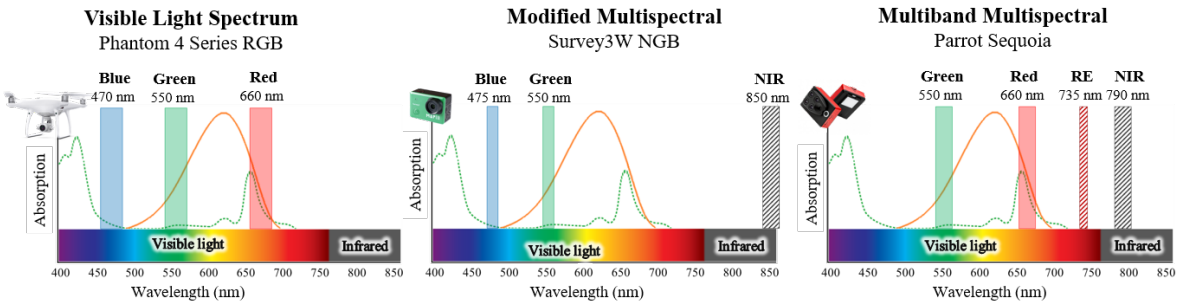

Figure 2.5. Central wavelength (nm) for the DJI Phantom 4 and Phantom 4 Pro integrated red, green, blue cameras (RGB), MAPIR Survey3W near-infrared, green, blue (NGB) modified 3-band multispectral sensors, and Parrot Sequoia multiband multispectral sensors utilized in this study, overlaid over the spectral absorbance of pigments found in all phytoplankton (i.e., chlorophyll-*a*; dashed green line) and unique to cyanobacteria (i.e., phycocyanin; solid orange line).

Chapter 3

Carlson's trophic state index is a poor predictor of cyanobacterial dominance in drinking water reservoirs

Abstract

A twenty-month survey of 71 surface drinking water utilities across 44 waterbodies was conducted to determine whether the commonly used Carlson's trophic state index (TSI) is a reliable indicator of the threat harmful algal blooms pose to drinking water sources. Raw water quality results showed that cyanobacteria, cyanotoxins (i.e., microcystin), and taste and odor (T&O) compounds (i.e., MIB and geosmin) were generally low in the utilities sampled. TSI values based on chlorophyll concentrations (TSI Chl-*a*) were closely related to phytoplankton, cyanotoxin, and T&O abundance and indicated most drinking water sources were mesotrophic or eutrophic. However, TSI values based on total phosphorus (TSI TP) indicated the drinking water sources were eutrophic or hypereutrophic. These results suggest TSI Chl-*a* is a better predictor of cyanobacteria and their compounds than TSI TP. Phytoplankton abundance decreased with depth, therefore managers should consider switching to deeper intakes when TSI Chl-*a* values increase to reduce removal costs.

Introduction

Determining the trophic state of aquatic ecosystems is useful for properly managing surface drinking water sources, as it quantifies the biological response of a system to increased nutrient availability. Water quality indices, such as Carlson's Trophic State Index (TSI), are commonly used for determining the trophic state of aquatic ecosystems, and can be used to estimate the abundance or potential abundance of phytoplankton, including potentially toxic cyanobacteria, which are becoming an increasing risk to drinking water surface utilities worldwide. The occurrence of cyanobacterial blooms is increasing worldwide as a result of elevated surface water temperatures and increased nutrient inputs from agricultural, industrial, and urban sources (Heisler et al. 2008; O'Neil et al. 2012; Glibert 2020). Several bloom-forming cyanobacteria produce toxic secondary metabolites (i.e., cyanotoxins), such as the hepatotoxins microcystin and cylindrospermopsin, that are linked to adverse health effects, such as upset stomach, diarrhea, vomiting, and liver and kidney damage in humans, livestock and domestic animals (Elleman et al. 1978; DeVries et al. 1993; Briand et al. 2003). To manage the potential health risks of cyanotoxin exposure, the United States Environmental Protection Agency (U.S. EPA) created a 10-Day Drinking Water Health Advisory for cyanotoxins encouraging some surface drinking water utilities to issue health advisories for children pre-school age and younger (i.e., <6 years old) when microcystin and cylindrospermopsin concentrations exceed 0.3 µg/L and 0.7 µg/L, respectively (USEPA 2015). Whereas, the 10-Day Drinking Water Health Advisory for school-age children and adults are 1.6 µg/L for microcystin and 3 µg/L for cylindrospermopsin. Yet, there are no federal standards for monitoring, response, and management of cyanotoxins that enter surface drinking water utilities, although such standards have been created in some states (Yeager and Carpenter 2019). A 2019 national survey found

that monitoring and management practices vary widely across states and that these approaches are more rigorous in states that record frequent harmful algal bloom (HAB) issues, such as Ohio (Yeager and Carpenter 2019).

Cyanobacteria further impair drinking water sources through the production of taste and odor compounds, such as geosmin and 2-methylisoborneol (MIB, Dunlap et al. 2015; Dietrich and Burlingame 2015; Olsen et al. 2016). Geosmin and MIB are volatile terpenes that give water a musty or muddy scent and flavor that can be detected by consumers at concentrations as low as 10 and 30 ng/L, respectively (Izaguirre et al. 1982). Detection at such low concentrations causes consumer complaints, as many gauge the quality and safety of their drinking water on aesthetic criteria (McGuire 1995). However, geosmin and MIB have no known health effects at environmentally relevant concentrations (Burgos et al. 2014). Therefore, there are no regulatory guidelines for managing geosmin and MIB in recreational waters or drinking water sources (Watson et al. 2016). Rather, drinking water utilities manage taste and odor compounds at their own discretion to meet customer demands and instill confidence in finished raw water quality.

Cyanobacteria, cyanotoxins, and taste and odor compound abundance can vary greatly seasonally and across years (Stumpf et al. 2012). For example, cyanotoxins and taste and odor compounds tend to increase during the warmer summer months when elevated temperatures and prolonged solar radiation stimulate cyanobacterial growth (Jöhnk et al. 2008; Watson et al. 2008). Trophic state can also play a major role, as nitrogen and phosphorus inputs facilitate cyanobacterial growth, with trophic state considered one of the main predictors of cyanobacterial and taste and odor compound abundance (Downing et al. 2001). However, the presence of cyanobacteria is not always indicative of elevated cyanotoxin and taste and odor compounds

levels, as not all cyanobacterial species are able to synthesize cyanotoxins or taste and odor compounds (Watson et al., 2008).

Conventional drinking water treatment methods remove cyanobacterial cells and low levels of cyanotoxins and taste and odor compounds from raw water (He et al. 2016). However, elevated and persistent levels of cyanotoxins and taste and odor compounds in source water can impose serious logistic and economic challenges to drinking water treatment (Khiari and Watson 2007; Dunlap et al. 2015). A survey of 800 surface drinking water utilities across the United States and Canada found that 4.5% of their annual budget was spent on taste and odor compound removal and management, on average (Khiari and Watson 2007). Therefore, monitoring and preventing HABs at the reservoir level is imperative as it determines the effectiveness and cost of water treatment and, ultimately, the final quality and safety of drinking water. Despite the potential health and economic impact of HABs, there are limited data on the presence of cyanotoxins in raw and finished drinking water, as cyanotoxins only recently became classified for health advisories and there are no official national monitoring programs for these compounds in the United States.

This study aims to determine the value of Carlson's Trophic State Index (TSI) for characterizing the prevalence of phytoplankton including cyanobacteria, cyanotoxins, and taste and odor compounds in all surface drinking water sources in the state of Alabama. Located in the southeastern United States, Alabama's elevated summer temperatures and high nutrient inputs from agricultural runoff could potentially promote high cyanobacterial abundance. To characterize the trophic state of Alabama reservoirs, the Alabama Department of Environmental Management (ADEM) calculated the average TSI (Carlson, 1977) based on growing season (i.e., summer) chlorophyll-*a* concentrations for 41 reservoirs from 1997 to 2007, and found that 58%

of such reservoirs were eutrophic, with higher chlorophyll-*a* values observed throughout the warmer summer months (Alabama Department of Environmental Management 2018). While elevated nutrient availability signifies an increased threat of HABs, there are limited data of the prevalence of HABs and the presence of cyanotoxins and taste and odor compounds in Alabama (Graham et al. 2017). To assess the threat of cyanotoxins and taste and odor compounds to drinking water across space and time, raw water samples were collected from the intake of every surface drinking water utility in Alabama to determine the presence of cyanobacterial toxins (i.e., microcystin, cylindrospermopsin, and saxitoxin), phytoplankton and cyanobacterial abundances, taste and odor compounds, and nutrients during the summers of 2017 and 2018. Moreover, the goal of this study was to generate monitoring and management criteria at the reservoir and processing plant level to support state-wide water resource management.

Materials and methods

Study site and sampling

Raw water samples were collected from the intakes of 71 surface drinking water utilities throughout the state of Alabama, USA, from April 2017 through November 2018 (Figure 3.1). One utility is located in Tennessee but was included in the study because it provides drinking water to Alabama residents located close to the border of the two states. Six utilities provided samples from two different water intake points, and one provided samples from four locations for a total of 83 raw water intakes. All participating utilities were asked to provide raw water samples during July of 2017 and 2018, and several utilities voluntarily provided additional samples throughout the year resulting in a total of 367 samples.

Drinking water utility managers were provided sampling kits that included standard operating procedures and all the necessary sampling equipment. Managers were instructed to allow raw intake water to run for at least 20 minutes before filling the provided acid-washed plastic bottles with the specified sample volume. Managers were also asked to provide intake depth (meters) relative to current surface level for every sample submitted for analysis. The managers did not specify whether the system was experiencing a visible algal bloom. Raw water samples were then placed in coolers with ice and shipped overnight to be immediately processed in the laboratory at Auburn University, Auburn, AL.

Sample preparation and analysis

Chlorophyll-*a*, phycocyanin, microcystin, saxitoxin, and cylindrospermopsin samples were prepared by filtering a known volume of well-mixed raw water through Pall A/E filters and stored frozen in the dark until analysis. Phytoplankton abundance was estimated using chlorophyll-*a* concentrations (µg/L) that were determined via fluorometric analysis (Turner Designs Trilogy fluorometer, non-acidification chlorophyll module) after extraction from filters with 90% aqueous ethanol in the dark at 4°C (Sartory and Grobbelaar 1984). Cyanobacterial abundance was estimated using phycocyanin filters that were ground and extracted in a 50mM phosphate buffer in the dark for four hours, centrifuged, and filtered through a <0.2 µm filter prior to fluorometric analysis (Turner Designs Trilogy fluorometer, orange module) to determine phycocyanin concentrations (µg/L, Sarada et al. 1999; Kasinak et al. 2015). Microcystin, saxitoxin, and cylindrospermopsin concentrations (µg/L) were determined via enzyme-linked immunosorbent assay (ELISA) after extraction from filters with acidified 75% aqueous methanol (An and Carmichael 1994). Toxin extracts were redissolved in 5 ml of phosphate buffer prior to ELISA.

Total nitrogen (TN) and total phosphorus (TP) raw water samples were stored frozen until analysis. Nutrient concentrations were determined via spectrophotometry using ultraviolet (total nitrogen; μg/L) or colorimetric (total phosphorus; μg/L) standard methods (Gross and Boyd 1998). Raw, whole-water samples were stored in glass vials sealed with parafilm at 4°C and analyzed within 7 days of collection for MIB and geosmin concentrations (ng/L) using solid-phase microextraction combined with gas chromatography/mass spectrometry (SPME GC/MS, Zimmerman et al. 2002).

Trophic status was determined using Carlson's trophic state index (TSI) calculations based on total phosphorus and chlorophyll-*a* concentrations as follows:

$$TSI\ (TP) = 14.42 \times \ln(TP) + 4.15 \quad (1)$$

$$TSI\ (Chl\text{-}a) = 9.81 \times \ln(CHL) + 30.6 \quad (2)$$

where TP = total phosphorus concentration (μg/L) and CHL = chlorophyll-*a* pigment concentration (μg/L). TSI values less than 30 typically indicate oligotrophic conditions, 50-70 typically indicate eutrophic conditions, and over 70 indicates a hypereutrophic lake or reservoir (Carlson 1977). Mean TSI for each reservoir was calculated by averaging the July 2017 and 2018 TSI values of each intake.

Statistical analysis

Trophic state index values were determined by averaging the July 2017 and 2018 samples as this was the only month in which every utility provided raw water samples. Pearson correlation coefficients were used to determine the relationship between chlorophyll-*a*, phycocyanin, microcystin, MIB, geosmin, TN, TP, TN:TP (by weight), and depth throughout the entire study period. Saxitoxin and cylindrospermopsin concentrations were low or undetectable through the study period and were therefore not included in statistical analyses. Differences in

measured pigments, cyanotoxins, and taste and odor compounds between the warmer summer months (July through October) and the rest of the sampling season were determined through analysis of variance (ANOVA). The *stats* package for the statistical software R Studio version 4.0.2 (RStudio Team 2015) was used for all statistical analyses.

Results

The temporal dynamics of chlorophyll-*a*, phycocyanin, microcystin, and taste and odor compound concentrations throughout the study are summarized in Table 3.1 and Figure 3.2. In general, phycocyanin, cyanotoxins, and taste and odor compounds remained low throughout the study despite a large range in reservoir nutrient concentrations. Chlorophyll-*a* and phycocyanin concentrations ranged from 0.03 to 66.05 μg/L (average 6.68 μg/L) and 0 to 26.51 μg/L (average 1.43 μg/L), respectively, throughout the entire study period (Table 3.1 and Figure 3.2). Chlorophyll-*a* concentrations were significantly lower through the warmer summer months (July-October) than the rest of the year (p =0.03), with chlorophyll-*a* averaging 5.87 μg/L (±0.83 95% C.I.) during the summer and 7.79 μg/L (±1.74 95% C.I.) the rest of the year (Table 3.2). Phycocyanin was higher during the summer, with phycocyanin concentrations averaging 1.60 μg/L (± 0.37 95% C.I) in the summer and 1.21 μg/L (± 0.46 95% C.I) the rest of the year, though this trend was not statistically significant (p =0.18). There was a significant relationship between the presence of the two pigments (r^2 =0.12, p <0.0001), with a 0.11 μg/L (± 0.03 95% C.I.) increase in phycocyanin for every 1 unit increase in chlorophyll-*a* (μg/L; Table 3.3).

Cyanotoxin concentrations were generally low throughout the study. Saxitoxin concentrations were below the 0.00067 limit of detection (LOD) for our assay throughout the study period, and cylindrospermopsin ranged from undetectable (below LOD of 0.0017 μg/L) to

0.0031 μg/L, suggesting these cyanotoxins were either low or not present in our samples. Microcystin concentrations ranged from undetectable (below LOD of 0.005 μg/L) to 0.21 μg/L (average 0.01 μg/L), and were generally higher during the warmer summer months, though the highest recorded concentration occurred in April 2017 at one site (Table 3.1, Figure 3.2). There was no significant relationship between microcystin and chlorophyll-*a* (r^2 <0.01, p =0.21) or phycocyanin (r^2 <0.01, p =0.78, Table 3.3).

MIB and geosmin concentrations ranged from the limit of detection (1 ng/L) to 115.91 ng/L (average 2.81 ng/L) and 21.11 ng/L (average 0.97 ng/L), respectively, throughout the sampling period (Table 3.1 and Figure 3.2). There was a significant correlation between the two taste and odor compounds (r^2 =0.25, p <0.0001), with a 2.25 ng/L (± 0.42 95% C.I.) increase in MIB for each one unit increase in geosmin (ng/L, Table 3.3). MIB and geosmin concentrations were 3.64 ng/L (± 2.16 95% C.I.) and 0.55 ng/L (± 0.48 95% C.I.) higher from July to October than the rest of the year, respectively ($p \leq 0.02$, Table 3.2). There was a significant positive relationship between MIB and chlorophyll-*a* (r^2 =0.01, p =0.03) and phycocyanin (r^2 =0.02, p =0.01), as well as geosmin and chlorophyll-*a* (r^2 =0.03, p <0.0005, Table 3.3). Geosmin and phycocyanin were not significantly correlated.

TN, TP, and TN:TP (by weight) ranged from 12.00 to 1,697.92 μg/L (average 463.84 μg/L), 9.24 to 212.1 μg/L (average 66.04 μg/L), and 0.1 to 44.14 (average 9.19), respectively, throughout the sampling period (Table 3.1, Figure 3.2). Chlorophyll-*a*, phycocyanin, and microcystin had a non-linear relationship with nutrients and TN:TP ratios. However, chlorophyll-*a* concentrations were 1.83 μg/L (±1.63 95% C.I.) higher when TN:TP ratios were under 10 (p =0.03, Table 3.2). There was also a trend of higher phycocyanin and MIB when

TN:TP was less than 10, although these trends were not statistically significant (Figure 3.3, Table 3.3).

The Carlson trophic state index (TSI) TP values ranged from 36.22 to 81.40 (average 62.06), while TSI Chl-*a* ranged from 0 to 71.71 (average 42.64) throughout the study period (Table 3.1). Interestingly, the average summer (July 2017 and 2018) TSI TP and TSI Chl-*a* values differed greatly, with TS TP values 19.26 (± 95% C.I. 17.8 – 20.82) higher than TSI-Chl-*a*, on average (p <0.0001). Based on summer TP data, 80% and 16% of our samples originated from a eutrophic or hypereutrophic source, respectively, while chlorophyll-*a* derived TSI values classified 31% as eutrophic and none as hypereutrophic (Figure 3.4). TSI Chl-*a* values were significantly correlated (p <0.03) with chlorophyll-*a*, phycocyanin, microcystin, MIB, and geosmin (Table 3.3). However, these relationships were not observed when compared to TSI TP. Chlorophyll-*a* was the only parameter closely related to TSI TP, with a 0.23 (±0.11 95% C.I.) unit increase in chlorophyll-*a* for every unit increase in TSI TP (r^2 =0.04, p <0.0001).

Surface drinking water intake depths ranged from surface intakes to 25.91 meters, with an average sampling depth of 4.81 meters (Table 3.1). Nineteen samples were collected from surface intakes (i.e., 0 meters). As depth increased, the abundance of phycocyanin, microcystin, and geosmin decreased, although these relationships were not statistically significant (Figure 3.5). However, chlorophyll-*a* and MIB concentrations were significantly higher in samples collected from intakes shallower than 5 meters (p <0.04, Table 3.2).

Discussion

Bloom-forming cyanobacteria thrive under elevated surface water temperatures, increased nitrogen and/or phosphorus availability, reduced nitrogen to phosphorus ratios

(TN:TP), and poor mixing conditions (Smith 1983; Downing et al. 2001; Paerl and Huisman 2008). While the surface drinking water sources sampled in this study had relatively high nutrients and summer surface water temperature conditions, cyanobacterial abundance was generally low and cyanotoxins remained below health advisory thresholds determined by the U.S. EPA (Figure 3.1, USEPA 2015).

Harmful algal blooms dominated by cyanobacteria are common during the warmer summer months when elevated temperatures and prolonged solar radiation facilitate their growth (Jöhnk et al. 2008). These trends were observed throughout the twenty-month sampling period with higher phycocyanin concentrations from July to October than the rest of the year (Table 3.2). Interestingly, chlorophyll-*a* concentrations were significantly higher from November to June. Due to the temporal and spatial variability of cyanobacterial abundance and cyanotoxin production, it is possible that the annual sampling of the utilities was not sufficient to capture the episodic trends of cyanobacterial growth in our systems.

Cyanotoxins were typically present at low to undetectable levels throughout the twenty-month study. Microcystin did not exceed the U.S. EPA drinking water health advisory of 0.3 μg/L for children under six years old (USEPA 2015) over the duration of this project with the highest observed concentration being 0.21 μg/L (Table 3.1). Microcystin was poorly correlated with algal abundance throughout the study period (Table 3.3), likely because not all cyanobacterial species have the ability to produce toxins, and the triggers for cyanotoxin synthesis, storage, and release vary by cyanobacterial species and even strain, leading to poor spatial and temporal relationships between cyanobacteria and their metabolites (Smith 1983; Downing et al. 2001; Watson et al. 2008). While some cyanobacteria can produce both cyanotoxins and taste and odor compounds, there was also no clear relationship between

microcystin and taste and odor compound abundance in our study (Table 3.3). There are conflicting data on the co-occurrence of phytoplankton, cyanotoxins, and taste and odor compounds, but poor relationships between the three parameters are not uncommon (Watson et al. 2008; Graham et al. 2017).

MIB and geosmin production by cyanobacteria are the main biological sources of taste and odor compounds in surface drinking water sources, particularly during elevated temperature and nutrient conditions (Jüttner and Watson 2007; Watson et al. 2008). MIB and geosmin were both significantly higher during the warmer summer months, which has been observed in previous field studies (Table 3.2, Sugiura et al., 1998; Westerhoff et al., 2005). Only 2% of the samples exceeded the human detection threshold concentration for MIB (30 ng/L), all of which occurred between July and September. MIB was closely related to chlorophyll-*a* and phycocyanin concentrations, which suggests cyanobacteria were the main producers of MIB in our systems (Table 3.3). Only 1% of the samples exceeded the human detection threshold concentration for geosmin (10 ng/L), all of which occurred between June and July. Geosmin concentrations were not significantly correlated to phycocyanin concentrations, which suggests the presence of benthic geosmin producer, such as benthic cyanobacteria or actinobacteria, in the studied systems (Izaguirre et al. 1982). Benthic MIB and geosmin producers may contribute to taste and odor compounds in the water column, although their contribution to drinking water sources is not as well studied as pelagic cyanobacterial species and this topic requires further study (Cai et al. 2017). There was a significant relationship between MIB and geosmin, though they did not occur exclusively in tandem. These results are surprising as taste and odor problems are common in the state of Alabama. A survey of rural Alabama drinking water consumers found 20% of consumers experience aesthetic issues (Wedgworth et al. 2014). The findings from our

study suggest that aesthetic issues reported by rural Alabama drinking water consumers are not related to cyanobacterial off-flavors.

Carlson's trophic state index (TSI) values based on whether average summer TSI calculations varied greatly were based on total phosphorus (TSI TP) or chlorophyll-*a* (TSI Chl-*a*) concentrations. TSI TP values suggest most of the samples were collected from either eutrophic (80%) or hypereutrophic (16%) systems. TSI Chl-*a* values reflect conditions common of more mesotrophic (53%) or eutrophic (31%) systems (Figure 3.4). The discrepancy between the two calculated TSI values suggests that our systems are nutrient-rich, but there is another factor suppressing cyanobacterial growth. Typically, this difference is observed in systems that have high turbidity which reduces light availability for phytoplankton (Carlson 1991). However, these patterns could also be related to summer stratification, in which surface water is warmer and high phytoplankton abundance reduces nutrient concentrations and deeper water is cooler, with low productivity due to low light availability and therefore have higher nutrient concentrations. In our study, chlorophyll-*a* and MIB were significantly higher in shallow (<5 m) intakes (Table 3.2). Chlorophyll-*a*, phycocyanin, microcystin, MIB, and geosmin were all significantly correlated to TSI Chl-*a* values (Table 3.3). The same relationship was not observed for TSI TP values, therefore TSI Chl-*a* was a better predictor of cyanobacteria and their metabolites in the drinking water sources monitored in this study than TSI TP. This is consistent with past studies that have shown that TSI Chl-*a* values are the best predictors of MIB and geosmin outbreaks in lentic systems (Downing et al. 2001).

There was a general trend in our systems of higher phytoplankton and cyanobacterial secondary metabolite abundance when TN:TP ratios (by weight) were below 10. In general, there is a tendency for cyanobacteria to dominate lentic systems when the TN:TP ratios are

below 30 (Smith 1983). Observational studies have found that MIB, geosmin, and microcystin concentrations were highest when TN:TP values were low (Smith et al. 2002; Harris et al. 2016; Perkins et al. 2019). Currently, the state of Alabama has not implemented state criteria for nitrogen and phosphorus concentrations in drinking water sources, though there are several lake-specific chlorophyll-*a* criteria implemented throughout the state (Alabama Department of Environmental Management 2017).

Due to the low abundance of cyanobacteria and cyanotoxins in our systems it is difficult to propose predictive models, but differences in vertical distribution presents an interesting management strategy for drinking water utilities. Cyanobacteria thrive and produce a higher concentration of cyanotoxins, MIB, and geosmin under elevated light conditions (Saadoun et al. 2001; Wang and Li 2015). Westerhoff et al. (2005) found that the highest concentrations of MIB occurred in the upper 10 m of the water column. In this study, chlorophyll-*a* and MIB were more abundant in shallow intakes (<5 m; Table 3.2). These findings present a low-cost preventative solution for reducing the cost of removing cyanobacteria and their secondary metabolites from drinking water. Switching to a deeper intake, when available, could reduce the abundance of phytoplankton entering water treatment plants at the intake level, thereby reducing the economic and logistic complications associated with removing these compounds from drinking water.

Conclusions

Harmful algal blooms threaten drinking water sources through the production of cyanotoxins and taste and odor compounds. The results of this twenty-month state-wide survey suggest that cyanobacteria, cyanotoxins, and taste and odor compounds were scarce in surface drinking water sources. TSI values based on chlorophyll-*a* concentrations suggest the majority of the drinking water sources were mesotrophic or eutrophic and correlated well with phytoplankton, cyanotoxin, and taste and odor compound abundance. Yet, TSI values based on total phosphorus suggest the systems were eutrophic or hypereutrophic and did not correlate well with cyanotoxins and taste and odor compounds. The discrepancy between the two TSI values suggests there may be an additional factor, such as stratification, suppressing cyanobacterial growth. When monitoring surface water sources, managers should prioritize chlorophyll-*a* over nutrient measurements, as TSI Chl-*a* values were closely related to cyanotoxins and taste and odor compounds. Moreover, calculating the TSI chl-*a* from several intakes, when available, can be useful for determining which intake has the lowest chance of containing cyanotoxin and taste and odor compounds without the need to directly measure these parameters. For this study, deeper intakes tended to have lower phytoplankton and taste and odor compound abundance. Although not tested in this study, directly measuring Sechhi depth can also be a reliable and low cost indicator of trophic state that could be used as an early warning sign to initiate more rigorous sampling.

Table 3.1. Photosynthetic pigment (chlorophyll-*a* and phycocyanin), cyanotoxin (microcystin), taste and odor compound (MIB and geosmin), total nitrogen (TN), total phosphorus (TP) and nitrogen to phosphorus ratio (TN:TP; by weight), trophic status index based on total phosphorus (TSI TP) and chlorophyll-*a* concentrations (TSI Chl-*a*), and raw water intake depth data for the 71 surface drinking water utilities sampled from April 2017 to November 2018 sampled for this study.

	Minimum	**Maximum**	**Mean**	**SD**	**n**
Chlorophyll-*a* (μg/L)	0.03	66.05	6.68	8.55	367
Phycocyanin (μg/L)	0.00	26.51	1.43	2.76	358
Microcystin (μg/L)	0.00	0.21	0.01	0.02	367
MIB (ng/L)	0.00	115.91	2.81	10.17	358
Geosmin (ng/L)	0.00	21.11	0.97	2.23	357
TN (μg/L)	12.00	1697.92	463.84	244.00	348
TP (μg/L)	9.24	212.10	66.04	244.16	366
TN:TP (by weight)	0.10	44.14	9.19	7.04	363
TSI TP	36.22	81.40	62.06	8.06	365
TSI Chl-*a*	0.00	71.71	42.64	12.12	367
Raw water intake depth (meters)	0.00	25.91	4.81	4.91	355

Table 3.2. Mean (± 95% C.I.) values for chlorophyll-*a*, phycocyanin, microcystin, MIB, and geosmin between the warmer summer months (July through October) and the rest of the year (November through June), above and below the apparent productivity cutoff for depth (5 m), and above and below the apparent 10 nitrogen to phosphorus ratio (TN:TP; by weight) cutoff.

	Chlorophyll (µg/L)	**Phycocyanin (µg/L)**	**Microcystin (µg/L)**	**MIB (ng/L)**	**Geosmin (ng/L)**	**n**
July to October	5.87 (0.83)	1.60 (0.37)	0.005 (0.003)	4.29 (1.72)	1.19 (0.34)	212
November to June	7.79 (1.74)	1.21 (0.46)	0.006 (0.002)	0.65 (0.55)	0.64 (0.28)	155
p-value	0.03	0.18	0.45	<0.01	0.02	
Below 10 TN:TP	7.26 (1.16)	1.44 (0.36)	0.004 (0.002)	2.87 (1.19)	0.90 (0.30)	252
Above 10 TN:TP	5.42 (0.93)	1.41 (0.47)	0.009 (0.005)	2.45 (2.18)	0.95 (0.30)	111
p-value	0.03	0.12	0.04	0.15	0.87	
Depth <5 m	7.58 (1.16)	1.50 (0.35)	0.005 (0.002)	3.42 (1.48)	1.03 (0.30)	258
Depth >5 m	4.64 (1.05)	1.24 (0.52)	0.004 (0.002)	0.83 (0.34)	0.71 (0.39)	97
p-value	0.004	0.45	0.55	0.04	0.23	

Table 3.3. Pearson correlation coefficients between chlorophyll-*a*, phycocyanin, microcystin, MIB, geosmin, trophic state index values based on chlorophyll-a (TSI Chl-*a*) and total phosphorus (TSI TP) collected from the raw water intakes of 71 surface drinking water utilities from April 2017 through November 2018.

Variable 1	**Variable 2**	**Effect Estimate**	**± 95% C.I.**	***p*-value**	**r^2**
Chlorophyll-*a*	Phycocyanin	0.11	0.03	<0.0001	0.12
Microcystin	Chlorophyll-*a*	0.00	0.00	0.21	<0.01
Microcystin	Phycocyanin	0.00	0.00	0.78	<0.01
MIB	Chlorophyll-*a*	0.14	0.13	0.03	0.01
MIB	Phycocyanin	0.47	0.38	0.01	0.02
Geosmin	Chlorophyll-*a*	0.05	0.03	<0.0005	0.03
Geosmin	Phycocyanin	0.07	0.08	0.08	0.01
Geosmin	MIB	2.25	0.42	<0.0001	0.25
Microcystin	MIB	0.00	0.00	0.69	<0.01
Microcystin	Geosmin	0.00	0.00	0.31	<0.01
Chlorophyll-*a*	TSI Chl-*a*	0.56	0.05	<0.0001	0.63
Phycocyanin	TSI Chl-*a*	0.05	0.02	<0.0001	0.05
Microcystin	TSI Chl-*a*	0.00	0.00	0.03	0.01
MIB	TSI Chl-*a*	0.11	0.09	0.01	0.02
Geosmin	TSI Chl-*a*	0.04	0.02	<0.0001	0.04
Chlorophyll-*a*	TSI TP	0.23	0.11	<0.0001	0.04
Phycocyanin	TSI TP	0.02	0.04	0.32	0.00
Microcystin	TSI TP	0.00	0.00	0.69	0.00
MIB	TSI TP	0.06	0.13	0.39	0.00
Geosmin	TSI TP	-0.01	0.03	0.57	0.00

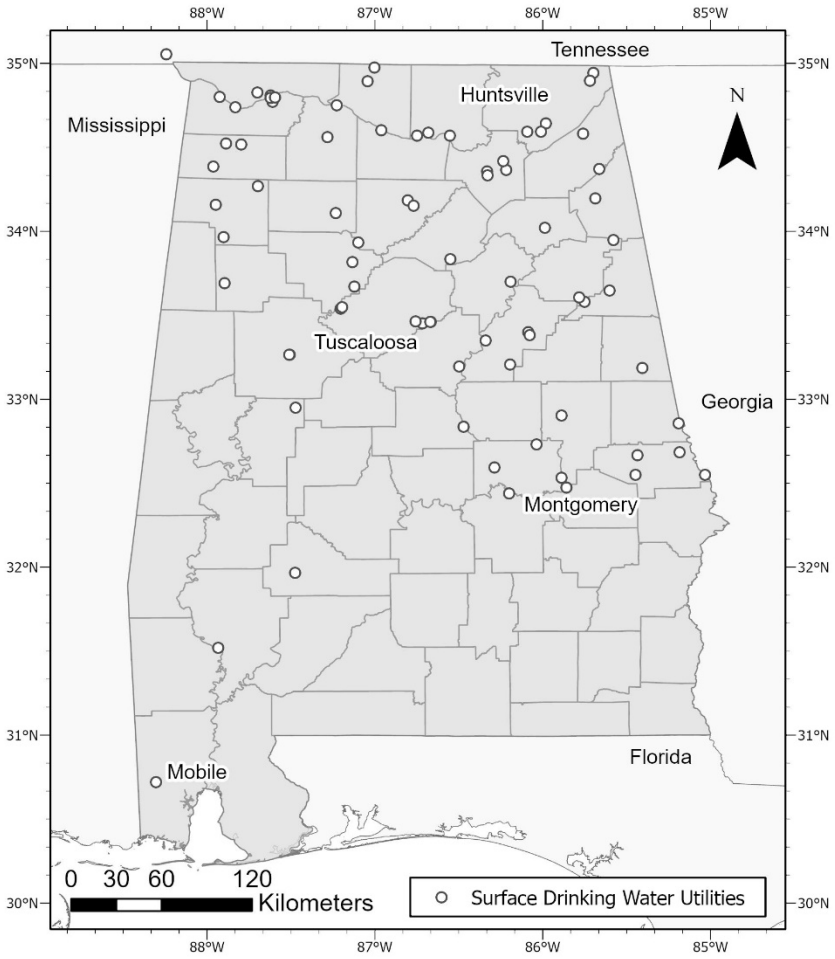

Figure 3.1. Map of the 83 raw water intake locations from the 71 surface drinking water utilities sampled in this study.

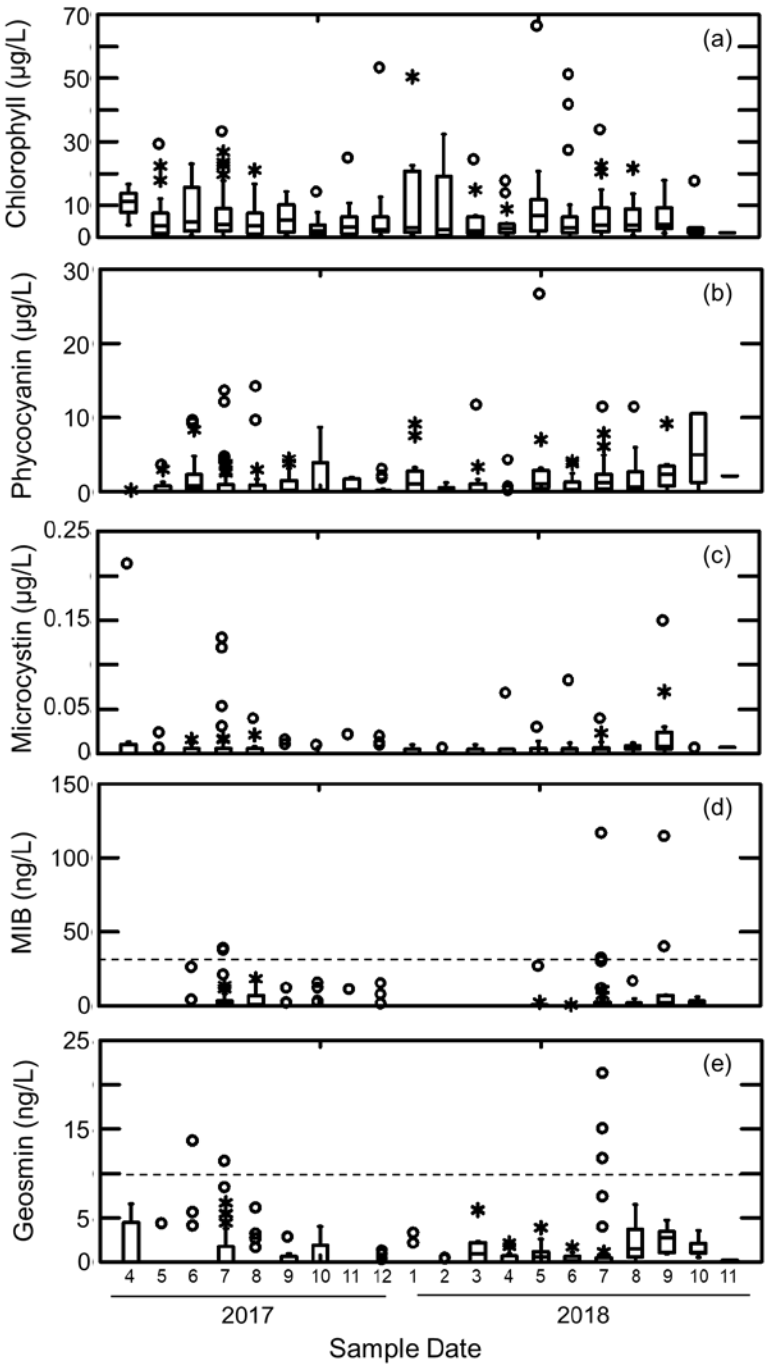

Figure 3.2. Chlorophyll-*a* (a), phycocyanin (b), microcystin (c), MIB (d), and geosmin (e) concentrations in raw water collected from the intakes of 71 surface drinking water utilities from April 2017 through November 2018. Dashed lines represent the human odor concentration threshold of MIB (30 ng/L) and geosmin (10 ng/L).

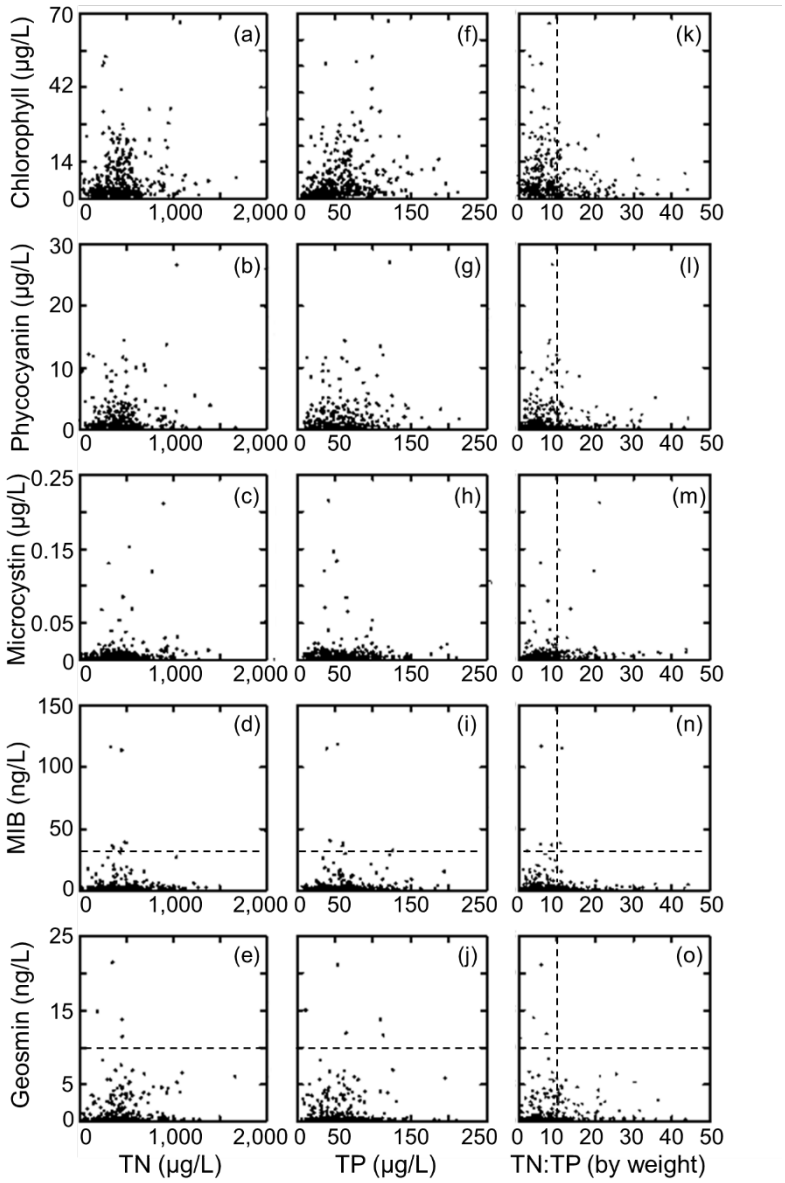

Figure 3.3. Relationship between chlorophyll-*a*, phycocyanin, microcystin, geosmin and MIB, and total phosphorus (TP; a-e), total nitrogen (TN; f-j), and total nitrogen to phosphorus ratio by weight (TN:TP; k-o). Black horizontal dashed lines represent the human odor concentration threshold of MIB (30 ng/L) and geosmin (10 ng/L). Vertical dashed lines represent the apparent TN:TP threshold for pigment and secondary metabolite abundance.

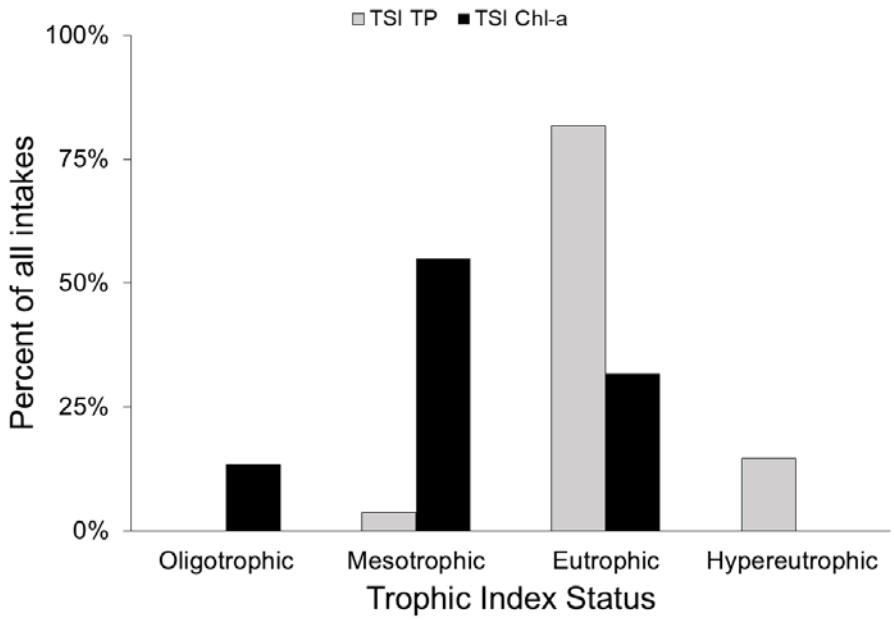

Figure 3.4. Trophic index status (TSI) estimates based on average total phosphorus concentrations (TSI TP) compared to chlorophyll-*a* concentrations (TSI Chl-*a*) collected from 83 raw surface water intakes from 71 drinking water utilities in July 2017 and 2018.

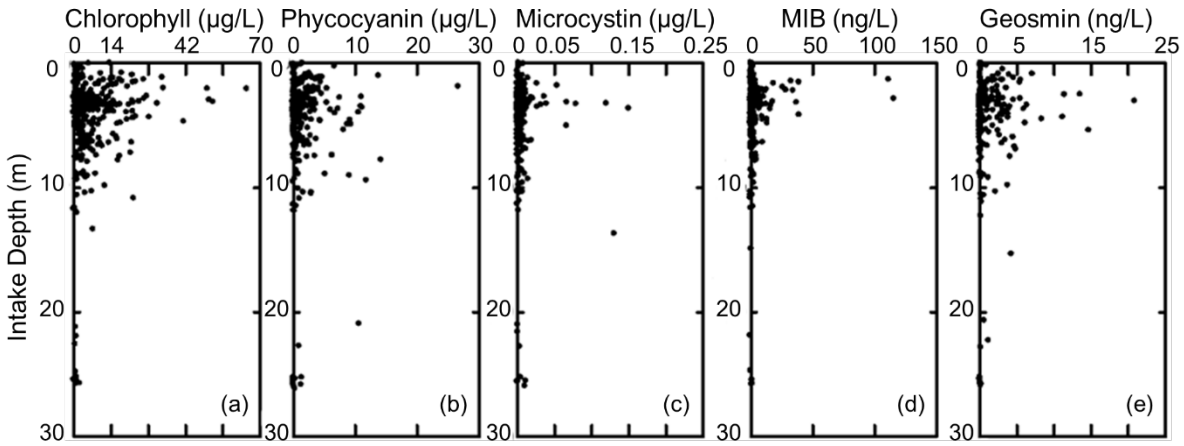

Figure 3.5. Chlorophyll-*a* (a), phycocyanin (b), microcystin (c), MIB (d), and geosmin (e) concentrations by intake depth (m) of raw water collected from 71 drinking water utilities from April 2017 through November 2018.

Chapter 4

Algal blooms in limbo: No sign of degradation or improvement over the past 30 years

Abstract

Algal blooms threaten aquatic ecosystems and local economies worldwide and are believed to be unanimously intensifying due to eutrophication and climate change. Here, we analyze 30 years (1990-2020) of algal bloom, eutrophication, and climate data for 650 lakes located across 11 freshwater ecoregions. Surprisingly, we found 67% of lakes were in a state of equilibrium and lakes that were significantly improving were doing so at a higher magnitude than lakes that were significantly decreasing in water quality. Algal bloom trends were positively correlated to eutrophication, and suggest nutrient management could be preventing further water quality degradation. Results indicate that algal bloom intensification may not be as pervasive as previously believed.

Main text

There is widespread scientific consensus that algal blooms are increasing in intensity and geographic distribution, attributed primarily to climate change and cultural eutrophication (Paerl and Huisman 2008; O'Neil et al. 2012; Taranu et al. 2015; Glibert 2020). Due to the extensive and potentially severe ecologic, economic and public health impacts related to algal blooms, legislations have been enacted in several countries to improve research, monitoring, and management of blooms and their triggers (Hudnell 2010; Zhou et al. 2017). In the United States, whether efforts to reduce nutrient transport have hindered the growing trend in algal blooms is unclear (Dove and Chapra 2015; United States Code 2018; Mahdiyan et al. 2021). We asked how recent algal bloom intensification trends vary spatially, and whether these trends are linked to changes in nutrient abundance, summertime temperature, and precipitation.

To explore algal bloom trends across a wide geographic region, 30-year time series (1990-2020) were generated from the annual median summertime chlorophyll concentrations (µg/L) of 650 lakes throughout 11 freshwater ecoregions (Figure 4.1). Mann-Kendall (M-K) trend statistics were calculated to determine algal bloom trend direction (M-K *S*), significance (M-K *z*, $p < 0.05$), and magnitude (Sen's Slope β), as this non-parametric test is robust despite high interannual variability of summertime chlorophyll concentrations (Gilbert 1987). M-K *S* statistics were also generated from total nitrogen (TN, µg/L), total phosphorus (TP, µg/L), Secchi depth (m, transparency measurement), and climate (i.e., temperature, precipitation, drought) data to determine whether environmental drivers explain algal bloom trends.

Results show that 438 of the 650 study lakes (67%) did not exhibit statistically significant increasing or decreasing trends in summertime algal bloom intensity (Figure 4.2). Lakes exhibiting significant increases in algal bloom intensity (n=103) were comparable in number and

spatial distribution to lakes with significant decreases in algal bloom intensity (n=109), indicating there is no clear spatial pattern of degradation or improvement among the study lakes (Figure 4.1). Moreover, lakes that are significantly improving are doing so at a significantly higher rate than those significantly decreasing in water quality, based on Sen's slope estimates (p = 0.001, Figure 4.2). Weak evidence of extensive algal bloom intensification was surprising, as decreasing trends in summertime algal blooms are rarely reported (Taranu et al. 2015; Ho et al. 2019), but see Oliver et al. 2017; Pi et al. 2021; Wilkinson et al. Accepted.

Lakes showing increasing and decreasing algal bloom trends were uniformly distributed across and within 10 of the 11 freshwater ecoregions (Figure 4.3). A notable exception are lakes located within the Central Prairie ecoregion, which show a significant increasing trend in algal bloom intensity (p <0.0001). There was no significant relationship between algal bloom trends and lake surface area (km^2) or surrounding population density (individuals/$mile^2$, p >0.05, Table 4.2).

Increasing global temperatures and erratic precipitation patterns are known to promote the growth and geographic expansion of bloom-forming and potentially toxic cyanobacteria in freshwater ecosystems (Paerl and Huisman 2008; O'Neil et al. 2012). Summertime air temperature increased across the 43 climate divisions included in the study, with a mean annual increase of 0.033°C. The effect of temperature trends on algal blooms was statistically significant but poorly correlated (p = 0.0007, r^2 =0.02) due to modest differences in temperature increases between the division (Table 4.2, Figure 4.4D). Moreover, elevated temperatures are more closely linked to cyanobacterial dominance and cyanotoxin production than overall phytoplankton abundance (Jöhnk et al. 2008; Kosten et al. 2012; Hayes et al. 2020). Phytoplankton community composition and cyanotoxin prevalence trends are beyond the scope

of this study as most lakes did not report cyanobacterial pigment concentrations (i.e., phycocyanin), phytoplankton counts, or cyanotoxin concentration data. Precipitation and drought trends were not significantly correlated to algal bloom trends (p >0.05, Table 4.2). High nutrient inputs due to intense rainfall events followed by prolonged droughts that increase water column stability and residence times can promote algal blooms in inland systems (Paerl and Huisman 2008; O'Neil et al. 2012). However, whether gradual increases in drought and precipitation affect algal bloom trends is not as well understood and could explain the poor relationship between these parameters and algal bloom trends in our study.

Eutrophication is a leading cause of waterbody impairment in the United States, with 40% and 35% of lakes showing excessive levels of phosphorus and nitrogen, respectively (USEPA 2016). Changes in nitrogen and phosphorus trends for the study lakes were generally statistically insignificant, although 28% of lakes show significant phosphorus reduction (Table 4.1). Nutrient and algal bloom intensification trends were significantly correlated in the study lakes, with a 0.67 (±0.07 95% C.I.) and 0.54 (±0.07 95% C.I.) increase in algal bloom M-K S for every unit increase in TN and TP M-K S, respectively (p <0.0001, Table 4.2, Figure 4.4). Algal bloom trends were also closely associated with Secchi depth trends, with a 0.82 (±0.07 95% C.I.) decrease in algal bloom M-K S for every one unit increase in Secchi depth M-K S (p <0.0001, r^2 = 0.59).

Results from this study contradict the tenet that algal blooms are unanimously intensifying. Most lakes did not show significant algal bloom trends, and there was no clear spatial pattern for the 212 lakes that were experiencing significant changes in algal bloom intensity (Figure 4.1). The paradox between our findings and those of others could be due to study lake physical characteristics (i.e., surface area, distribution), sampling frequency and

length, number of study lakes, or disproportionate research attention being focused on impaired systems. Eutrophication was a stronger predictor of algal bloom intensification than climate variations in our systems, but understanding the interaction between these two drivers will be important for informing resource management as temperatures continue to increase (Taranu et al. 2015; Chapra et al. 2017). Admittedly, while 30-year time series demonstrate recent trends in chlorophyll concentrations, they provide limited information of the pre-industrial prevalence of algal blooms in these lakes (Taranu et al. 2015; Waters 2016). However, this study focuses on whether algal blooms are continuing to intensify despite increases in research, monitoring, and management initiatives. Based on the close relationship between nutrients and algal bloom trends, it appears that legislation and research associated with managing nutrients (United States Code 2018) may be preventing further degradation of aquatic ecosystems.

Methods

Lake data for this study were collected from the Florida Water Atlas, Iowa Department of Natural Resources (DNR), Missouri DNR, US Long-Term Ecological Research Network - Madison Lake Area, Vanni 2019, and Wilkinson et al. (USEPA 2009, 2016; Vanni et al. 2019; Jones et al. 2020; Iowa DNR 2021; Wilkinson et al. Accepted). Lakes were included in the study if the lake was sampled (1) for at least 10 years (Kendall, 1975), (2) with less than a three-year gap between samples for the first 10 years of sampling, and (3) the most recent sample was collected on or after 2016. Lake data were restricted to 1990-2020 samples, as sampling was increasingly inconsistent and sporadic before 1990. Additionally, chlorophyll data had to be collected via alcohol or acetone extraction followed by fluorometric analysis of *in situ* samples, rather than raw fluorescence units or remote sensing chlorophyll estimates. A total of 650 lakes met such criteria, with an average of 22 sample years. For each lake, summertime (July-September) chlorophyll (µg/L), total nitrogen (TN, µg/L), total phosphorus (TP, µg/L), and Secchi depth (m) values, as well as lake physical characteristics were recorded.

Climate division scale annual summertime air temperature (°C), precipitation (mm), and drought (Palmer Z Index) data were accessed through the Climate at a Glance National Oceanic and Atmospheric Administration (NOAA) application (NOAA 2021). Mean summer air temperature values were used to estimate lake surface temperatures, as summer air temperatures are a significant predictor of surface water temperatures (O'Reilly et al. 2015).

Spatial distribution of the lakes was based on freshwater ecoregions, which largely correspond to major watersheds and are designed to spatially divide areas based on freshwater biodiversity (Abell et al. 2008). To simplify statistical analysis, the three study lakes located within the Laurentian Great Lakes freshwater ecoregion were reclassified to the nearest

freshwater ecoregion, as they were less than 3 km from the next neighboring ecoregion. Such lakes were: DeRuyter Reservoir (0.58 km from Chesapeake Bay), Lake Como (2.71 km from Chesapeake Bay), and Millsite Lake (0.6 km from St. Lawrence). 57% of the lakes included in this study were located in the Florida Peninsula freshwater ecoregion. To verify that observations from the Florida Peninsula were not disproportionately driving study trends, the dataset was split between the Florida Peninsula lakes (n=373) and those located within the remaining 10 freshwater ecoregions (n=277). Split datasets did not differ significantly in algal bloom trend significance or magnitude (ANOVA, p >0.05).

The Mann-Kendall trend test (M-K) was utilized to test for the presence of monotonic time trends, as this non-parametric test does not require data to be normally distributed and has low sensitivity to missing values (Mann 1945; Kendall 1975; Gilbert 1987). When lakes had multiple observations per year, annual medians were calculated and used as the representative annual value to reduce the effects of autocorrelation and conform to the required single observation per time period for the M-K test (Gilbert 1987).

The M-K test statistics, S, was calculated by determining the difference between later measured values (y_j) and earlier measured values (y_i) as:

$$S = \sum_{i=1}^{n-1} \sum_{j=i+1}^{n} sign\,(y_j - y_i)$$

$$sign\,(y_j - y_i) = \begin{cases} 1 & if\ sign\,(y_j - y_i) > 0 \\ 0 & if\ sign\,(y_j - y_i) = 0 \\ -1 & if\ sign\,(y_j - y_i) < 0 \end{cases}$$

Where S >1 values indicate that later observations tend to be higher than earlier observations, and the opposite is true when S <-1. The variance of S, $var(S)$, was then calculated as:

$$var(S) = \frac{1}{18}\left[n(n-1)(2n+5) - \sum_{p=1}^{g} t_p\,(t_p-1)(2t_p+5)\right]$$

Where g is the number of tied groups and t_p is the number of data in the pth group. The M-K z statistic was calculated to determine trend significance as follows:

$$z = \begin{cases} (S-1)/\sqrt{var(S)} & if\ S > 1 \\ 0 & if\ S = 0 \\ (S+1)/\sqrt{var(S)} & if\ S < 0 \end{cases}$$

Where a positive or negative $z \geq 1.96$ indicates a significant increasing or decreasing trend, respectively, at a significance level of 0.05 (Gilbert 1987). Sen's slope was calculated to determine trend magnitude, as this method is not greatly affected by missing data or outliers (Sen 1968; Gilbert 1987). Sen's slope (β) is calculated by determining the slope of all pairs of data used to compute S, and then calculating the median of those slopes as:

$$\beta = Median\ \frac{(y_j - y_i)}{(x_j - x_i)} \quad (1 \leq i \leq n)$$

Where y_j and y_i are the time series data at time x_j and x_i, respectively.

Pearson correlation coefficients were calculated to determine the relationship between algal bloom and environmental trends. Algal bloom trends differences amongst freshwater ecoregions were determined through analysis of variance (ANOVA). All statistical analyses were executed utilizing the *trend* and *Kendall* packages of R version 4.0.3 (McLeod 2011; Pohlert 2020).

Table 4.1. Number of lakes showing decreasing, increasing or no change in median summertime chlorophyll (µg/L), Secchi depth (m), total nitrogen (µg/L), total phosphorus (µg/L) trends from 1990-2020 (M-Z *z*, significance level of $p < 0.05$).

	Significant decrease	**Decrease**	**No change**	**Increase**	**Significant increase**	**Total**
Chlorophyll	103	214	20	204	109	650
Secchi depth	68	126	4	129	68	395
Total nitrogen	93	109	4	104	86	396
Total phosphorus	110	123	2	92	69	396

Table 4.2. Relationship between long-term algal bloom trends (chlorophyll, µg/L) and Secchi depth (m) trends, total nitrogen (TN, µg/L) trends, total phosphorus (TN, µg/L) trends, temperature (°C) trends, precipitation (mm) trends, drought (Palmer Z Index) trends, population density (individuals/ mile^2), and lake surface area (km^2). Trends were measured as M-K *S*.

		Effect Estimate (± 95% C.I.)	***p*-value**	**r^2**	**n**
M-K *S* Chlorophyll	M-K *S* Secchi	-0.82 (0.07)	<0.0001	0.59	395
	M-K *S* TN	0.67 (0.07)	<0.0001	0.51	396
	M-K *S* TP	0.54 (0.07)	<0.0001	0.34	396
	M-K *S* Temperature	-0.34 (0.20)	0.0007	0.02	650
	M-K *S* Precipitation	0.11 (0.18)	0.22	0.00	650
	M-K *S* Drought	0.05 (0.19)	0.61	0.00	650
	Population density	0.00 (0.00)	0.17	0.00	650
	Lake surface area	0.26 (0.34)	0.12	0.00	650

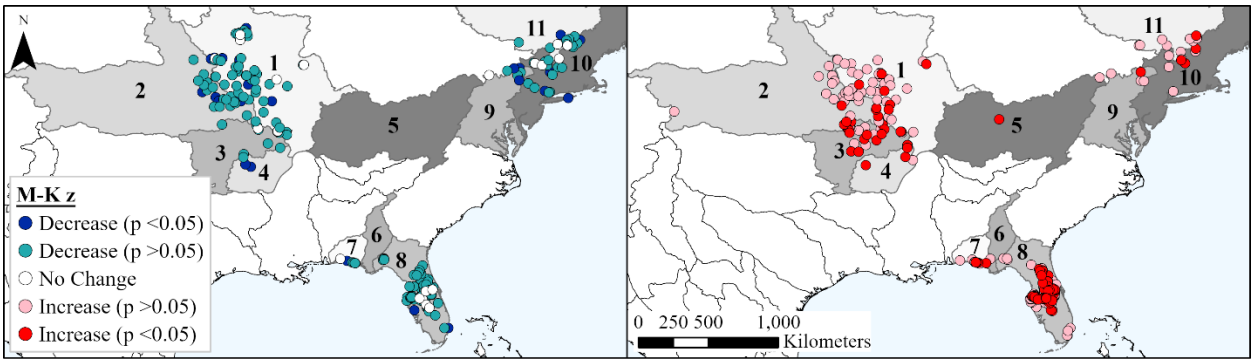

Figure 4.1. Geographic distribution of the 650 study lakes. Fill colors indicate the direction and significance (M-K *z*, significance level 0.05) of algal bloom trends from 1990 to 2020. Freshwater ecoregions are identified by numbers: Upper Mississippi (1), Middle Missouri (2), Central Prairie (3), Ozark Highlands (4), Teays (5), Apalachicola (6), West Florida Gulf (7), Florida Peninsula (8), Chesapeake Bay (9), Atlantic Drainages (10), and St. Lawrence (11).

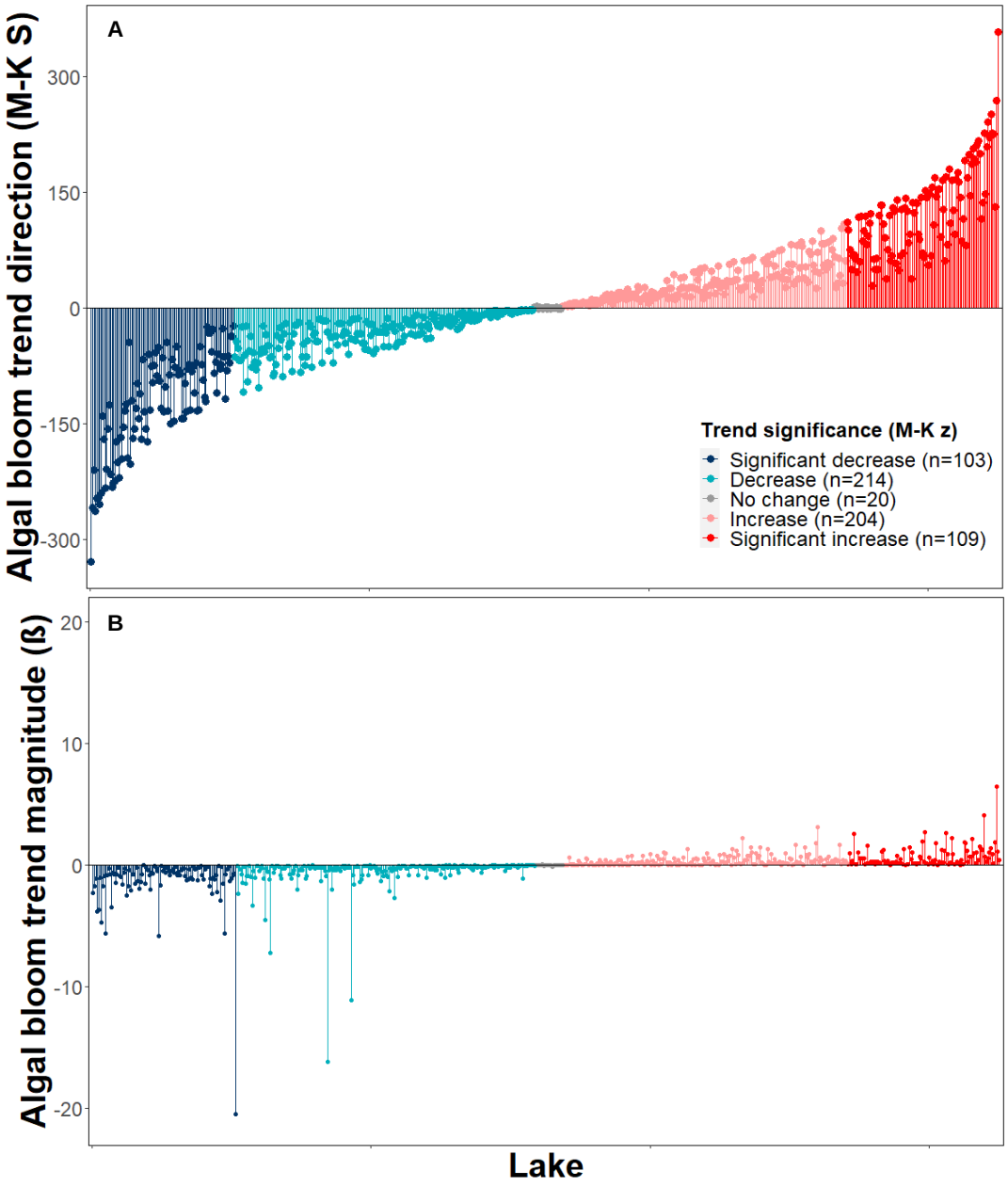

Figure 4.2. Algal bloom intensity trend direction (A, M-K *S*) and magnitude (B, Sen's Slope β) from 1990 to 2020 for 650 lakes. Trend statistic $S < -1$ and $S > 1$ indicate a decrease or increase in algal bloom intensity, respectively. The 650 lakes are arranged in order of increasing trend significance (M-Z *z*), based on a significance level of $p < 0.05$.

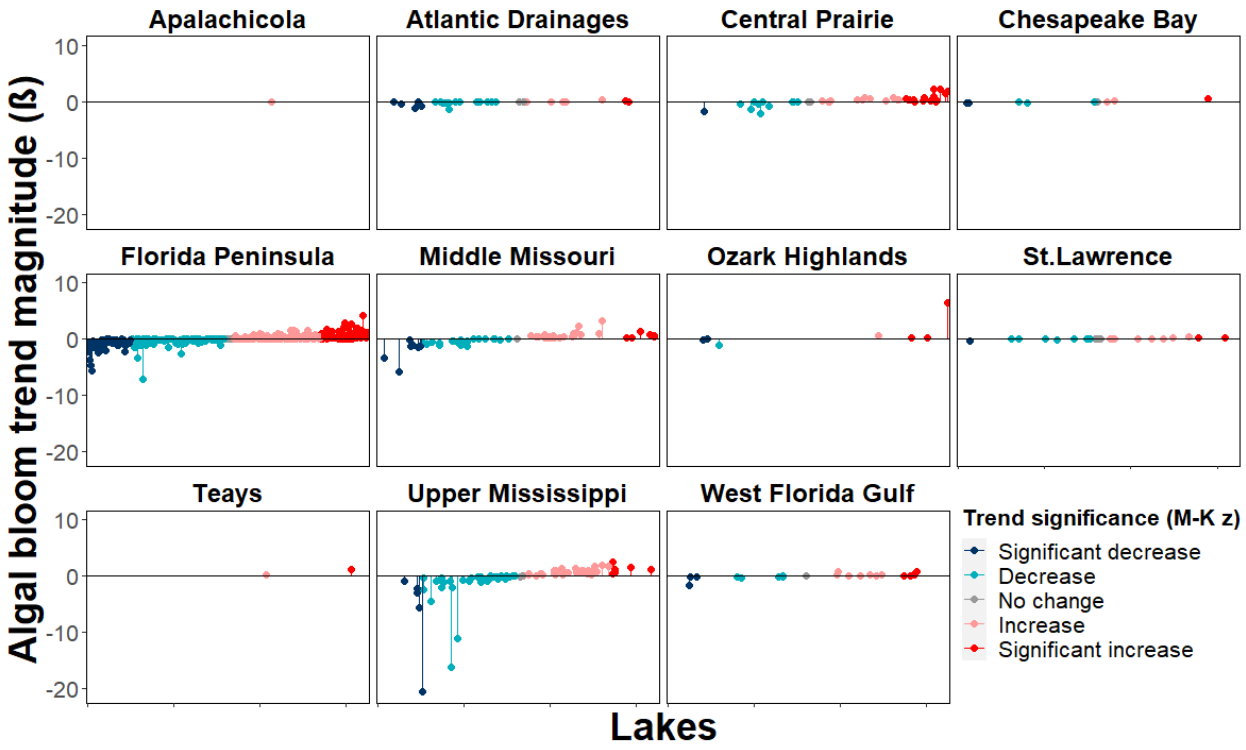

Figure 4.3. Algal bloom intensity trend magnitude (Sen's Slope β) from 1990 to 2020 for 650 lakes, grouped by freshwater ecoregion. The lakes are arranged in order of increasing trend significance (M-Z *z*), based on a significance level of $p < 0.05$.

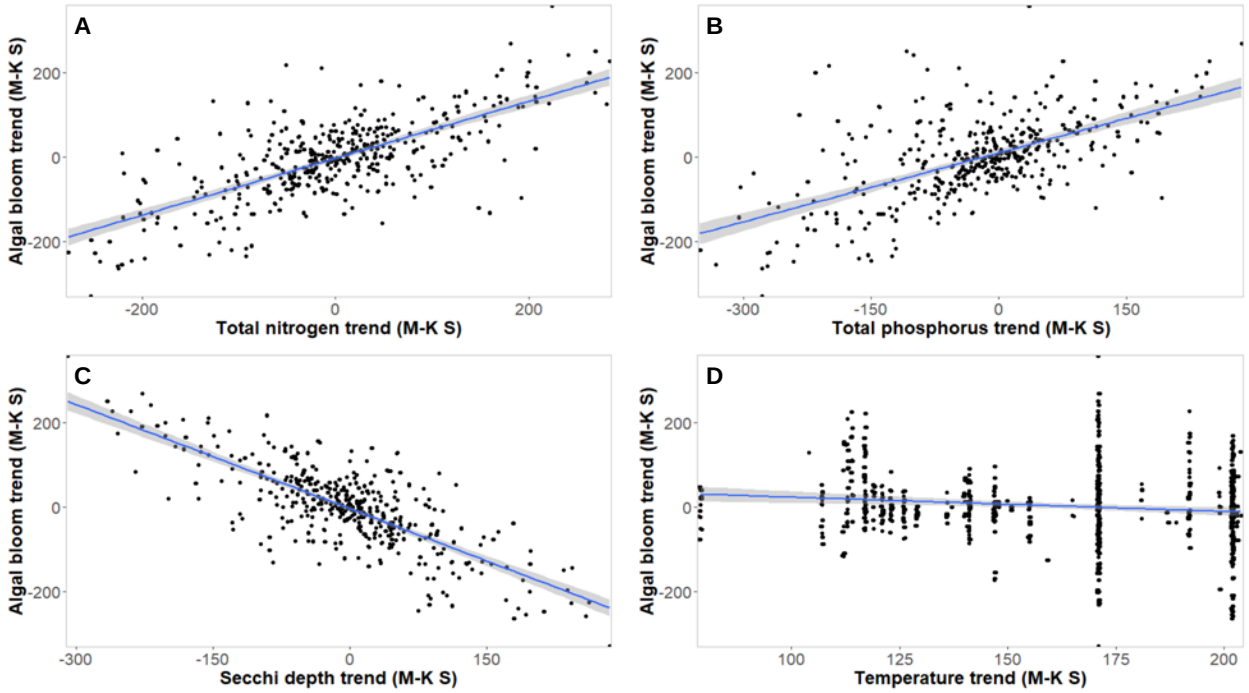

Figure 4.4. Relationship between algal bloom intensity and total nitrogen (A), total phosphorus (B), Secchi depth (C), and summertime temperature (D) trend direction (M-K *S*) from 1990 to 2020 for 650 lakes. Trend statistic $S < -1$ and $S > 1$ indicate a decrease or increase in parameter values, respectively. Gray shading represents 95% confidence intervals.

References

Abell, R., M. L. Thieme, C. Revenga, and others. 2008. Freshwater ecoregions of the world: a new map of biogeographic units for freshwater biodiversity conservation. BioScience **58**: 403–414. doi:10.1641/B580507

Alabama Department of Environmental Management. 2017. Chapter 335-6-10: Water quality criteria. Water division - Water quality program.

Alabama Department of Environmental Management. 2018. Alabama integrated water quality monitoring and assessment report: Water quality in Alabama 2016-2018. Alabama Department of Environmental Management.

Allan, J. D. 1976. Life history patterns in zooplankton. The American Naturalist **110**: 165–180.

An, J., and W. W. Carmichael. 1994. Use of a colorimetric protein phosphatase inhibition assay and enzyme linked immunosorbent assay for the study of microcystins and nodularins. Toxicon **32**: 1495–1507. doi:10.1016/0041-0101(94)90308-5

Barnes, E. M., T. R. Clarke, S. E. Richards, and others. 2000. Coincident detection of crop water stress, nitrogen status and canopy density using ground based multispectral data. *Fifth International Conference on Precision Agriculture*. Proceedings of the International Conference on Precision Agriculture and Other Resource Management.

Beck, R., S. Zhan, H. Liu, and others. 2016. Comparison of satellite reflectance algorithms for estimating chlorophyll-a in a temperate reservoir using coincident hyperspectral aircraft imagery and dense coincident surface observations. Remote Sens. Environ. **178**: 15–30. doi:10.1016/j.rse.2016.03.002

Beisner, B., E. Mccauley, and F. Wrona. 1996. Temperature-mediated dynamics of planktonic food chains: the effect of an invertebrate carnivore. Freshwater Biol. **35**: 219–232. doi:10.1046/j.1365-2427.1996.00492.x

Bendig, J., K. Yu, H. Aasen, A. Bolten, S. Bennertz, J. Broscheit, M. L. Gnyp, and G. Bareth. 2015. Combining UAV-based plant height from crop surface models, visible, and near infrared vegetation indices for biomass monitoring in barley. Int. J. Appl. Earth Obs. Geoinf. **39**: 79–87. doi:10.1016/j.jag.2015.02.012

Bollard-Breen, B., J. D. Brooks, M. R. L. Jones, and others. 2015. Application of an unmanned aerial vehicle in spatial mapping of terrestrial biology and human disturbance in the McMurdo Dry Valleys, East Antarctica. Polar Biol. **38**: 573–578. doi:10.1007/s00300-014-1586-7

Brando, V. E., and A. G. Dekker. 2003. Satellite hyperspectral remote sensing for estimating estuarine and coastal water quality. IEEE Trans. Geosci. Remote Sens. **41**: 1378–1387. doi:10.1109/TGRS.2003.812907

Briand, J.-F., S. Jacquet, C. Bernard, and J.-F. Humbert. 2003. Health hazards for terrestrial vertebrates from toxic cyanobacteria in surface water ecosystems. Vet. Res. **34**: 361–377. doi:10.1051/vetres:2003019

Brivio, P. A., C. Giardino, and E. Zilioli. 2001. Determination of chlorophyll concentration changes in Lake Garda using an image-based radiative transfer code for Landsat TM images. Int. J. Remote Sens. **22**: 487–502. doi:10.1080/014311601450059

Burgos, L., M. Lehmann, D. Simon, and others. 2014. Agents of earthy-musty taste and odor in water: Evaluation of cytotoxicity, genotoxicity and toxicogenomics. Sci. Total Environ. **490**: 679–685. doi:10.1016/j.scitotenv.2014.05.047

Cai, F. F., G. L. Yu, K. Zhang, and others. 2017. Geosmin production and polyphasic characterization of *Oscillatoria limosa* Agardh ex Gomont isolated from the open canal of a large drinking water system in Tianjin City, China. Harmful Algae **69**: 28–37. doi:10.1016/j.hal.2017.09.006

Camargo Neto, J. 2004. A combined statistical-soft computing approach for classification and mapping weed species in minimum -tillage systems. ETD collection for University of Nebraska - Lincoln 1–170.

Cao, Q., Y. Miao, H. Wang, S. Huang, S. Cheng, R. Khosla, and R. Jiang. 2013. Non-destructive estimation of rice plant nitrogen status with crop circle multispectral active canopy sensor. Field Crops Res. **154**: 133–144. doi:10.1016/j.fcr.2013.08.005

Carlson, R. E. 1977. A trophic state index for lakes. Limnol. Oceanogr. **22**: 361–369. doi:10.4319/lo.1977.22.2.0361

Carlson, R. E. 1991. Expanding the trophic state concept to identify non-nutrient limited lakes and reservoirs. *Proceedings of a National Conference on Enhancing the States' Lake Management Programs*. Proceedings of the National Conference on Enhancing the States' Lake Management Programs. 59–71.

Chapra, S. C., B. Boehlert, C. Fant, and others. 2017. Climate Change Impacts on Harmful Algal Blooms in U.S. Freshwaters: A Screening-Level Assessment. Environ. Sci. Technol. **51**: 8933–8943. doi:10.1021/acs.est.7b01498

Chen, J. M. 1996. Evaluation of Vegetation Indices and a Modified Simple Ratio for Boreal Applications. Can. J. Remote Sens. **22**: 229–242. doi:10.1080/07038992.1996.10855178

Cheng, K. H., S. N. Chan, and J. H. W. Lee. 2020. Remote sensing of coastal algal blooms using unmanned aerial vehicles (UAVs). Mar. Pollut. Bull. **152**: 110889. doi:10.1016/j.marpolbul.2020.110889

Chislock, M. F., R. B. Kaul, K. A. Durham, O. Sarnelle, and A. E. Wilson. 2019a. Eutrophication mediates rapid clonal evolution in *Daphnia pulicaria*. Freshwater Biol. **64**: 1275–1283. doi:10.1111/fwb.13303

Chislock, M. F., O. Sarnelle, L. M. Jernigan, V. R. Anderson, A. Abebe, and A. E. Wilson. 2019b. Consumer adaptation mediates top–down regulation across a productivity gradient. Oecologia **190**: 195–205. doi:10.1007/s00442-019-04401-4

Chislock, M. F., O. Sarnelle, B. K. Olsen, E. Doster, and A. E. Wilson. 2013. Large effects of consumer offense on ecosystem structure and function. Ecology **94**: 2375–2380. doi:10.1890/13-0320.1

Choo, Y., G. Kang, D. Kim, and S. Lee. 2018. A study on the evaluation of water-bloom using image processing. Environ. Sci. Pollut. Res.remote **25**: 36775–36780. doi:10.1007/s11356-018-3578-6

Cillero Castro, C., J. A. Domínguez Gómez, J. Delgado Martín, B. A. Hinojo Sánchez, J. L. Cereijo Arango, F. A. Cheda Tuya, and R. Díaz-Varela. 2020. An UAV and satellite multispectral data approach to monitor water quality in small reservoirs. Remote Sens. **12**: 1514. doi:10.3390/rs12091514

Claska, M. E., and J. J. Gilbert. 1998. The effect of temperature on the response of *Daphnia* to toxic cyanobacteria. Freshwater Biol. **39**: 221–232. doi:10.1046/j.1365-2427.1998.00276.x

Clissold, F. J., and S. J. Simpson. 2015. Temperature, food quality and life history traits of herbivorous insects. Curr. Opin. Insect Sci. **11**: 63–70. doi:10.1016/j.cois.2015.10.011

DeVries, S. E., F. D. Galey, M. Namikoshi, and J. C. Woo. 1993. Clinical and pathologic findings of blue-green algae (*Microcystis aeruginosa*) intoxication in a dog. J VET Diagn Invest **5**: 403–408. doi:10.1177/104063879300500317

Dietrich, A. M., and G. A. Burlingame. 2015. Critical review and rethinking of USEPA secondary standards for maintaining organoleptic quality of drinking water. Environ. Sci. Technol. **49**: 708–720. doi:10.1021/es504403t

Dodson, S. I., and T. Hanazato. 1995. Commentary on effects of anthropogenic and natural organic chemicals on development, swimming behavior, and reproduction of *Daphnia*, a key member of aquatic ecosystems. Environ. Health Perspect. **103**: 7–11.

Dove, A., and S. C. Chapra. 2015. Long-term trends of nutrients and trophic response variables for the Great Lakes. Limnol. Oceanogr. **60**: 696–721. doi:https://doi.org/10.1002/lno.10055

Downing, J. A., S. B. Watson, and E. McCauley. 2001. Predicting cyanobacteria dominance in lakes. Can. J. Fish. Aquat. Sci. **58**: 1905–1908. doi:10.1139/cjfas-58-10-1905

Drozd, A., P. de T. Pinto, V. Fernández, M. Bazzalo, F. Bordet, and G. Ibañez. 2020. Hyperspectral remote sensing monitoring of cyanobacteria blooms in a large South American reservoir: high- and medium-spatial resolution satellite algorithm simulation. Mar. Freshwater Res. **71**: 593–605. doi:10.1071/MF18429

Dudgeon, D., A. H. Arthington, M. O. Gessner, and others. 2007. Freshwater biodiversity: importance, threats, status and conservation challenges. Biol. Rev. Cambridge Philos. Soc. **81**: 163–182. doi:10.1017/S1464793105006950

Dunlap, C. R., K. S. Sklenar, and L. J. Blake. 2015. A costly endeavor: Addressing algae problems in a water supply. Journal AWWA **107**: E255–E262. doi:10.5942/jawwa.2015.107.0055

Dupuis, A. P., and B. J. Hann. 2009. Warm spring and summer water temperatures in small eutrophic lakes of the Canadian prairies: potential implications for phytoplankton and zooplankton. J. Plankton Res. **31**: 489–502. doi:10.1093/plankt/fbp001

Ebert, D. 2005. Ecology, epidemiology, and evolution of parasitism in *Daphnia*, National Center for Biotechnology Information (US).

Elleman, T. C., I. R. Falconer, A. R. Jackson, and M. T. Runnegar. 1978. Isolation, characterization and pathology of the toxin from a *Microcystis aeruginosa* (= *Anacystis cyanea*) bloom. Aust. J. Biol. Sci. **31**: 209–218. doi:10.1071/bi9780209

Flynn, K. F., and S. C. Chapra. 2014. Remote sensing of submerged aquatic vegetation in a shallow non-turbid river using an unmanned aerial vehicle. Remote Sens. **6**: 12815–12836. doi:10.3390/rs61212815

Fox, J., Z. Nie, and J. Byrnes. 2017. sem: Structural Equation Modeling, RStudio, Inc.

Gamon, J. A., and J. S. Surfus. 1999. Assessing leaf pigment content and activity with a reflectometer. New Phytol. **143**: 105–117. doi:10.1046/j.1469-8137.1999.00424.x

Gilbert, R. O. 1987. Statistical methods for environmental pollution monitoring, Van Nostrand Reinhold Co.

Gitelson, A. A., and M. N. Merzlyak. 1998. Remote sensing of chlorophyll concentration in higher plant leaves. Adv. Space Res. **22**: 689–692. doi:10.1016/S0273-1177(97)01133-2

Gitelson, A. A., R. Stark, U. Grits, D. Rundquist, Y. Kaufman, and D. Derry. 2002. Vegetation and soil lines in visible spectral space: A concept and technique for remote estimation of

vegetation fraction. Int. J. Remote Sens. **23**: 2537–2562. doi:10.1080/01431160110107806

Gitelson, A. A., A. Viña, T. J. Arkebauer, D. C. Rundquist, G. Keydan, and B. Leavitt. 2003. Remote estimation of leaf area index and green leaf biomass in maize canopies. Geophys. Res. Lett. **30**. doi:10.1029/2002GL016450

Glibert, P. M. 2020. Harmful algae at the complex nexus of eutrophication and climate change. Harmful Algae **91**: 101583. doi:10.1016/j.hal.2019.03.001

Graham, J. L., N. M. Dubrovsky, and S. Eberts. 2017. Cyanobacterial harmful algal blooms and U.S. Geological Survey Science Capabilities. Open-File Report 2016–1174. 2016–1174 U.S. Geological Survey.

Griffith, A. W., and C. J. Gobler. 2020. Harmful algal blooms: A climate change co-stressor in marine and freshwater ecosystems. Harmful Algae **91**: 101590. doi:10.1016/j.hal.2019.03.008

Gross, A., and C. E. Boyd. 1998. A digestion procedure for the simultaneous determination of total nitrogen and total phosphorus in pond water. J. World Aquacult. Soc. **29**: 300–303. doi:10.1111/j.1749-7345.1998.tb00650.x

Hague, T., N. D. Tillett, and H. Wheeler. 2006. Automated crop and weed monitoring in widely spaced cereals. Precis. Agric. **7**: 21–32. doi:10.1007/s11119-005-6787-1

Hairston, N. G., W. Lampert, C. E. Caceres, and others. 1999. Lake ecosystems - Rapid evolution revealed by dormant eggs. Nature **401**: 446–446. doi:10.1038/46731

Harris, T. D., V. H. Smith, J. L. Graham, D. B. Van de Waal, L. P. Tedesco, and N. Clercin. 2016. Combined effects of nitrogen to phosphorus and nitrate to ammonia ratios on

cyanobacterial metabolite concentrations in eutrophic Midwestern USA reservoirs. Inland Waters **6**: 199–210. doi:10.5268/iw-6.2.938

Hayes, N. M., H. A. Haig, G. L. Simpson, and P. R. Leavitt. 2020. Effects of lake warming on the seasonal risk of toxic cyanobacteria exposure. Limnol. Oceanogr. Lett. **5**: 393–402. doi:https://doi.org/10.1002/lol2.10164

He, X., Y.-L. Liu, A. Conklin, and others. 2016. Toxic cyanobacteria and drinking water: Impacts, detection, and treatment. Harmful Algae **54**: 174–193. doi:10.1016/j.hal.2016.01.001

Heisler, J., P. M. Glibert, J. M. Burkholder, and others. 2008. Eutrophication and harmful algal blooms: A scientific consensus. Harmful Algae **8**: 3–13. doi:10.1016/j.hal.2008.08.006

Hering, D., L. Carvalho, C. Argillier, and others. 2015. Managing aquatic ecosystems and water resources under multiple stress — An introduction to the MARS project. Sci. Total Environ. **503–504**: 10–21. doi:10.1016/j.scitotenv.2014.06.106

Hietala, J., C. Laurén-Määttä, and M. Walls. 1997. Sensitivity of *Daphnia* to toxic cyanobacteria: effects of genotype and temperature. Freshwater Biol. **37**: 299–306. doi:10.1046/j.1365-2427.1997.d01-555.x

Hlina, B. L. 2019. ecotox: Analysis of Ecotoxicology, RStudio, Inc.

Ho, J. C., A. M. Michalak, and N. Pahlevan. 2019. Widespread global increase in intense lake phytoplankton blooms since the 1980s. Nature **574**: 667–670. doi:10.1038/s41586-019-1648-7

Hochmuth, J. D., and K. A. C. D. Schamphelaere. 2014. The effect of temperature on the sensitivity of *Daphnia magna* to cyanobacteria is genus dependent. Environ. Toxicol. Chem. **33**: 2333–2343. doi:10.1002/etc.2681

Hu, C. 2009. A novel ocean color index to detect floating algae in the global oceans. Remote Sens. Environ. **113**: 2118–2129. doi:10.1016/j.rse.2009.05.012

Hudnell, H. K. 2010. The state of U.S. freshwater harmful algal blooms assessments, policy and legislation. Toxicon **55**: 1024–1034. doi:10.1016/j.toxicon.2009.07.021

Huisman, J., G. A. Codd, H. W. Paerl, B. W. Ibelings, J. M. H. Verspagen, and P. M. Visser. 2018. Cyanobacterial blooms. Nat. Rev. Microbiol. **16**: 471–483. doi:10.1038/s41579-018-0040-1

Iowa DNR. 2021. Iowa Department of Natural Resources Water Quality Monitoring and Assessment.

Izaguirre, G., C. J. Hwang, S. W. Krasner, and M. J. McGuire. 1982. Geosmin and 2-Methylisoborneol from cyanobacteria in three water supply systems. Appl. Environ. Microbiol. **43**: 708–714. doi:10.1128/AEM.43.3.708-714.1982

Jiang, Z., A. R. Huete, Y. Kim, and K. Didan. 2007. 2-band enhanced vegetation index without a blue band and its application to AVHRR data. Proceedings of the Optical Engineering + Applications. 667905.

Jöhnk, K. D., J. Huisman, J. Sharples, B. Sommeijer, P. M. Visser, and J. M. Stroom. 2008. Summer heatwaves promote blooms of harmful cyanobacteria. Global Change Biol. **14**: 495–512. doi:10.1111/j.1365-2486.2007.01510.x

Jones, J., A. Argerich, D. Obrecht, A. Thorpe, and R. North. 2020. Missouri lakes and reservoirs long-term limnological dataset. Dataset. doi:10.6073/pasta/86d8d176e91410566b4de51df44c2624

Jüttner, F., and S. B. Watson. 2007. Biochemical and ecological control of geosmin and 2-methylisoborneol in source waters. Appl. Environ. Microbiol. **73**: 4395–4406. doi:10.1128/aem.02250-06

Kasinak, J.-M. E., B. M. Holt, M. F. Chislock, and A. E. Wilson. 2015. Benchtop fluorometry of phycocyanin as a rapid approach for estimating cyanobacterial biovolume. J. Plankton Res. **37**: 248–257. doi:10.1093/plankt/fbu096

Kataoka, T., T. Kaneko, H. Okamoto, and S. Hata. 2003. Crop growth estimation system using machine vision. *2003 IEEE/ASME International Conference on Advanced Intelligent Mechatronics (AIM 2003)*. IEEE. 1079–1083.

Kendall, M. G. 1975. Rank correlation methods, 4th ed. Griffin.

Khiari, D., and S. Watson. 2007. Tastes and odours in drinking water: where are we today? Water Sci. Technol. **55**: 365–366. doi:10.2166/wst.2007.199

Kilham, S., D. Kreeger, C. Goulden, and S. Lynn. 1997. Effects of nutrient limitation on biochemical constituents of *Ankistrodesmus falcatus*. Freshwater Biol. **38**: 591–596. doi:10.1046/j.1365-2427.1997.00231.x

Kislik, C., I. Dronova, and M. Kelly. 2018. UAVs in support of algal bloom research: A review of current applications and future opportunities. Drones **2**: 35. doi:10.3390/drones2040035

Korpelainen, H. 1986. The effects of temperature and photoperiod on life history parameters of *Daphnia magna* (Crustacea: Cladocera). Freshwater Biol. **16**: 615–620. doi:10.1111/j.1365-2427.1986.tb01004.x

Kosten, S., V. L. M. Huszar, E. Bécares, and others. 2012. Warmer climates boost cyanobacterial dominance in shallow lakes. Global Change Biol. **18**: 118–126. doi:10.1111/j.1365-2486.2011.02488.x

Kutser, T. 2004. Quantitative detection of chlorophyll in cyanobacterial blooms by satellite remote sensing. Limnol. Oceanogr. **49**: 2179–2189. doi:10.4319/lo.2004.49.6.2179

Kutser, T., L. Metsamaa, N. Strömbeck, and E. Vahtmäe. 2006. Monitoring cyanobacterial blooms by satellite remote sensing. Estuarine Coastal Shelf Sci. **67**: 303–312. doi:10.1016/j.ecss.2005.11.024

Lampert, W. 1987. Laboratory studies on zooplankton-cyanobacteria interactions. N. Z. J. Mar. Freshwater Res. **21**: 483–490. doi:10.1080/00288330.1987.9516244

Lampert, W. 1993. Phenotypic plasticity of the size at first reproduction in *Daphnia*: The importance of maternal size. Ecology **74**: 1455–1466. doi:10.2307/1940074

Lampert, W., and I. Trubetskova. 1996. Juvenile growth rate as a measure of fitness in *Daphnia*. Funct. Ecol. **10**: 631–635. doi:10.2307/2390173

Larsson, P., and S. Dodson. 1993. Invited review - Chemical communication in planktonic animals. Arch. Hydrobiol. Suppl. **129**: 129–155. doi:10.1127/archiv-hydrobiol/129/1993/129

Lomax, A. S., W. Corso, and J. F. Etro. 2005. Employing unmanned aerial vehicles (UAVs) as an element of the Integrated Ocean Observing System. *OCEANS 2005 MTS/IEEE*. Proceedings of the OCEANS 2005 MTS/IEEE. 184-190 Vol. 1.

Lu, B., Y. He, and P. D. Dao. 2019. Comparing the performance of multispectral and hyperspectral images for estimating vegetation properties. IEEE J. Sel. Top. Appl. Earth Obs. Remote Sens. **12**: 1784–1797. doi:10.1109/JSTARS.2019.2910558

Mahdiyan, O., A. Filazzola, L. A. Molot, D. Gray, and S. Sharma. 2021. Drivers of water quality changes within the Laurentian Great Lakes region over the past 40 years. Limnol. Oceanogr. **66**: 237–254. doi:https://doi.org/10.1002/lno.11600

Malzahn, A. M., D. Doerfler, and M. Boersma. 2016. Junk food gets healthier when it's warm. Limnol. Oceanogr. **61**: 1677–1685. doi:10.1002/lno.10330

Mann, H. B. 1945. Nonparametric Tests Against Trend. Econometrica **13**: 245–259. doi:10.2307/1907187

Manzi, F., R. Agha, Y. Lu, F. Ben-Ami, and J. Wolinska. 2020. Temperature and host diet jointly influence the outcome of infection in a *Daphnia*-fungal parasite system. Freshwater Biol. **65**: 757–767. doi:10.1111/fwb.13464

MAPIR CAMERA. 2020. Processing Survey3 Camera Images. MAPIR CAMERA.

Masclaux, H., A. Bec, M. J. Kainz, C. Desvilettes, L. Jouve, and G. Bourdier. 2009. Combined effects of food quality and temperature on somatic growth and reproduction of two freshwater cladocerans. Limnol. Oceanogr. **54**: 1323–1332. doi:10.4319/lo.2009.54.4.1323

MaxMax. 2015. Enhanced Normalized Difference Vegetation Index (ENDVI). MaxMax.com.

McGuire, M. J. 1995. Off-flavor as the consumer's measure of drinking water safety. Water Sci. Technol. **31**: 1–8. doi:10.1016/0273-1223(95)00448-V

McLeod, A. I. 2011. Package 'Kendall': Kendall rank correlation and Mann-Kendall trend test,.

Merel, S., D. Walker, R. Chicana, S. Snyder, E. Baurès, and O. Thomas. 2013. State of knowledge and concerns on cyanobacterial blooms and cyanotoxins. Environ. Int. **59**: 303–327. doi:10.1016/j.envint.2013.06.013

Müller-Navarra, D. C., M. T. Brett, A. M. Liston, and C. R. Goldman. 2000. A highly unsaturated fatty acid predicts carbon transfer between primary producers and consumers. Nature **403**: 74–77. doi:10.1038/47469

NOAA. 2021. NOAA National Centers for Environmental Information, Climate at a glance: divisional time series.

Nõges, P., C. Argillier, Á. Borja, and others. 2016. Quantified biotic and abiotic responses to multiple stress in freshwater, marine and ground waters. Sci. Total Environ. **540**: 43–52. doi:10.1016/j.scitotenv.2015.06.045

Oliver, R. L., D. P. Hamilton, J. D. Brookes, and G. G. Ganf. 2012. Physiology, blooms and prediction of planktonic cyanobacteria, p. 155–194. *In* B.A. Whitton [ed.], Ecology of Cyanobacteria II: Their Diversity in Space and Time. Springer Netherlands.

Oliver, S. K., S. M. Collins, P. A. Soranno, T. Wagner, E. H. Stanley, J. R. Jones, C. A. Stow, and N. R. Lottig. 2017. Unexpected stasis in a changing world: Lake nutrient and chlorophyll trends since 1990. Global Change Biol. **23**: 5455–5467. doi:https://doi.org/10.1111/gcb.13810

Olsen, B. K., M. F. Chislock, and A. E. Wilson. 2016. Eutrophication mediates a common off-flavor compound, 2-methylisoborneol, in a drinking water reservoir. Water Res. **92**: 228–234. doi:10.1016/j.watres.2016.01.058

O'Neil, J. M., T. W. Davis, M. A. Burford, and C. J. Gobler. 2012. The rise of harmful cyanobacteria blooms: The potential roles of eutrophication and climate change. Harmful Algae **14**: 313–334. doi:10.1016/j.hal.2011.10.027

Orcutt, J. D., and K. G. Porter. 1984. The synergistic effects of temperature and food concentration on life history parameters of *Daphnia*. Oecologia **63**: 300–306. doi:10.1007/BF00390657

O'Reilly, C. M., S. Sharma, D. K. Gray, and others. 2015. Rapid and highly variable warming of lake surface waters around the globe. Geophys. Res. Lett. **42**: 10,773-10,781. doi:https://doi.org/10.1002/2015GL066235

Ortega-Terol, D., D. Hernandez-Lopez, R. Ballesteros, and D. Gonzalez-Aguilera. 2017. Automatic hotspot and sun glint detection in UAV multispectral images. Sensors **17**. doi:10.3390/s17102352

Paerl, H. W., and J. Huisman. 2008. Climate - Blooms like it hot. Science **320**: 57–58. doi:10.1126/science.1155398

Paul, R. J., T. Lamkemeyer, J. Maurer, O. Pinkhaus, R. Pirow, M. Seidl, and B. Zeis. 2004. Thermal acclimation in the microcrustacean *Daphnia*: a survey of behavioural, physiological and biochemical mechanisms. J. Therm. Bio **29**: 655–662. doi:10.1016/j.jtherbio.2004.08.035

Peng Gong, Ruiliang Pu, G. S. Biging, and M. R. Larrieu. 2003. Estimation of forest leaf area index using vegetation indices derived from Hyperion hyperspectral data. IEEE Trans. Geosci. Remote Sens. **41**: 1355–1362. doi:10.1109/TGRS.2003.812910

Perkins, R. G., E. I. Slavin, T. M. C. Andrade, and others. 2019. Managing taste and odour metabolite production in drinking water reservoirs: The importance of ammonium as a key nutrient trigger. J. Environ. Manage. **244**: 276–284. doi:10.1016/j.jenvman.2019.04.123

Pi, X., L. Feng, W. Li, and others. 2021. Chlorophyll-a concentrations in 82 large alpine lakes on the Tibetan Plateau during 2003–2017: temporal–spatial variations and influencing factors. Int. J. Digital Earth **0**: 1–22. doi:10.1080/17538947.2021.1872722

Pohlert, T. 2020. Package 'trend': non-parametric trend tests and change-point detection,.

Przytulska, A., M. Bartosiewicz, M. Rautio, F. Dufresne, and W. F. Vincent. 2015. Climate effects on high latitude *Daphnia* via food quality and thresholds. PLoS ONE **10**: 1–15. doi:10.1371/journal.pone.0126231

Rouse, W., R. H. Haas, J. A. Schell, and D. W. Deering. 1974. Monitoring vegetation systems in the Great Plains with ERTS. Proceedings of the Proceedings of the Third Earth Resources Technology Satellite- 1 Symposium. 301–317.

RStudio Team. 2015. RStudio: Integrated Development for R, RStudio, Inc.

Saadoun, I. M. K., K. K. Schrader, and W. T. Blevins. 2001. Environmental and nutritional factors affecting geosmin synthesis by *Anabaena* sp. Water Res. **35**: 1209–1218. doi:10.1016/s0043-1354(00)00381-x

Sarada, R., M. G. Pillai, and G. A. Ravishankar. 1999. Phycocyanin from *Spirulina* sp: influence of processing of biomass on phycocyanin yield, analysis of efficacy of extraction methods and stability studies on phycocyanin. Process Biochem. **34**: 795–801. doi:10.1016/S0032-9592(98)00153-8

Sarnelle, O., and A. E. Wilson. 2005. Local adaptation of *Daphnia pulicaria* to toxic cyanobacteria. Limnol. Oceanogr. **50**: 1565–1570. doi:doi.org/10.4319/lo.2005.50.5.1565

Sartory, D. P., and J. U. Grobbelaar. 1984. Extraction of chlorophyll-a from freshwater phytoplankton for spectrophotometric analysis. Hydrobiologia **114**: 177–187. doi:10.1007/BF00031869

Schaffner, L. R., L. Govaert, L. De Meester, and others. 2019. Consumer-resource dynamics is an eco-evolutionary process in a natural plankton community. Nat. Ecol. Evol. **3**: 1351–1358. doi:10.1038/s41559-019-0960-9

Sen, P. K. 1968. Estimates of the Regression Coefficient Based on Kendall's Tau. J. Am. Stat. Assoc. **63**: 1379–1389. doi:10.1080/01621459.1968.10480934

Shi, K., Y. Zhang, Y. Zhou, X. Liu, G. Zhu, B. Qin, and G. Gao. 2017. Long-term MODIS observations of cyanobacterial dynamics in Lake Taihu: Responses to nutrient enrichment and meteorological factors. Sci. Rep. **7**. doi:10.1038/srep40326

Smith, V. H. 1983. Low nitrogen to phosphorus ratios favor dominance by blue-green algae in lake phytoplankton. Science **221**: 669–671. doi:10.1126/science.221.4611.669

Smith, V. H., J. Sieber-Denlinger, F. deNoyelles, S. Campbell, S. Pan, S. J. Randtke, G. T. Blain, and V. A. Strasser. 2002. Managing taste and odor problems in a eutrophic drinking water reservoir. Lake Reservoir Manage. **18**: 319–323. doi:10.1080/07438140209353938

Sperfeld, E., and A. Wacker. 2009. Effects of temperature and dietary sterol availability on growth and cholesterol allocation of the aquatic keystone species *Daphnia*. J. Exp. Biol. **212**: 3051–3059. doi:10.1242/jeb.031401

Strayer, D. L. 2010. Alien species in fresh waters: ecological effects, interactions with other stressors, and prospects for the future. Freshwater Biol. **55**: 152–174. doi:10.1111/j.1365-2427.2009.02380.x

Stumpf, R. P., T. T. Wynne, D. B. Baker, and G. L. Fahnenstiel. 2012. Interannual variability of cyanobacterial blooms in Lake Erie. PLoS ONE **7**: e42444. doi:10.1371/journal.pone.0042444

Sugiura, N., N. Iwami, Y. Inamori, O. Nishimura, and R. Sudo. 1998. Significance of attached cyanobacteria relevant to the occurrence of musty odor in Lake Kasumigaura. Water Res. **32**: 3549–3554. doi:10.1016/s0043-1354(98)00153-5

Taranu, Z. E., I. Gregory-Eaves, P. R. Leavitt, and others. 2015. Acceleration of cyanobacterial dominance in north temperate-subarctic lakes during the Anthropocene. Ecol. Lett. **18**: 375–384. doi:10.1111/ele.12420

Tucker, C. J. 1979. Red and photographic infrared linear combinations for monitoring vegetation. Remote Sens. Environ. **8**: 127–150. doi:10.1016/0034-4257(79)90013-0

Tucker, C. S., and K. K. Schrader. 2020. Off-flavors in pond-grown ictalurid catfish: causes and management options. J. World Aquacult. Soc. **51**: 7–92. doi:10.1111/jwas.12672

United States Code. 2018. 33 U.S.C. - Navigation and navigable waters. 33 U.S.C.

USEPA. 2009. National Lakes Assessment: A Collaborative Survey of the Nation's Lakes. EPA 841-R-09-001. EPA 841-R-09-001 U.S. Environmental Protection Agency, Office of Water and Office of Research and Development.

USEPA. 2015. 2015 drinking water health advisories for two cyanobacterial toxins. EPA 820F15003. EPA 820F15003 U.S. Environmental Protection Agency, Office of Water and Office of Research and Development.

USEPA. 2016. National Lakes Assessment 2012: A Collaborative Survey of Lakes in the United States. U.S. Environmental Protection Agency.

Vagner, M., T. Lacoue-Labarthe, J.-L. Z. Infante, D. Mazurais, E. Dubillot, H. Le Delliou, P. Quazuguel, and C. Lefrancois. 2015. Depletion of essential fatty acids in the food source affects aerobic capacities of the golden grey mullet *Liza aurata* in a warming seawater context. PLoS One **10**: e0126489. doi:10.1371/journal.pone.0126489

Van der Merwe, D., and K. Price. 2015. Harmful algal bloom characterization at ultra-high spatial and temporal resolution using small unmanned aircraft systems. Toxins **7**: 1065–1078. doi:10.3390/toxins7041065

Vanderploeg, H. A., J. R. Liebig, W. W. Carmichael, M. A. Agy, T. H. Johengen, G. L. Fahnenstiel, and T. F. Nalepa. 2001. Zebra mussel (*Dreissena polymorpha*) selective filtration promoted toxic *Microcystis* blooms in Saginaw Bay (Lake Huron) and Lake Erie. Can. J. Fish. Aquat. Sci. **58**: 1208–1221. doi:10.1139/cjfas-58-6-1208

Vanni, M. J., M. J. Gonzalez, and W. H. Renwick. 2019. Long term limnological measures in Acton Lake, a southwest Ohio reservoir, and its inflow streams: 1992-2017. Environmental Data Initiative. doi:10.6073/pasta/92453dbf5e885748819fa6cbbf46a376

Wacker, A., and E. von Elert. 2003. Food quality controls reproduction of the zebra mussel (*Dreissena polymorpha*). Oecologia **135**: 332–338. doi:10.1007/s00442-003-1208-5

Walsby, A. E., P. K. Hayes, R. Boje, and L. J. Stal. 1997. The selective advantage of buoyancy provided by gas vesicles for planktonic cyanobacteria in the Baltic Sea. New Phytol. **136**: 407–417. doi:10.1046/j.1469-8137.1997.00754.x

Wang, Z. J., and R. H. Li. 2015. Effects of light and temperature on the odor production of 2-methylisoborneol-producing *Pseudanabaena* sp and geosmin-producing *Anabaena ucrainica* (cyanobacteria). Biochem. Syst. Ecol. **58**: 219–226. doi:10.1016/j.bse.2014.12.013

Waters, M. N. 2016. A 4700-year history of cyanobacteria toxin production in a shallow subtropical lake. Ecosystems **19**: 426–436. doi:10.1007/s10021-015-9943-0

Watson, S. B., P. Monis, P. Baker, and S. Giglio. 2016. Biochemistry and genetics of taste- and odor-producing cyanobacteria. Harmful Algae **54**: 112–127. doi:10.1016/j.hal.2015.11.008

Watson, S. B., J. Ridal, and G. L. Boyer. 2008. Taste and odour and cyanobacterial toxins: impairment, prediction, and management in the Great Lakes. Can. J. Fish. Aquat. Sci. **65**: 1779–1796. doi:10.1139/f08-084

Wedgworth, J., J. Brown, P. Johnson, J. B. Olson, M. Elliott, R. Forehand, and C. E. Stauber. 2014. Associations between perceptions of drinking water service delivery and measured drinking water quality in rural Alabama. Int. J. Environ. Res. Public Health **11**: 7376–7392. doi:10.3390/ijerph110707376

Weider, L. J., W. Lampert, M. Wessels, J. K. Colbourne, and P. Limburg. 1997. Long–term genetic shifts in a microcrustacean egg bank associated with anthropogenic changes in the Lake Constance ecosystem. Proc. R. Soc. London, Ser. B **264**: 1613–1618. doi:10.1098/rspb.1997.0225

Westerhoff, P., M. Rodriguez-Hernandez, L. Baker, and M. Sommerfeld. 2005. Seasonal occurrence and degradation of 2-methylisoborneol in water supply reservoirs. Water Res. **39**: 4899–4912. doi:10.1016/j.watres.2005.06.038

Wilkinson, G. M., J. A. Walter, C. D. Buelo, and M. L. Pace. Accepted. No evidence of widespread algal bloom intensification in hundreds of lakes. Front. Ecol. Environ.

Wilson, A. E., D. C. Gossiaux, T. O. Höök, J. P. Berry, P. F. Landrum, J. Dyble, and S. J. Guildford. 2008. Evaluation of the human health threat associated with the hepatotoxin microcystin in the muscle and liver tissues of yellow perch (*Perca flavescens*). Can. J. Fish. Aquat. Sci. **65**: 1487–1497. doi:10.1139/F08-067

Wilson, A. E., and M. E. Hay. 2007. A direct test of cyanobacterial chemical defense: Variable effects of microcystin-treated food on two *Daphnia pulicaria* clones. Limnol. Oceanogr. **52**: 1467–1479. doi:10.4319/lo.2007.52.4.1467

Wilson, A. E., O. Sarnelle, and A. R. Tillmanns. 2006. Effects of cyanobacterial toxicity and morphology on the population growth of freshwater zooplankton: Meta-analyses of laboratory experiments. Limnol. Oceanogr. **51**: 1915–1924. doi:doi.org/10.4319/lo.2006.51.4.1915

Wynne, T. T., R. P. Stumpf, M. C. Tomlinson, and J. Dyble. 2010. Characterizing a cyanobacterial bloom in Western Lake Erie using satellite imagery and meteorological data. Limnol. Oceanogr. **55**: 2025–2036. doi:10.4319/lo.2010.55.5.2025

Xu, F., Z. Gao, X. Jiang, J. Ning, X. Zheng, D. Song, J. Ai, and M. Chen. 2017. Mapping of green tide using true color aerial photographs taken from a unmanned aerial vehicle. *Remote Sensing and Modeling of Ecosystems for Sustainability XIV*. Proceedings of the Remote Sensing and Modeling of Ecosystems for Sustainability XIV. International Society for Optics and Photonics. 104050M.

Xu, F., Z. Gao, X. Jiang, W. Shang, J. Ning, D. Song, and J. Ai. 2018. A UAV and S2A data-based estimation of the initial biomass of green algae in the South Yellow Sea. Mar. Pollut. Bull. **128**: 408–414. doi:10.1016/j.marpolbul.2018.01.061

Xue, J., and B. Su. 2017. Significant remote sensing vegetation indices: A review of developments and applications. J. Sens. **2017**: e1353691. doi:10.1155/2017/1353691

Yacobi, Y. Z., W. J. Moses, S. Kaganovsky, B. Sulimani, B. C. Leavitt, and A. A. Gitelson. 2011. NIR-red reflectance-based algorithms for chlorophyll-a estimation in mesotrophic

inland and coastal waters: Lake Kinneret case study. Water Res. **45**: 2428–2436. doi:10.1016/j.watres.2011.02.002

Yang, Z., P. Willis, and R. Mueller. 2008. Impact of band-ratio enhanced AWIFS image to crop classification accuracy. Proceedings of the 17th William T. Pecora Memorial Remote Sensing Symposium.

Yeager, N., and A. Carpenter. 2019. State approaches to addressing cyanotoxins in drinking water. AWWA Water Sci. **1**: e1121. doi:10.1002/aws2.1121

Zhou, Y., J. Ma, Y. Zhang, and others. 2017. Improving water quality in China: Environmental investment pays dividends. Water Res. **118**: 152–159. doi:10.1016/j.watres.2017.04.035

Zimmerman, L. R., A. C. Ziegler, and E. M. Thurman. 2002. Method of analysis and quality-assurance practices by the U.S. Geological Survey Organic Geochemistry Research Group; determination of geosmin and methylisoborneol in water using solid-phase microextraction and gas chromatography/mass spectrometry. USGS Numbered Series 2002–337. 2002–337 U.S. Geological Survey.

Appendix A. Juvenile percent survival of the six *Daphnia pulicaria* genotypes used in this study

Table A1. Juvenile percent survival of six *Daphnia pulicaria* genotypes fed a diet of 100% *Ankistrodesmus falcatus* or 100% microcystin-producing *Microcystis aeruginosa* for 9 days. The six genotypes were isolated in 2017 from the surface sediment of six small glacial lakes in southern Michigan. Three of the lakes are oligotrophic and three lakes are moderately to highly eutrophic, based on total phosphorus concentrations (µg/L). Average total phosphorus concentrations are based on data reported by Chislock et al. (2019). SE = standard error.

Source Lake	**Average TP_{spring}** (µg/L)	**Isolate ID**	**Survival on 100% *Ankistrodesmus* diet (SE)**	**Survival on 100% *Microcystis* diet (SE)**
Sensitive genotypes				
Sherman	8	Sherman-7	83 (17)	50 (17)
Bassett	10	Bassett-411	83 (17)	0 (0)
Lawrence	13	Lawrence-401	83 (17)	17 (17)
Tolerant genotypes				
Duncan	62	Duncan-1	100 (0)	100 (0)
Baseline	36	Base-4	83 (17)	50 (50)
Kent	25	Kent-1	100 (0)	67 (33)

Appendix B. *Daphnia pulicaria* survivorship results

Table B1. ANOVA results of survival (measured as LT50) over 10 days by cyanobacteria-tolerant and cyanobacteria-sensitive *Daphnia pulicaria* genotypes exposed to two temperatures (20°C and 28°C) and five diet treatments (*Ankistrodesmus* only (0% *Microcystis*), 75% *Ankistrodesmus* and 25% *Microcystis* (25% *Microcystis*), 50% *Ankistrodesmus* and 50% *Microcystis* (50% *Microcystis*), and 25% *Ankistrodesmus* and 75% *Microcystis* (75% *Microcystis*), and a starvation treatment (starved)). Extra sum of squares *F*-test results determine whether two- and three-way ANOVAs are a significant improvement in fit to the data compared to one-way ANOVA. df = degrees of freedom; MS= means square error.

Test	**Source**	**df**	**MS**	**F-ratio**	***p*-value**
One-way ANOVA	Temperature	1	31.65	0.89	0.36
	Genotype	1	4.88	0.14	0.72
	Cyanobacteria	1	157.73	4.43	0.05
	Error	16	35.63		
Two-way ANOVA	Temperature	1	31.65	1.36	0.26
	Genotype	1	4.88	0.21	0.65
	Cyanobacteria	1	157.73	6.79	0.02
	Temperature x Genotype	1	3.60	0.16	0.70
	Temperature x Cyanobacteria	1	219.45	9.44	0.01
	Cyanobacteria x Genotype	1	44.88	1.93	0.19
	Error	13	23.24		
				F-drop test *p*-value:	0.04
Three-way ANOVA	Temperature	1	32.65	1.30	0.28
	Genotype	1	4.88	0.20	0.66
	Cyanobacteria	1	157.73	6.49	0.03
	Temperature x Genotype	1	3.60	0.15	0.71
	Temperature x Cyanobacteria	1	219.45	9.03	0.01
	Cyanobacteria x Genotype	1	44.88	1.85	0.19
	Genotype x Temperature x Cyanobacteria	1	10.43	0.43	0.52
	Error	12	24.31		
				F-drop test *p*-value:	0.52

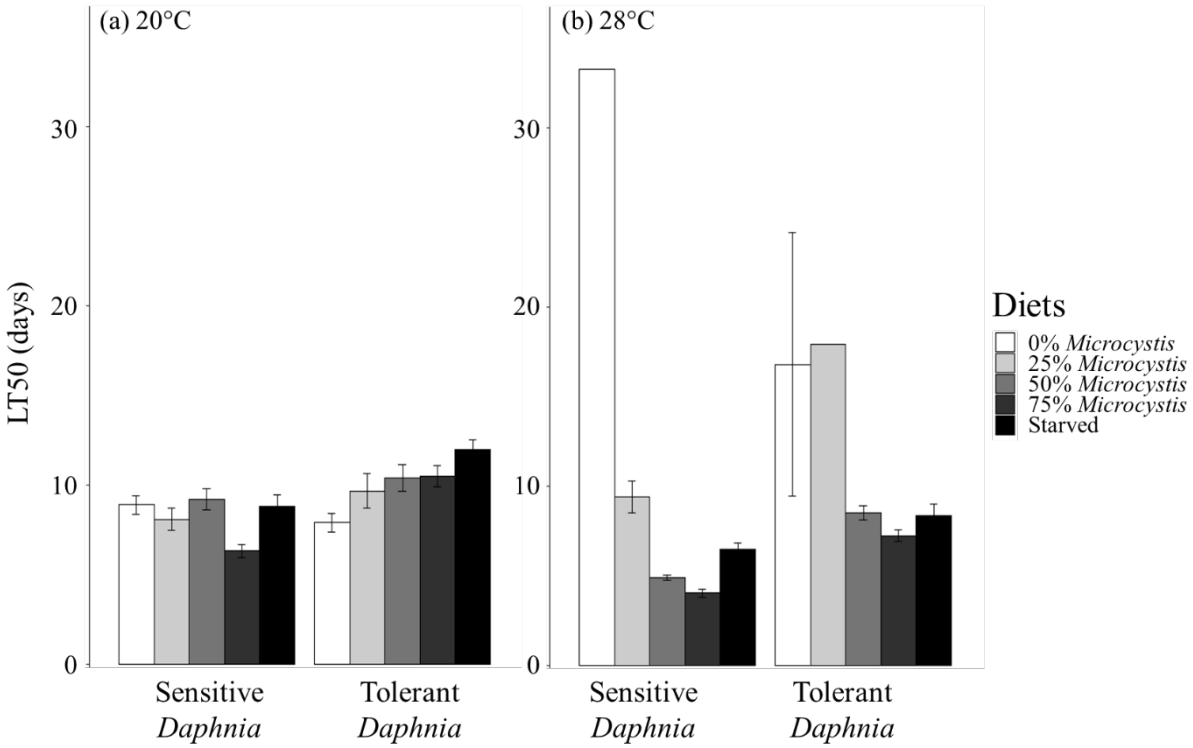

Figure B1. Time needed to kill 50% (i.e., LT50) of cyanobacteria-tolerant and cyanobacteria-sensitive *Daphnia pulicaria* genotype females cultured at (a) 20°C or (b) 28°C. Diet treatments included *Ankistrodesmus* only (0% *Microcystis*), 75% *Ankistrodesmus* and 25% *Microcystis* (25% *Microcystis*), 50% *Ankistrodesmus* and 50% *Microcystis* (50% *Microcystis*), and 25% *Ankistrodesmus* and 75% *Microcystis* (75% *Microcystis*), and a starvation treatment (starved). Error bars = ± 1 SE. Sample size per treatment = 4.

Appendix C. *Daphnia pulicaria* juvenile somatic growth rate results

Table C1. ANOVA results for juvenile somatic growth rate (length, micrometers per day) over 7 days by cyanobacteria-tolerant and cyanobacteria-sensitive *Daphnia pulicaria* genotypes exposed to two temperatures (20°C and 28°C) and five diet treatments (*Ankistrodesmus* only (0% *Microcystis*), 75% *Ankistrodesmus* and 25% *Microcystis* (25% *Microcystis*), 50% *Ankistrodesmus* and 50% *Microcystis* (50% *Microcystis*), and 25% *Ankistrodesmus* and 75% *Microcystis* (75% *Microcystis*), and a starvation treatment (starved)). Extra sum of squares *F*-test results determine whether two- and three-way ANOVAs are a significant improvement in fit to the data, compared to one-way ANOVA. df = degrees of freedom; MS= means square error.

Test	**Source**	**df**	**MS**	**F-ratio**	***p*-value**
One-way ANOVA	Temperature	1	0.0002	0.75	0.39
	Genotype	1	0.0065	31.74	<0.0001
	Cyanobacteria	4	0.0068	33.44	<0.0001
	Error	60	0.0002		
Two-way ANOVA	Temperature	1	0.0013	8.16	0.01
	Genotype	1	0.0059	37.41	<0.0001
	Cyanobacteria	4	0.0066	41.42	<0.0001
	Temperature x Genotype	1	0.0000	0.21	0.65
	Temperature x Cyanobacteria	4	0.0004	2.47	0.05
	Cyanobacteria x Genotype	4	0.0006	3.78	0.01
	Error	51	0.0002		
				F-drop test *p*-value:	0.01
Three-way ANOVA	Temperature	1	0.0013	8.33	0.01
	Genotype	1	0.0060	38.20	<0.0001
	Cyanobacteria	4	0.0066	42.30	<0.0001
	Temperature x Genotype	1	0.0001	0.63	0.43
	Temperature x Cyanobacteria	4	0.0004	2.45	0.05
	Cyanobacteria x Genotype	4	0.0006	3.84	0.01
	Genotype x Temperature x Cyanobacteria	2	0.0002	1.54	0.22
	Error	49	0.0002		
				F-drop test *p*-value:	0.22

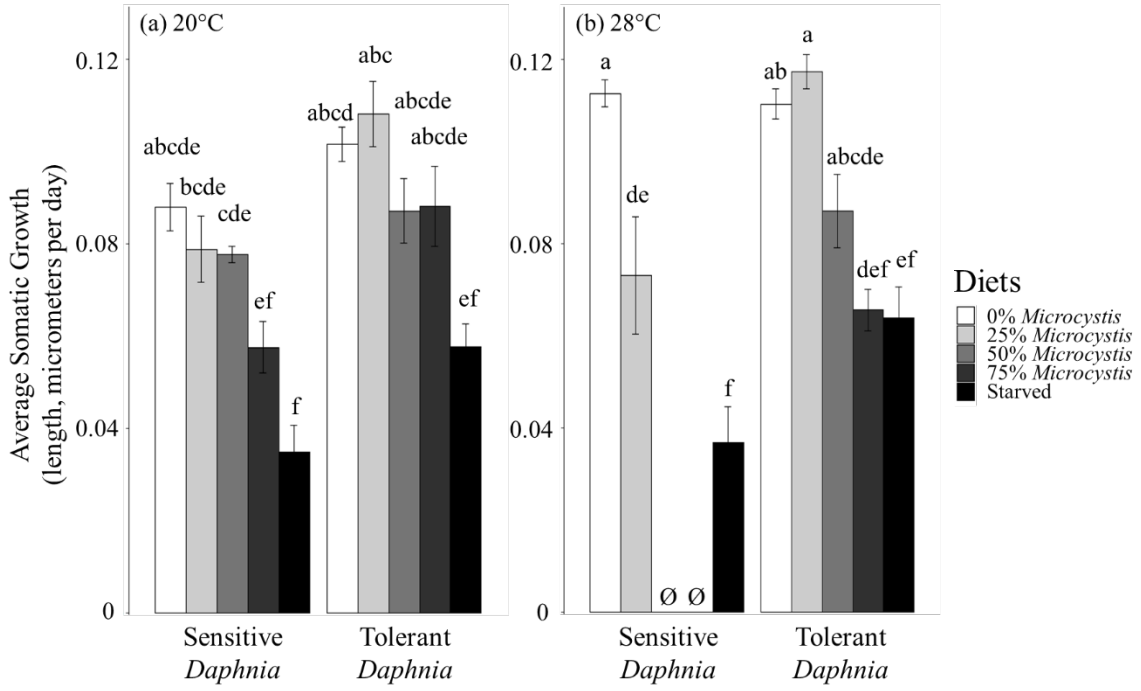

Figure C1. Average juvenile somatic growth rates (length, micrometers per day) of cyanobacteria-tolerant and cyanobacteria-sensitive *Daphnia pulicaria* genotype females cultured at (a) 20°C or (b) 28°C over 7 days. Diet treatments included *Ankistrodesmus* only (0% *Microcystis*), 75% *Ankistrodesmus* and 25% *Microcystis* (25% *Microcystis*), 50% *Ankistrodesmus* and 50% *Microcystis* (50% *Microcystis*), and 25% *Ankistrodesmus* and 75% *Microcystis* (75% *Microcystis*), and a starvation treatment (starved). Unique letters represent statistically different observations (p <0.05) across genotypes and temperature treatments. Error bars = ± 1 SE. Sample size per treatment = 4.

Appendix D. Number of neonates produced per female *Daphnia pulicaria*

Table D1. ANOVA results for number of neonates produced per female over 10 days by cyanobacteria-tolerant and cyanobacteria-sensitive *Daphnia pulicaria* genotype females exposed to two temperatures (20°C and 28°C) and five diet treatments (*Ankistrodesmus* only (0% *Microcystis*), 75% *Ankistrodesmus* and 25% *Microcystis* (25% *Microcystis*), 50% *Ankistrodesmus* and 50% *Microcystis* (50% *Microcystis*), and 25% *Ankistrodesmus* and 75% *Microcystis* (75% *Microcystis*), and a starvation treatment (starved)). Extra sum of squares *F*-test results determine whether two- and three-way ANOVAs are a significant improvement in fit to the data, compared to one-way ANOVA. df = degrees of freedom; MS= means square error.

Test	**Source**	**df**	**MS**	**F-ratio**	***p*-value**
One-way ANOVA	Temperature	1	28.03	3.828	0.05
	Genotype	1	77.2	10.55	0.0017
	Cyanobacteria	4	255.77	34.94	<0.0001
	Error	73	7.32		
Two-way ANOVA	Temperature	1	28.03	5.88	0.01
	Genotype	1	77.24	16.23	0.0002
	Cyanobacteria	4	255.77	53.74	<0.0001
	Temperature x Genotype	1	0.04	0.01	0.93
	Temperature x Cyanobacteria	4	23.05	4.84	0.002
	Cyanobacteria x Genotype	4	34.40	7.23	<0.0001
	Error	64	4.76		
			F-drop test *p*-value: <0.0001		
Three-way ANOVA	Temperature	1	28.03	5.963	0.01
	Genotype	1	77.24	16.44	0.0001
	Cyanobacteria	4	255.77	54.42	<0.0001
	Genotype x Temperature	1	0.04	0.01	0.93
	Temperature x Cyanobacteria	4	23.05	4.90	0.001
	Cyanobacteria x Genotype	4	34.40	7.32	<0.0001
	Genotype x Temperature x Cyanobacteria	4	5.65	1.20	0.32
	Error	60	4.70		
				F-drop test *p*-value: 0.32	

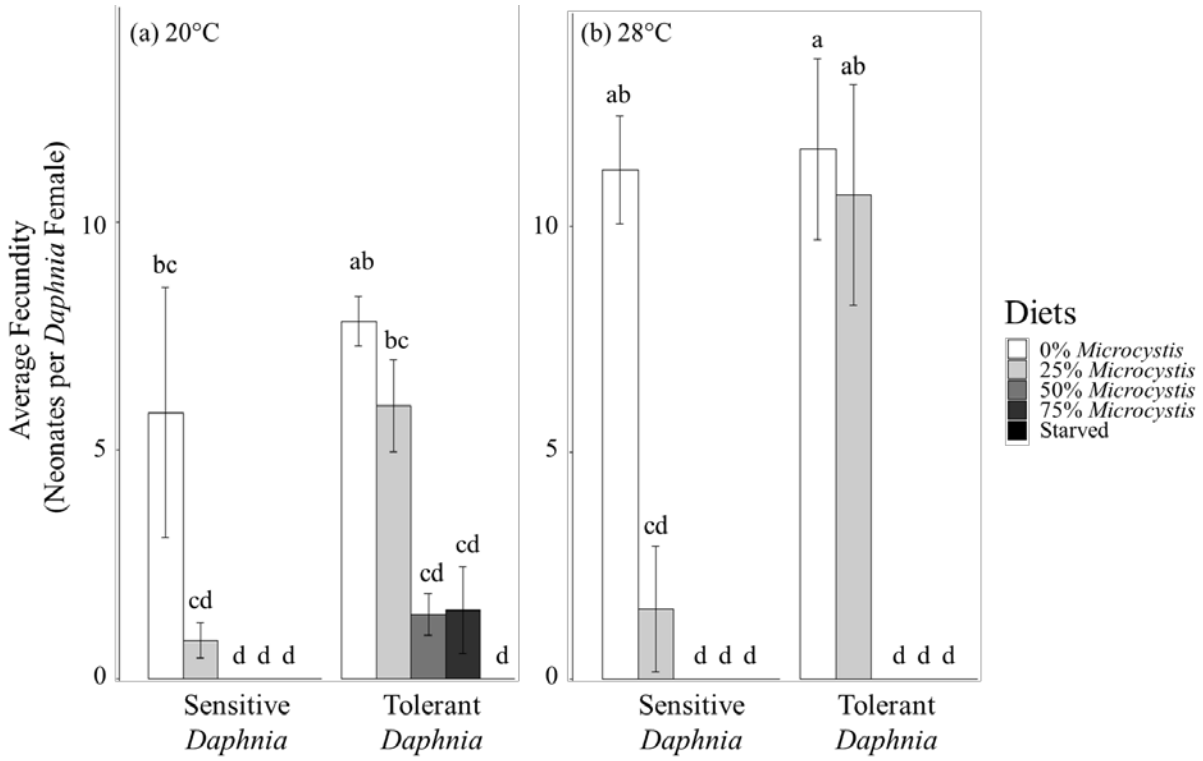

Figure D1. Average fecundity of cyanobacteria-tolerant and cyanobacteria-sensitive *Daphnia pulicaria* genotype females cultured at (a) 20°C or (b) 28°C, measured as total number of neonates produced per female over 10 days. Diet treatments included *Ankistrodesmus* only (0% *Microcystis*), 75% *Ankistrodesmus* and 25% *Microcystis* (25% *Microcystis*), 50% *Ankistrodesmus* and 50% *Microcystis* (50% *Microcystis*), and 25% *Ankistrodesmus* and 75% *Microcystis* (75% *Microcystis*), and a starvation treatment (starved). Unique letters represent statistically different observations (p <0.05) across genotypes and temperature treatments. Error bars = ± 1 SE. Sample size per treatment = 4.